Galaxy Interactions and Star Formation

Autor: María Sol Alonso

Presentado ante la Facultad de Matemática, Astronomía y Física
como parte de los requerimientos para la obtención del grado de
Doctor en Astronomía de la

UNIVERSIDAD NACIONAL DE CÓRDOBA

Mayo, 2007

Director: Dr. Diego García Lambas

A mi amor Gastón,
que ilumina y da alegría
a cada día de mi vida.

CONTENTS

Abstract

In this Thesis we analyse samples of galaxies in pairs obtained from the largest galaxy surveys at the present, the Two Degree Field Galaxy Redshift Survey (2dFGRS) and the Sloan Digital Sky Survey (SDSS). We have constructed accordingly two galaxy pair catalogs comprising 6067 and 11461 pairs for 2dFGRS and SDSS respectively. These are large databases suitable for statistical studies of galaxy interactions in the local Universe, $z \leq 0.1$. Galaxy pairs were selected by relative radial velocity (ΔV) and projected separation (r_p) thresholds determined by requiring star formation activity within neighbours to be significantly enhanced.

We study field galaxy pairs, that is, nearly isolated from other bright galaxies, and also we assess the effects of galaxy-galaxy interactions in dense environments by analysing pairs in groups and clusters of galaxies with virial masses in the range $10^{13} - 10^{15} M_{\odot}$. We find that star formation in galaxy pairs in the field is significantly enhanced over that of galaxies without companions for $r_p < 25$ kpc h^{-1} and $\Delta V < 100$ km s^{-1}. For those pairs in galaxy groups, a smaller limit $r_p < 15$ kpc h^{-1} provied the threshold of higher star formation activity in comparison to other group member galaxies.

Furthermore, we analyse star formation rates derived for galaxies in pairs in different environments using a projected galaxy density parameter derived from the fifth brightest neighbour of each galaxy, with a convenient luminosity threshold. We find that the star formation birthrate parameter is a strong function of the global environment as well as r_p and ΔV values. We observe that galaxy interactions are more effective at triggering important star formation activity in low and moderate density environments with respect to the control sample of galaxies without a close companion.

We have also analysed the star formation activity in a sample of 31 late-type satellite galaxies, with four of them showing signs of interactions, orbiting spiral galaxies. For these objects, we present narrow-band observations of the Hα emission, which was detected in all the spiral and irregular galaxies with fluxes in the range $1.15 - 49.80 \times 10^{-14}$ erg cm^{-2} s^{-1}. The four objects with higher current star formation rates (SFR) show clear signs of interaction with close companions of comparable brightness at projected distances of 25, 20 and 2 kpc, respectively. The other satellite with the largest current SFR (apart from the interacting systems) corresponds to the satellite galaxy, NGC 3154a, which has the smallest projected distance from its progenitor (19 kpc). These findings suggest that the proximity between

galaxies (i.e. satellite-satellite, satellite-primary) can produce an efficient enhancement of the star formation activity.

As a further study of the effects of interactions, we have performed an analysis of active galactic nuclei (AGN) host characteristics and nuclear activity for AGNs in pairs and without companions. An eye-ball classification of images of 1607 close pairs ($r_p < 25$ kpc h^{-1}, $\Delta V < 350$ km s^{-1}) according to the evidence of interaction through distorted morphologies and tidal features provides us with a more confident assessment of galaxy interactions from this sample. We find AGN hosts to be redder and with a larger concentration morphological index than non-AGN galaxies. This effect does not depend on whether AGN hosts are in pairs or in isolation. The $[OIII]$ luminosity of AGNs with strong interaction features is found to be significantly larger than that of other AGNs, either in pairs or in isolation. Estimations of the accretion rate, $L[OIII]/M_{BH}$, show that AGNs in merging pairs are actively feeding their black holes, regardless of their stellar masses.

Resumen

En esta Tesis se analizan muestras de galaxias pares obtenidas a partir de los dos mayores relevamientos de galaxias existentes al presente, Two Degree Field Galaxy Redshift Survey (2dFGRS) y Sloan Digital Sky Survey (SDSS). Construimos dos catálogos de galaxias pares que comprenden 6067 y 11461 pares a partir de 2dFGRS y SDSS, respectivamente, los cuales representan la mayor base de datos para realizar estudios de interacciones de galaxias en el Universo local, $z \leq 0.1$. Las galaxias pares fueron seleccionadas con límites de velocidades radiales relativas (ΔV) y separaciones proyectadas (r_p), determinados por una actividad de formación estelar notablemente mayor respecto a galaxias vecinas.

Estudiamos galaxias pares de campo, cercanamente aisladas respecto a galaxias brillantes, y evaluamos el efecto de las interacciones galaxia-galaxia en ambientes de mayor densidad, analizando pares en grupos y cúmulos de galaxias con masas viriales en un rango de $10^{13} - 10^{15} M_{\odot}$. Encontramos que la formación estelar en galaxias pares de campo se observa notablemente incrementada respecto a galaxias sin compañeras cercanas para $r_p < 25$ kpc h^{-1} y $\Delta V < 100$ km s^{-1}. En galaxias pares en grupos, un límite menor, $r_p < 15$ kpc h^{-1} provee una tendencia de alta actividad de formación estelar en comparación con las otras galaxias miembros de grupos.

Además, analizamos la razón de formación estelar para galaxias pares en diferentes ambientes, usando un parámentro de densidad proyectado derivado a partir del quinto vecino mas brillante de cada galaxia, con un umbral conveniente de luminosidad. Encontramos que la formación estelar es una fuerte función del ambiente global, así como de los valores de r_p y ΔV. Observamos que las interacciones de galaxias son más eficientes en disparar una actividad de formación estelar intensa en ambientes de densidad bajos y moderados, respecto a una muestra control de galaxias sin compañeras cercanas.

Investigamos la actividad de formación estelar en una muestra de 31 galaxias satélites de tipo tardías, donde cuatro de ellas muestran signos de interacción, orbitando galaxias espirales. Para estos objetos, presentamos observaciones de emisión en banda angosta Hα, que se detectaron en todas las galaxias espirales e irregulares, con flujos comprendidos dentro de un rango $1.15 - 49.80 \times 10^{-14}$ erg cm^{-2} s^{-1}. Los cuatro objetos con mayor actividad de formación estelar (SFR) muestran claros signos de interacción con compañeras cercanas de brillos comparables a distancias proyectadas de 25, 10 y 2 kpc, respectivamente. El otro satélite con mayor SFR (aparte de los sistemas en interacción) corresponde a la galaxia satélite NGC

3154a, la cual tiene la menor distancia proyectada respecto a su galaxia progenitora (19 kpc). Estos resultados sugieren que la proximidad entre galaxias (por ej. satélite-satélite, satélite-galaxia primaria) pueden producir un eficiente aumento de la actividad de formación estelar.

Además del estudio de los efectos de las interacciones, realizamos un análisis de las características de las galaxias huéspedes de núcleos activos (AGN) y de la actividad nuclear para AGNs en galaxias pares y sin compañeras cercanas. Una clasificación visual de imágenes de 1607 pares cercanas ($r_{\rm p} < 25$ kpc h^{-1}, $\Delta V < 350$ km s^{-1}) de acuerdo a la evidencia de distorsiones morfológicas y características de fuerzas de mareas, nos brinda una mayor confianza para el estudio de las interacciones de galaxias. La luminosidad del $[OIII]$ de AGNs con fuertes características de interacción se encuentra notablemente incrementada respecto a otras AGNs, ya sean en pares o aisladas. Estimas de la razón de acreción, $L[OIII]/M_{\rm BH}$, muestran que AGNs en pares en fusión presentan agujeros negros con actividad nuclear eficiente, respecto a otros sistemas de similares masas estelares.

CHAPTER 1

INTRODUCTION

1.1 Galaxy Mergers and Interactions

Galaxies may be viewed as the basic building blocks of the large-scale structure of the visible Universe. Hubble (1926) introduced a scheme that classifies most galaxies into ellipticals, normal and barred spirals. The galaxies that do not fit into these categories are classified separately as irregular galaxies. This Hubble classification system refers principally to normal galaxies and labels all peculiar galaxies as Type II Irregulars. Several of these peculiar systems appear to be in a highly disturbed state, often involving jets, tails, or ringlike structures. However these objects exhibit a wide variety of morphologies, having in common the lack of a well defined morphological pattern. Several examples can be found in Arp's *Atlas of Peculiar Galaxies* (1966), in Vorontsov-Velyaminov (1968) and in Arp & Madore (1987). It was firstly believed that these irregular systems could be exploding galaxies, although in the 1970s it was set the idea that most of these objects were actually colliding systems.

We presently know that interactions play a fundamental role in galaxy evolution as an efficient mechanism that modifies the mass distribution and trigger star formation (SF) activity. During the last thirty years the study of mergers and interacting galaxies has been acquiring an increasing importance mainly due to the wide range of phenomena observed in this type of objects. The works of Toomre & Toomre (1972), in theory, and those of Larson & Tinsley (1978), in observations, were the pioneers in this topic. Since this epoch, mounting evidence indicated that interactions between galaxies can affect almost any aspect of the evolution of these objects.

1.1.1 Galaxy Formation: the role of mergers and interactions

Over the last twenty five years, a standard paradigm has emerged for the formation and evolution of structure in the Universe assuming that structure forms by hierarchical aggregation (Peebles 1974, White & Rees 1978). In such scenario, mergers and interacting galaxies are frequent and play a crucial role in determining galaxy properties. Galaxies and galaxy systems grew via gravitational instability from small-amplitude Gaussian density fluctuations, generated by physical processes in the early Universe. Hierarchical models, such as the cold dark matter (CDM) model assume that the amplitude of the fluctuations decreases with increasing scale, resulting in the formation of low-mass objects, forming first, and then, mergers building up more massive structures (clusters, superclusters, filaments, etc.).

A halo of any given mass may have a variety of merging histories, and the properties of galaxies that form within this halo presumably depend to some extent on the details of this history. Assuming an initial random Gaussian field of fluctuations, Press & Schechter (1974) derived an analytic approximation for the mass distribution of nonlinear objects at a given time. Starting from the Press-Schechter formalism (or any of its extensions e.g. Bond et al. 1991, Bower 1991, Lacey & Cole 1993), one may derive halo dark matter merger histories. All this information is contained in the so called *merger tree*, such as that schematically shown in Fig. 1.1. The computation of these mean quantities within the Press-Schechter model is straightforward. Also, the semi-analytic approach to modeling galaxy formation (e.g. Kauffmann, White & Guiderdoni 1993, Cole et al. 1994) attempts to describe the formation history, supernova feedback, galaxy-galaxy merging, and stellar population synthesis. These models rely on the construction of a merger tree, with estimates of the masses of progenitors and the redshifts at which they merge to form larger halos.

1.1.2 Physical Processes in Merging Galaxies

Since galaxy mergers and interactions drive the evolution of galaxies and galaxy populations, the physics involved in close encounters must be properly addressed.

When two galaxies interact, certain processes may turn on such as shock waves and compression of the gas. The densest parts of these gas clouds may cool efficiently and collapse rapidly, forming a new generation of stars. The pre-existing stars, however, will not be greatly affected. Distances between stars are large with respect to the size of the stars themselves, hence, in a high speed collision of two galaxies, the stellar systems of each

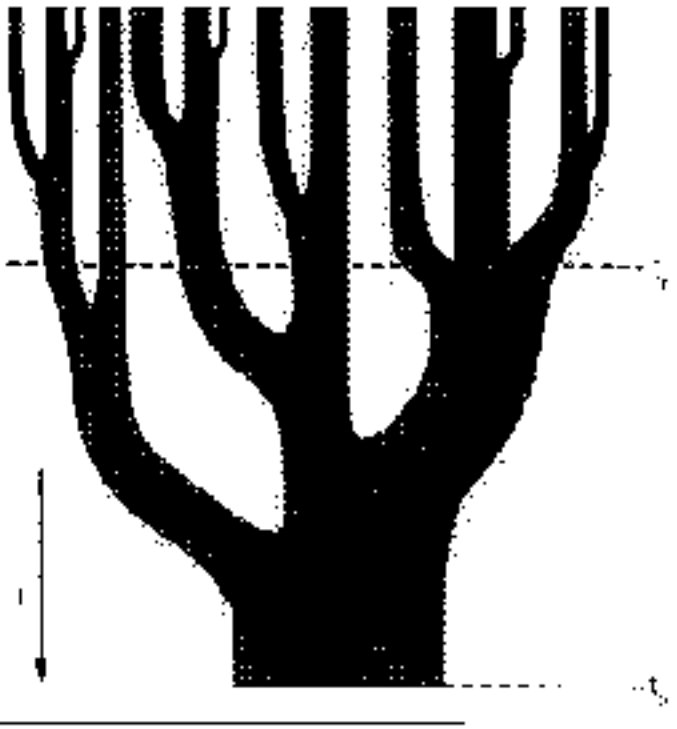

Fig. 1.1: A schematic representation of a *merger tree* depicting the growth of the halo as the result of a series of mergers. Time increases from top to bottom in this figure and the widths of the branches of the tree represent the masses of the individual parent halos. A size through the tree horizontally gives the distribution of masses in the parent halos at a given time. The present time t_0 and the formation time t_f are marked by horizontal lines, where the formation time is defined as the time at which a parent halo containing in excess of half of the mass of the final halo was first created (Lacey & Cole 1993).

galaxy will pass through each other, causing no significant global effects (Barnes & Hernquist 1992). Numerical simulations show that, as the systems are assembled, mergers and interactions can trigger star formation with an efficiency that seems to depend mainly on the internal structure of the systems. By using pre-prepared mergers, Barnes & Hernquist (1996) showed how the gas component experiences torques originated in the companion, increases its gas density and triggers a starburst during the orbital decay phase of the neighbour galaxy. These starbursts are fed by gas inflows tidally-induced if the axisymmetrical character of the potential well is lost during the interaction. The stability of the systems can be assured by a dominating central mass concentration and a second starburst could be generated at the actual fusion of the baryonic cores. Cosmological hydrodynamical simulations showed that these processes take place in the formation of galactic systems in a hierarchical aggregation scenario in a similar way to that shown by pre-prepared mergers (e.g. Barnes 1988, Barnes

& Hernquist 1992, 1996).

Besides triggering star formation, gas inflows could also feed a central black hole and help initiate or increase the nuclear activity (Sanders et al. 1988). The evolution of galaxies and the knowledge of the black hole properties is now better understood than a few years ago, however, many issues remain still unclear (Heckmann et al. 2004). The collisional disruption and gas dissipation in galaxy interactions could feed the nuclear activity of galaxies (Toomre & Toomre 1972) and several authors (e.g. Schwartz 1981; Shlosman, Begelman & Frank 1990) suggested that internal instabilities such as bars could be effective in transporting the gas into the centre of galaxies. Moreover, there are findings of more than one supermassive black hole in the nucleus of merger remnants (Begelman, Blanford & Rees 1980, Milosavljevic & Merritt 2001, Yu 2002).

N-body simulations show that the *slowest* encounters are often the most disruptive. When two galaxies are in close proximity, tidal forces become important, often creating tidal tails and bridges. During encounters, the orbital energy of the two galaxies is gradually converted into internal motions within the galaxies themselves; a mechanism referred to as dynamical friction (Chandrasekhar 1943, Binney & Tremaine 1987). Depending on relative velocities, orientation, and masses involved, this process may lead to a merger. When a merger occurs between two galaxies of comparable mass (a major merger), the end product will usually look like an elliptical galaxy (e.g. Barnes 1988). Numerical simulations of minor mergers (between galaxies with dissimilar masses) show that tidal torques from minor companions induce non-axisymmetrical structure in the main disk galaxy (Hernquist & Mihos 1995). However, in many close encounters a merger may not occur, although the encounter may still have a noticeable effect on the galaxies involved.

1.1.3 Mergers and Interactions: Environment and Epoch

Most galaxies in our local neighbourhood do not appear to be undergoing major mergers. Taking this into account, one must look in those environments most favorable to encounters. A first requirement would appear to be a high density of galaxies which would enhance the rate of potential interactions (cores of rich clusters, compact groups, or close pairs of galaxies). However, low relative velocities are required for interactions to be effective. Rich clusters with velocity dispersions of the order of 1000 km s^{-1} (e.g. Carlberg et al. 1996) are not suitable, while compact groups (e.g. Hickson et al. 1992) and close pairs (e.g. Charlton

& Salpeter 1991) with typical velocity dispersions of < 400 km s^{-1} are one of the better locations for studying the effects of galaxy interactions.

Within the hierarchical paradigm for galaxy formation it is expected that the merger rate was significantly higher in the past. This is so, since the universe is expanding, so that the space density of galaxies was higher before. Theoretical models (e.g. Toomre 1977, Carlberg 1990) predict that mergers would have been much more frequent, even at modest redshifts. Tissera et al. (2002) showed that the effects of interactions are different at dissimilar stages of evolution of the systems, being more efficient at higher z when the systems are in early stages of evolution. Also, the effects of mergers and interactions on star formation rates (SFR) are expected to be greater, since galaxies were generally more gas rich than they are at the present epoch. Observationally, these expectations appear to be validated by high resolution imaging of distant field galaxies. In addition, several studies of close pairs of galaxies at moderate redshift (e.g. Zepf & Koo 1989; Carlberg, Pritchet, & Infante 1994; Yee & Ellingson 1995) have estimated the change in the merger rate with redshift; the results of these studies are consistent with an increase with redshift. This can also be inferred from studies of *IRAS* galaxies (Lonsdale et al. 1990), radio galaxies (e.g. Windhorst et al. 1995), and quasars (e.g. Bahcall et al. 1997). Similar results have also shown that the merger rates (e.g., Woods, Fahlman & Richer 1995; Le Fevre et al. 2000; Patton et al. 2002) and the star formation activity of galaxies increase with redshift, suggesting a change in the impact of interactions on the star formation process as galaxies evolve.

1.1.4 Star Formation and Galaxy Interactions

The rate of star formation in galaxies

There is a wide range of young stellar content and star formation activity along the Hubble sequence, a basic feature of the Hubble classification itself.

Several authors (e.g. Tinsley 1968, 1972, Searle et al. 1973) derived the first estimates of star formation rates from evolutionary synthesis models of galaxy colours. These early studies confirmed the trends in SFRs and SF histories along the Hubble sequence, and led to the first predictions of the evolution of the SFR with cosmic lookback time. Subsequent modeling of blue galaxies by Bagnuolo (1976), Huchra (1977) and Larson & Tinsley (1978) revealed the importance of star formation bursts in the evolution of low-mass galaxies and

interacting systems.

The SFRs in galaxies, expressed in terms of the total mass of stars formed per year, show a large spread: approximately zero in gas-poor ellipticals, S0s, and dwarf galaxies; to 20 $M_\odot$/yr in gas-rich spirals. Much larger global SFRs (up to 100 $M_\odot$ yr^{-1} or more) can be found in optically-selected starburst galaxies and ultra-luminous infrared galaxies (ULIRGs). These objects are likely associated with the merger of the two nuclei (Sanders & Mirabel 1996). The highest SFR are associated almost uniquely with strong tidal interactions and mergers.

Dependence of star formation on environment

Fundamental studies by Dressler (1980), Postmann & Geller (1984), Sandage (1986), Ferguson & Sandage (1991) analysed the morphology-density relation showing that the star formation activity resides preferentially in disc galaxies populating low density regions. Different physical processes may play a role in driving the morphology-density relation and among them, mergers and interactions stands out in a hierarchical scenario. Even for systems in the field or in groups, the cumulative effects of many weaker encounters (Richstone 1976; Moore et al. 1996), or few merger events could have imprinted important features in their astrophysical properties.

Regarding the dependence of star formation activity on environment, Martínez et al. (2002) and Domínguez et al. (2002) analysed the relative fractions of passively star-forming galaxies in high density regions corresponding to groups of galaxies extracted from the Two degree Galaxy Redshift Survey (2dFGRS), finding that star formation activity increases with the distance to the group centre. A similar analysis carried out by Gomes et al. (2003) and Balogh et al. (2004) in the Sloan Digital Sky Survey (SDSS) and 2dFGRS surveys, also gave a clear indication of a strong dependence of star formation on environment consisting of decreasing activity with increasing density. Loveday, Tresse & Maddox (1999) found that galaxies with prominent emission-lines have weaker clustering than more quiescent galaxies. Tegmark & Bromley (1999) also found that early spectral type galaxies are more strongly clustered than late types. Besides, Carter et al. (2002) suggest that the triggering of star formation occurs on a small spatial scale, and whether a galaxy forms stars or not is strongly correlated with the surrounding galaxy density averaged over a scale of a few Mpc. Lewis et al. (2002) confirmed this last result by studying the environmental dependence of galaxy star formation rates near clusters, finding that it is insensitive to the global large-scale struc-

ture in which the galaxy is embedded. The authors also obtained that the distribution of star-formation rates is correlated with both the distance from the cluster centre and the local projected density (see also Domínguez et al. 2002). More recently, Balogh et al. (2004) found that, at fixed galaxy luminosity, the fraction of red galaxies is a strong function of local density, increasing up to ~ 70 per cent of the population in the highest density environments. Similar trends were obtained by Hogg et al. (2003), who showed that red galaxies, regardless of luminosity, are found in overdense regions. Kauffmann et al. (2004) used a complete sample of galaxies from SDSS, to study the structure and star formation activity as a function of local density and stellar mass, finding that the star formation activity was the galaxy property most sensitive to environment, with the strongest dependence for smallest stellar mass systems. These authors also claimed that mergers could lead to this dependence, although environment driven processes such as tidal stripping, which could remove gas from galaxies inhibiting further star formation activity, might be important in high density regions, principally for low stellar mass systems.

Effects of interactions on star formation

Several observational studies showed that mergers and interactions of galaxies affect star formation activity in galaxies in the Local Universe (e.g., Larson & Tinsley 1978; Donzelli & Pastoriza 1997; Barton, Geller & Kenyon 2000; Petrosian et al. 2002). Although the relevance of these violent events on the formation of structure and star formation history is now widely accepted, many questions remain to be answered. For example, as it has been reported by some authors (e.g., Petrosian et al. 2002), many interacting systems show weak star formation activity suggesting that the particular internal conditions (such as the gas content) within these systems may be needed to trigger star formation.

An insight into the nature of interactions can be obtained from studies of close pairs of galaxies. Yee & Ellingson (1995) and Patton et al. (1996) adopted a minimum projected separation of 20 kpc h^{-1} to define close pairs, finding no significant differences between mean properties of paired and isolated galaxies, although those which appear to be undergoing interactions or mergers have strong emission lines and blue rest-frame colours. A similar result was found by Zepf & Koo (1989), who studied close faint galaxy pairs, separated by less than 4.5 arcsec, finding that their colours correspond to recent star formation activity with an overall distribution consistent with field galaxies. Kennicutt et al. (1987) examined the H_α equivalent widths, UBV colours and far-infrared fluxes of a complete sample of local

pairs of galaxies finding that these pairs exhibit a general trend of enhanced star formation and nuclear activity but with a wide dispersion about the mean behavior. Barton et al. (2000) analysed a sample of approximately 500 galaxy pairs in the field, showing a correlation between their relative projected separation and radial velocity, and the H_α equivalent width. Although these authors found a tendency for increasing star formation activity for close pairs (both in projection and relative velocity), their sample is still small to carry out a thoughtful statistical study of the effects of interactions and their cosmological evolution.

1.2 Outline of this Thesis

The main aim of the work presented in this Thesis is to shed new light on the effects of mergers and interactions in galaxy properties such as star formation activity, galaxy colours and nuclear activity, from a statistical point of view.

For this purpose, we constructed two galaxy pair catalogs from the 2dF Galaxy Redshift Survey and the Sloan Digital Sky Survey. These pair catalogs are the largest samples up to date including several thousands galaxy pairs, suitable to analyse into detail how mergers and interactions affect galaxy properties.

In Chapter 2 we describe both surveys, 2dFGRS and SDSS, and the construction of the galaxy pair catalogs. We also provide details of a sample of satellites taken from Zaritsky et al. 1997.

In Chapters 3 and 4, we study pair galaxies in two different environments, field and groups/clusters. We investigate the effects of interactions on the star formation activity of galaxies in the field based on a comparative analysis of the properties of isolated galaxies and galaxies in interacting pairs. We analyse pairs in groups and clusters with virial masses in the range $10^{13} - 10^{15} M_\odot$, in Chapter 4. The effects of close companions in different density environments are analysed in Chapter 5.

In Chapter 6, we present observations of Hα emission in a sample of satellites orbiting isolated giant spiral galaxies. Four of these objects have clear signs of interaction with close companions and exhibit high star formation rates.

With the aim of unveiling the role of interactions in triggering active galactic nuclei (AGN), we analyse the effects of interactions in AGNs in close pairs, in comparison with AGNs without companions. This study is described in Chapter 7, where we investigate the power of nuclear activity and the estimated black hole accretion rate for AGNs with companions and in isolation.

Finally, in Chapter 8 we describe the principal conclusions and discussion.

This Thesis is based on the following articles:

1) Lambas D. G., Tissera P. B., Alonso M. S., Coldwell G., 2003, MNRAS, 346, 1189.

2) Alonso M. S., Tissera P. B., Coldwell G., Lambas D. G., 2004, MNRAS, 352, 1081.

3) Alonso, M. S., Lambas, D.G., Tissera, P.B. & Coldwell, G., 2006, MNRAS, 367, 1029.

4) Gutiérrez, C.M., Alonso M. S., Funes J. G., Ribeiro, M. B, 2006, AJ, 132, 596.

5) Alonso, M. S., Lambas, D.G., Tissera, P.B. & Coldwell, G., 2007, MNRAS, 375, 1017.

CHAPTER 2

OBSERVATIONAL DATA AND GALAXY PAIR CATALOGS

2.1 Abstract

In this Chaptet we obtain and describe pair galaxy samples from 2dFGRS and SDSS surveys. We describe the selection procedure of galaxy pairs from both surveys that give origin to the 2dF Galaxy Pair Catalog (2dFGPC) and the SDSS Galaxy Pair Catalog (SDSSGPC), comprising 6067 and 11461 pairs, respectively. Galaxy pairs were selected by relative radial velocity (ΔV) and projected separation (r_p) thresholds determined by an analysis of the star formation activity of neighbours. We also discuss possible aperture effects in both pair catalogs and incompleteness problems of SDSS pairs.

We have also obtained a sample of 31 satellite galaxies orbiting late spirals compiled by Zaritsky et al. (1997). For this sample we present the observational program and data reduction comprising photometry in optical broad and narrow-band filters.

2.2 2dF Galaxy Redshift Survey

The Two degree Field Galaxy Redshift Survey (2dFGRS; Colless et al. 2001) is one of the largest present-day spectroscopic surveys. It includes spectra for 245591 objects, with determined redshifts for approximately 240000 galaxies brighter than a limit magnitude b_j = 19.45. The source catalog for the survey is a revised and extended version of the APM Galaxy Catalog. The survey covers an area of approximately 2000 square degrees in three regions: NGP strip, SGP strip and 100 random fields. The strip in the North Galactic Hemisphere has 90000 galaxies and covers 75° × 10°. There are approximately 170000 galaxies in the 80° × 15° South Galactic Hemisphere strip centered on the South Galactic Pole; in

addition, there are 100 fields spread over the southern Galactic cap. A map of the survey fields on the sky is shown in Fig. 2.1 and the spatial distribution of the galaxies in the survey strips is shown in Fig. 2.2. This figure is the projection of the full width of the strips (10° in the NGP and 15° in the SGP).

The 2dFGRS uses the 2dF multi-fibre spectrograph on the Anglo-Australian Telescope, which is capable of observing 400 objects simultaneously over a 2° diameter field. Adaptive tiling is used to give a highly uniform sampling rate of 93% over the whole survey region. Redshifts are measured from spectra covering 3600–8000Å at a two-pixel resolution of 9.0Å and a median S/N of 13 pixel^{-1}.

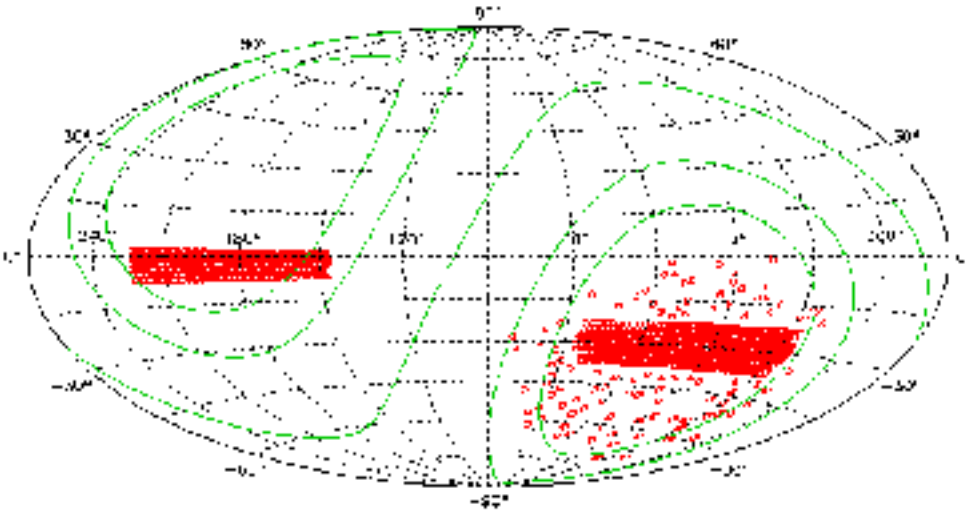

Fig. 2.1: The 2dFGRS regions shown in an Aitoff projection of Right Ascension and Declination, with individual 2dF fields marked as small circles. Also shown are the lines of Galactic latitude $|b|$=0°, 30°, 45°.

The 2dF data comprise information on redshift (z), angular separation, spectral type (η) and blue magnitude (m_b).

The spectral type parameter η is defined by Madgwick et al. (2002, hereafter M02), as a linear combination of the first two projections derived from a Principal Component Analysis (PCA), where it was found to be related to the morphological type and the strength of the absorption-emission features.

In Fig. 2.3 the distribution of the η parameter is shown for galaxies in the 2dFGRS. Also shown in the same figure is the η-morphology relation for a sample of galaxies from the Kennicutt Atlas (Kennicutt 1992). Comparing the two data sets shows that there is a

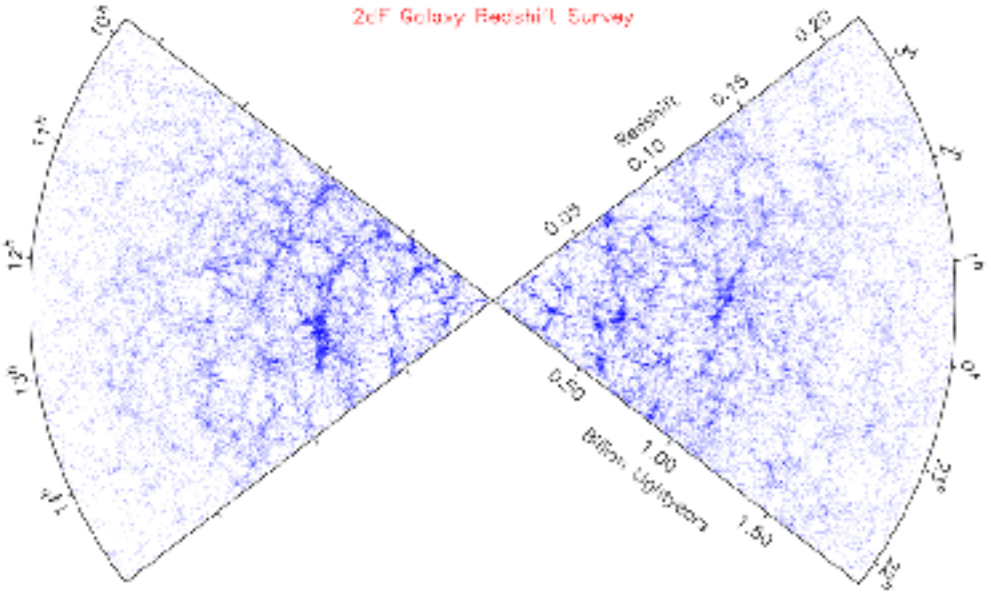

Fig. 2.2: The projected distribution of the galaxies in the NGP (top) and SGP (bottom) strips, as a function of redshift and R.A.; the variations in the galaxy density with R.A. are due to variations in the effective widths of the strips (Colless et al. 2001).

correspondence between the sequence of η and that of morphology.

Moreovet, the η parameter identifies the average emission and absorption line strength in the galaxy rest-frame spectrum. M02 suggest four different spectral Types, based on the relative prominence of emission lines with star formation efficiency increasing with galaxy Type:

Type 1: $\eta < -1.4$ (passive star formation)

Type 2: $-1.4 \leq \eta < 1.1$ (low to moderate star formation)

Type 3: $1.1 \leq \eta < 3.5$ (moderate to strong star formation)

Type 4: $\eta \geq 3.5$. (strong star formation)

The typical spectrum of each type is shown in Fig. 2.4. The good correlation found between η and EW(H_α) (the equivalent width of the Hα line) by M02 supports the interpretation of this parameter as a good indicator of star formation activity.

We have estimated galaxy luminosities and we have applied the K-corrections obtained by M02 to derive restframe values. The public 2dF data have galaxies with redshifts up to

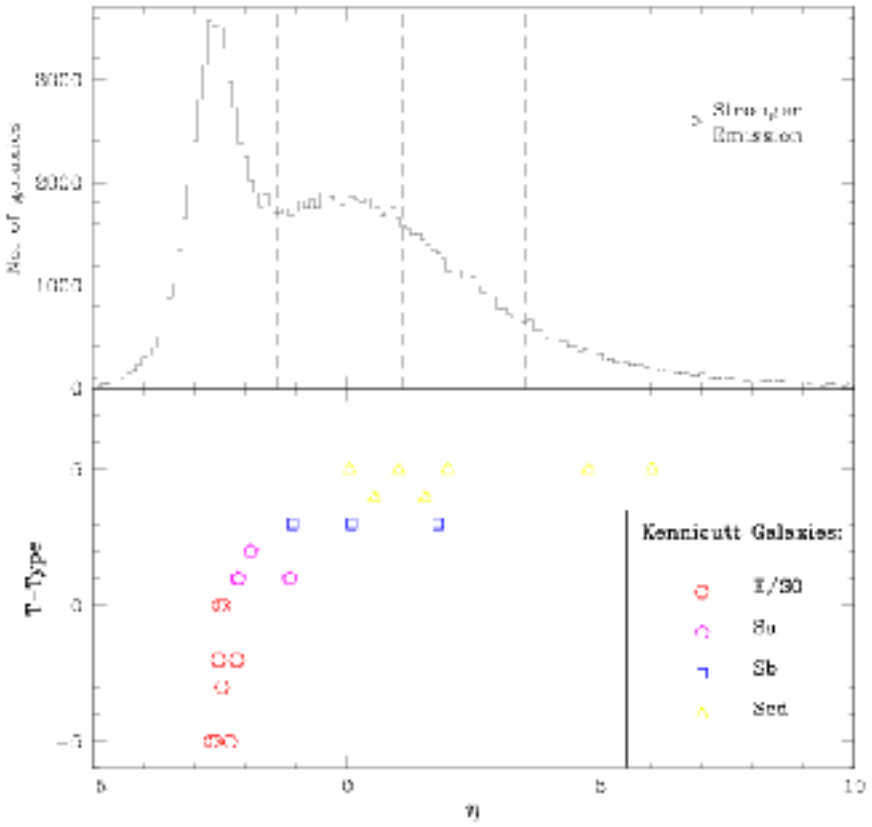

Fig. 2.3: The observed distribution of spectral types measured by η. Also shown are the four divisions that one can use to divide the dataset (see Fig. 2.4 for mean spectra). The bottom panel shows the correlation between η and morphological type using a training set of galaxies taken from the Kennicutt Atlas (Kennicutt 1992) (Madgwick et al. 2002).

$z \approx 0.3$, however, for the purpose of defining galaxy pairs we restrict our analysis to the range $0.01 \leq z \leq 0.1$ in order to prevent against strong biases in galaxy luminosities at too low redshift by peculiar velocities and unreliable spectral type estimates for distant galaxies.

2.2.1 Galaxy Pair Catalog from 2dFGRS

As we discussed in Chapter 1, Barton et al. (2000) presented a sample of approximately 500 galaxies in pairs which were selected to have projected separations $r_p < 50$ kpc h^{-1} (r_p corresponds to the distance between the two galaxies projected on the plane of the sky) and relative radial velocity differences $\Delta V \leq 1000$ km s^{-1} (defined as $\Delta V = c(z_1 - z_2)$, where z_1 and z_2 are the redshifts of the galaxies in the pair). These authors studied the possibility

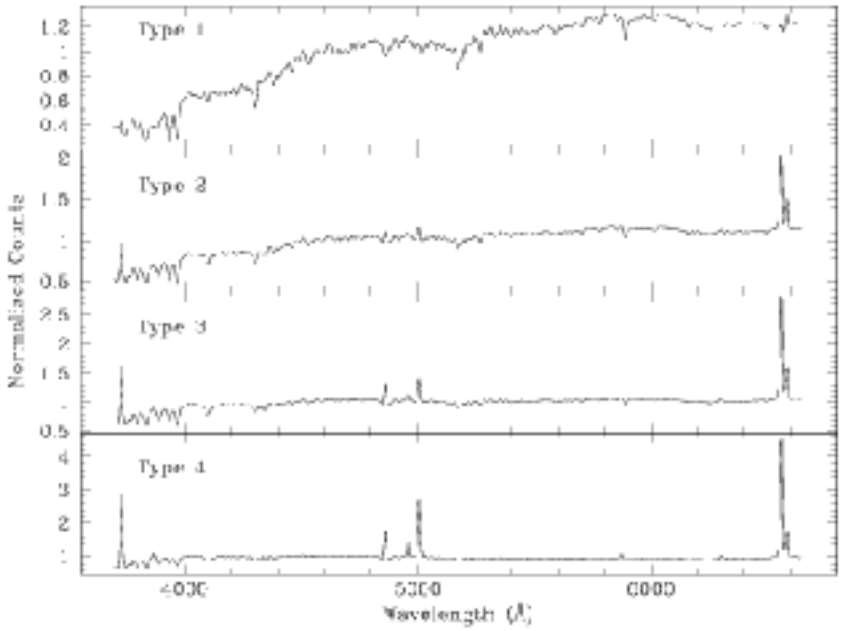

Fig. 2.4: The average 2dFGRS spectrum of each spectral type is shown. Each spectrum is in units of counts per pixel and has been normalized to have average counts of unity (Madgwick et al. 2002).

that tidal interactions induced star formation. However, it is not clear from their work, if there are critical spatial and velocity separations which could establish limits for tidal interactions to be effective star formation triggering mechanisms.

We have estimated the stellar birthrate parameter, $b = SFR/\langle SFR \rangle$, as the ratio of the current star formation rate to the average over the life time of the galaxy (Scalo 1986). This parameter has been found to correlate with the morphological type (Kennicutt 1992) in the sense that late-type spirals and irregulars have larger b values.

In order to compute the b parameter we adopt a linear relation between η and EW(H_α) values, which provide a reasonable fit to the data given by M02 (see Fig. 2.5):

$$EW(H_\alpha) = 5.64\eta + 10.9.$$

The relation between EW(H_α) and b was obtained by fitting a linear regression of the form:

$b = 0.045 EW(H_\alpha) + 0.61$

to the data of star forming galaxies given in Carter et al. (2001), see Fig. 2.6.

The resulting equation that relates linearly b with η is therefore:

$b = 0.25\eta + 1.06.$

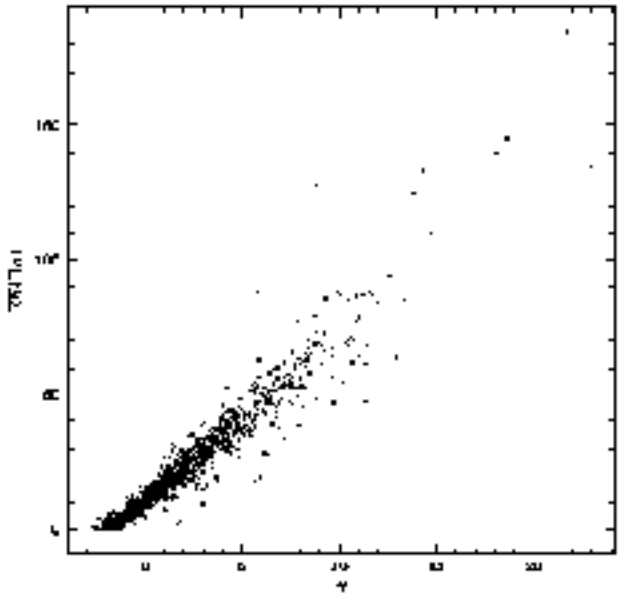

Fig. 2.5: Correlation between EW(H_α) and η parameter (Madgwick et al. 2002).

We notice that b, estimated by Madgwick et al. (2002), follows a quadratic relation with η, not a linear one as adopted in this work. We notice, however, that given the scatter shown in Fig. 2.5 both fits are equivalently suitable. It should be taken into account that the birthrate parameter b is linked to models for the star formation history and so the results are reliable on a global or statistical sense. Therefore, the conclusions obtained here are not expected to depend crucially on the particular dependence of b on η as far as η provides a useful measure of star formation in galaxies.

For the purpose of analysing the way b depends on r_p and ΔV, we computed the mean star formation rate parameter $\langle b \rangle$ of neighbours within $r_p \leq 1$ Mpc h^{-1} and $\Delta V \leq 1000$ km s^{-1} of a given galaxy. We considered two sub-samples according to the η spectral type of the

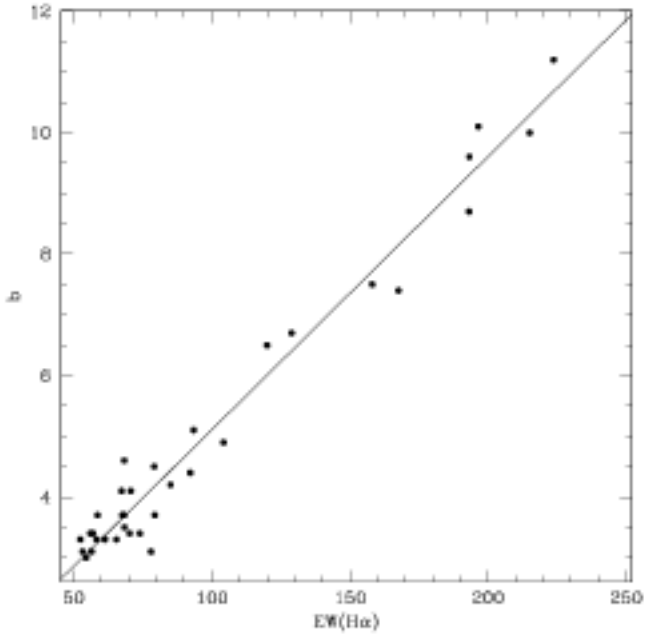

Fig. 2.6: Correlation between b and EW(H_α) (Carter et al. 2001).

galaxy centre. Sub-samples I and II take as a centre a galaxy with $\eta > 3.5$ (Type 4, strong star forming galaxies) and $\eta > -1.4$ (this subsample excludes Type 1 objects, consisting of passively star forming galaxies), respectively. For comparison with the general 2dF survey, we also use the total galaxy sample without restricting the values of η of the central galaxy.

In Fig. 2.7 we show the mean birthrate parameter for each sub-sample and the total galaxy sample in r_p bins. Error bars in the figure correspond to bootstrap resampling of the data.

The results shown in this figure highlight that the closest neighbours experience the strongest star formation activity in each sample. This effect is more significant when the central galaxy is also experiencing strong star formation activity ($\eta > 3.5$). Similar calculations where performed for velocity bins within $\Delta V < 1000\,\mathrm{km\ s^{-1}}$. In Fig. 2.8 we show $\langle b \rangle$ as a function of ΔV for these sub-samples finding that a maximum relative velocity of 350 $\mathrm{km\ s^{-1}}$ (vertical dotted line), is a suitable threshold for galaxies in pairs to have an enhanced star formation activity.

We can appreciate in Fig 2.7 and Fig 2.8 the general trend of decreasing star formation for smaller relative separation and radial velocity as expected according to the morphology-density relation. We stress that this tendency is sharply changed at the threshold $r_p \leq 100$

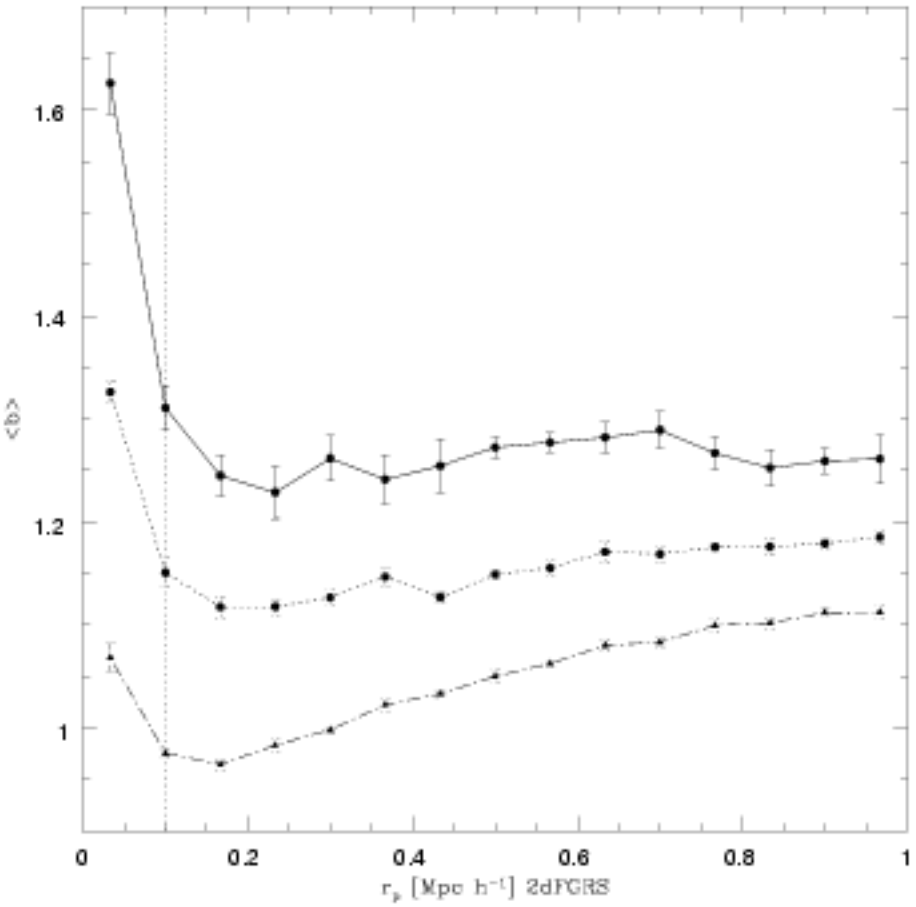

Fig. 2.7: Mean birthrate parameter $\langle b \rangle$ as a function of relative projected separation r_p of galaxies with $\eta > 3.5$ (solid line), $\eta > -1.4$ (dotted line) and no η restriction (dotted-dashed line). The dotted vertical line depicts the spatial separation threshold identification.

kpc h^{-1} and $\Delta V \leq 350$ km s^{-1}, where star formation strongly increases as one approaches the central galaxy.

Therefore, according to this analysis, $r_p \leq 100$ kpc h^{-1} and $\Delta V \leq 350$ km s^{-1} can be defined as reliable upper limits for the projected distance and relative radial velocity criteria to select galaxy pairs with enhanced star formation activity compared to average galaxies in 2dFGRS. The signals are more significant for centre galaxies of spectral Type 4, the same threshold applies to the other samples of centres. Hence these values of projected separation and relative radial velocity may be considered as suitable thresholds for the triggering of star formation induced by interactions.

By adopting these thresholds, the 2dF Galaxy Pair Catalog (2dFGPC) comprises 6067 galaxy pairs, with a redshift range $0.01 \leq z \leq 0.1$.

2.3 Sloan Digital Sky Survey

The Sloan Digital Sky Survey (SDSS; York et al. 2000) has produced both imaging and spectroscopic surveys over a large area of the sky mapping one-quarter of the entire sky and giving redshifts for galaxies and quasars.

The survey uses a dedicated wide-field 2.5 m telescope (Gunn et al. 2006) at Apache Point Observatory, New Mexico USA, equipped with a large format mosaic CCD camera to image the sky in five optical bands, $u\,g\,r\,i\,z$, spanning the range from 3000 to 10000 Å (Fukugita et al. 1996), on moonless photometric (Hogg et al. 2001) nights of good seeing.

Objects are selected from the imaging data for spectroscopy, including a complete sample of galaxies with reddening-corrected (Schlegel, Finkbeiner, & Davis 1998) Petrosian (1976) r magnitudes brighter than 17.77 (Strauss et al. 2002).

2.3.1 The Fourth Data Release (DR4)

The fourth data release (DR4) includes all data in previous outputs (DR1, DR2 and DR3).

The DR4's imaging portion comprises 6670 square degrees, containing photometric parameters of 180 million objects. The Main Galaxy Sample is essentially a magnitude limited spectroscopic sample (Petrosian magnitude) $r_{\rm lim} < 17.77$, most of galaxies span a redshift range $0 < z < 0.25$ with a mean redshift at $z = 0.1$ (Strauss et al. 2002).

The SDSS imaging data are taken along a series of strips, great circles on the sky which aim to fill a contiguous area in the Northern Galactic Cap, and three non-contiguous strips in the Southern Galactic Cap. The top panel of Fig. 2.9 shows the region of sky included in DR4. As this figure shows, the Northern Galactic Cap is covered by two contiguous regions, one centered roughly on the Celestial Equator, and the other at around $\delta = +40°$.

The SDSS-DR4 has more than half a millon galaxy spectra and includes different galaxy parameters such as magnitudes, star formation indicators, concentration index parameters, etc. The lower panel of Fig. 2.9 shows the 4783 deg^2 sky coverage of the spectroscopic data.

2.3.2 Galaxy Pair Catalog from SDSS

To construct the Galaxy Pair Calalog from the SDSS-DR4, we followed a similar procedure to that used to obtain pairs from 2dFGRS.

First, we have estimated the stellar birthrate parameter:

$b = (1 - R)t_H(SFR/M^*)$,

where t_H is the Hubble time, R is the fraction of the total stellar mass initially formed that is returned to the interstellar medium over the lifetime of the galaxy, and SFR/M^* is the present star formation rate normalised to the total mass in stars given by Brinchmann et al. (2004): we notice (SFR/M^*) has units of yr^{-1} and indicates the inverse of the global star formation time scale. We use a mean value $R = 0.5$ as estimated by Brinchmann et al. (2004).

As in the 2dFGRS case we have considered a redshift range $0.01 < z < 0.1$ in order to avoid strong incompleteness at larger distances as well as significant contributions from peculiar velocities at low redshifts. In order to find suitable limits in projected distance r_p and relative velocity ΔV to identify galaxy pairs with star formation enhancement in SDSS, we followed the procedure described in the previous Section. Namely, we analyse neighbours in concentric spheres within $r_p < 1$ Mpc h^{-1} and $\Delta V < 1000$ km s^{-1}, centered at a given galaxy. For these neighbours, we show in Fig.2.10 the mean birthrate parameter $\langle b \rangle$ as a function of projected separation, r_p, and relative velocity, ΔV. As it can be appreciated from this figure, there is a clear trend for the closest neighbours to have higher star formation activity. We find a significant increase of $\langle b \rangle$ for galaxies with companions with $r_p <$ 100 kpc h^{-1} and $\Delta V < 350$ km s^{-1} (vertical lines) compared to the mean stellar birthrate parameter value of the total SDSS survey, $\langle b \rangle = 0.35$. We notice the same pattern found for 2dFGRS pairs (Fig 2.7 and Fig 2.8), that is a decreasing star formation activity at closer separations and radial velocities, and a sharp change of this trend at the same projected separation and relative radial velocity thresholds. We also notice the smaller value of $\langle b \rangle$ for SDSS compared to 2dFGRS derived from the η parameter. In Chapter 5 we use common pairs in 2dFGRS and SDSS with these two different SFR estimates to homogenise the analysis an assess the agreement of the results of the two surveys. By imposing these thresholds, a SDSS galaxy pair catalog of 13485 galaxy pairs was built up which includes information

on the star formation activity of all its members. These thresholds are the same than those inferred from the 2dFGRS catalog, confirming that these limits are reliable to select pair galaxies with statistically enhanced star formation activity.

Contamination by active galactic nuclei (AGN) could contribute to the emission in spectral features, affecting our interpretation of star formation activity. In order to exclude AGNs from our sample, we cross-correlated the Brinchmann et al. (2004) AGN catalog with the SDSS pair catalog. From this analysis we found that $\approx 17\%$ of galaxies in the total pair sample are classified as AGNs.

After remotion of these common objects we obtain the final SDSS Galaxy Pair Catalog (SDSSGPC) consisting of 11461 pairs (free of AGNs contamination).

2.4 Aperture and Incompleteness Effects in Pair Catalogs

We discuss the possible presence of systematics that could bias our star formation rate estimates and pair definition, namely *aperture* and *incompleteness* effects.

Fibers for spectroscopy have finite angular sizes, and so spectral characteristics of the galaxies can be extracted only for the central regions of extended galaxies. On the other hand, incompleteness refers to the lack of galaxy measurement due to the maximum number of fibers in a given field so that it depends on the observational strategy of a survey. Fiber angular sizes are $2''$ and $3''$ for 2dFGRS and SDSS respectively, so we expect similar aperture effects for both surveys. On the other hand, due to the repeated scanning of 2dF (and not in SDSS), incompleteness is expected to affect more strongly the SDSS catalog. Here we evaluate incompleteness effects for the SDSS by combining the photometric and spectroscopic catalogs.

2.4.1 Possible Aperture Effects

By biasing the measurements towards the central region of galaxies, aperture effects can lead to underestimate the effects of star formation in large disc galaxies. Possible effects of aperture bias have been discussed in some detail by several authors (Baldry et al. 2002; Gomes, et al. 2003; Balogh et al. 2004; Kauffmann et al. 2004; Brinchmann et al. 2004).

Balogh et al. (2004) analysed the aperture effects in different environments finding that there was no significant trend of galaxy size with local density. Therefore, the effect of aper-

ture bias depends mainly on the spatial distribution of star formation across the galaxy with a lack of strong environment biases. For galaxies in SDSS, Brinchmann et al. (2004) found that there are still strong aperture effects in the estimates of SFR/M^* values for galaxies with $\log M^* > 10.5$. This is expected since these galaxies often have prominent bulges, in which the specific SFR is expected to be low. This would affect the star formation rate of the most massive galaxies in our sample, but not the intermediate and low mass systems, which dominate our statistics of interacting pairs ($\sim 70\,\%$ of the sample).

Based on these analysis we conclude that this potential bias is not likely to have a large effect on our analysis of star formation in pair galaxies in different environments.

2.4.2 Incompleteness Effects

In order to assess the effects of incompleteness, we built up a subsample of pairs free from incompleteness effects by cross-correlating the spectroscopic and the photometric surveys. We explored the fields in the photometric SDSS survey around each spectroscopic pair restricted to $m_* = 17.5$[1], searching for those galaxy pairs without any extra galaxy companion in the photometric survey within a projected distance of 100 kpc h^{-1} and with $m_* \leq 17.5$, which could contaminate our sample due to incompleteness of spectroscopy. This new pair sample is suitable to test the results obtained against incompleteness effects which could introduce other nearby galaxy whose redshift was not determined in the spectroscopic sample. By comparison between both pair samples (clean and raw), we estimated that the spectroscopic catalog has an incompleteness of $\approx 9.5\%$. Although this is not a large fraction, we have examined the possible effects in our analysis in Chapter 5, where we conclude that there is not a serious bias in our results.

2.5 Observing Program

For the purpose of completing the statistical analysis of star formation activity, we have conducted an observational program for the analysis of the star formation activity in satellite galaxies orbiting giant isolated spiral galaxies. The observational program comprises photometry in optical broad and narrow-band filters. For this study, we use narrow-band observations in Hα to estimate the current star formation rate of a subsample comprising late

[1] With this magnitude restriction we are considering ≈ 70 per cent of the total sample but with a much higher completeness than at the 17.77 original limit

type objects.

2.5.1 The Sample

The initial sample is the catalog of satellite galaxies compiled by Zaritsky et al. (1997). The catalog contains 115 objects orbiting 69 primary isolated spiral galaxies. Basically, the satellites were selected according to their relative brightness (at least 2.2 magnitudes fainter than their parents), projected distances (< 500 kpc h^{-1}) and relative velocity (< 500 km s^{-1}) from the primaries. The objects analyzed here correspond to a subsample comprising most of the objects classified by Gutiérrez & Azzaro (2004) as spirals or irregulars. In total, 31 objects have been observed and analyzed (most of the late type objects observable from the northern hemisphere). The objects span a considerable range in luminosity ($-19 < M_B < -15$), and constitute a sample useful for statistical studies of the population of late-type galaxies present in the halos of large spiral galaxies.

2.5.2 Observations and Data Reduction

Hα images and the broad-band for continuum estimation were acquired during three observing runsseven nights each in December 2001, May 2002, and December 2002 with the 1.80m Vatican Advanced Technology Telescope (VATT) at the Mt Graham International Observatory by J. G. Funes, C. M. Gutiérrez and M. B. Ribeiro. Most of the observations analyzed here were obtained in the first two runs and in photometric conditions. A back-illuminated 2048×2048 Loral CCD was used as the detector at the aplanatic Gregorian focus, $f/9$. It yielded a field of view of $6.4' \times 6.4'$ with an image scale of 0.4 pixel^{-1} after 2×2 pixel binning. The seeing varied between $1.1''$ and $2.3''$ with a mean value of $1.5''$. For each galaxy we have obtained typically 3×1800s narrow-band images using an apptopriate interference filters with ~ 70 Å widths that isolate the spectral region characterized by the redshifted Hα and [N II] λ6548,6583 Å emission lines. To cover the range in velocity spanned for the galaxies presented in this work, three filters were needed with central wavelength of 6584.7, 6632.8 and 6736.2 Å (another filter exists centered at 6683.1 Å but it was not necessary for any of the galaxies analyzed in this work). The nominal normalized spectral responses of these filters are presented in Fig. 2.11. Table 2.2 presents a summary of the observations and properties of the images obtained. Each filter is denoted according to its central wavelength in nm.

For absolute astronomical calibration we observed spectrophotometric standard stars

from the list provided by Oke (1990). In general, we observed one of these stars just before or after the narrow-band observations for each galaxy. In each case, stars were selected with a similar airmass rather than to calibrate the target. The exposure times for these stars ranged between 12 and 300 s, depending on the magnitude of the star. These details are shown in Table 2.2. The data were reduced using IRAF packages[2]. We performed standard data reduction, comprising, bias subtraction, flat-field correction using sky twilight observations in the appropriate filters and narrow-band images, and co-addition of the narrow-band images. This combination eliminates most of the artifacts due to bad pixels or cosmic rays.

To isolate the possible Hα emission of the targeted galaxies, the contribution of the stellar continuum emission of the galaxy needs to be removed. This was done by appropriately scaling the R-band image and subtracting it from the Hα images. The scaling factor was estimated by comparing the brightness of several field stars in the broad and in the narrow bands respectively. We measured the flux of these stars in a circular aperture $\sim$6 FWHM of the image. Depending on the field, the number of stars considered was in the range 3–12, with a typical number of 5.

2.6 *Summary of Samples*

In this Chapter, we have obtained two large samples of pairs from existing galaxy surveys: the 2dF Galaxy Pair Catalog and the SDSS Galaxy Pair Catalog, which comprise 6067 and 11461 pairs respectively. We have also obtained a sample of 31 satellite galaxies orbiting large late spirals compiled by Zaritsky et al. (1997) and we present the observational program and data reduction.

We use the 2dF Galaxy Pair Catalog in Chapters 3, 4 and 5. In Chapter 3 we analyse pairs in the field, excluding pairs in high density regions. In Chapter 4 we study pairs in groups and clusters of galaxies. We study the SDSS Galaxy Pair Catalog in Chapters 5 and 7. In Chapter 5 we analyse pairs in different environments from both 2dF and SDSS Galaxy Pair Catalogs. In Chapter 6, we analyse the star formation activity in the satellite galaxy sample orbiting late spirals. In Chapter 7, we consider active galactic nuclei in pairs from the SDSS Galaxy Pair Catalog.

A summary of the sample characteristics is given in Table 2.1.

[2]IRAF is the Image Reduction and Analysis Facility, written and supported by the IRAF programming group at the National Optical Astronomy Observatory (NOAO) in Tucson, Arizona.

Tab. 2.1: Catalogs

Catalog	Galaxy Numbers	Chapters
2dFGPC	6067 pair galaxies	3, 4 and 5
SDSSGPC	11461 pair galaxies	5 and 7
Satellite Sample	31 satellites	6

Note: 2dFGPC: 2dF Galaxy Pair Catalog; SDSSGPC: SDSS Galaxy Pair Catalog.

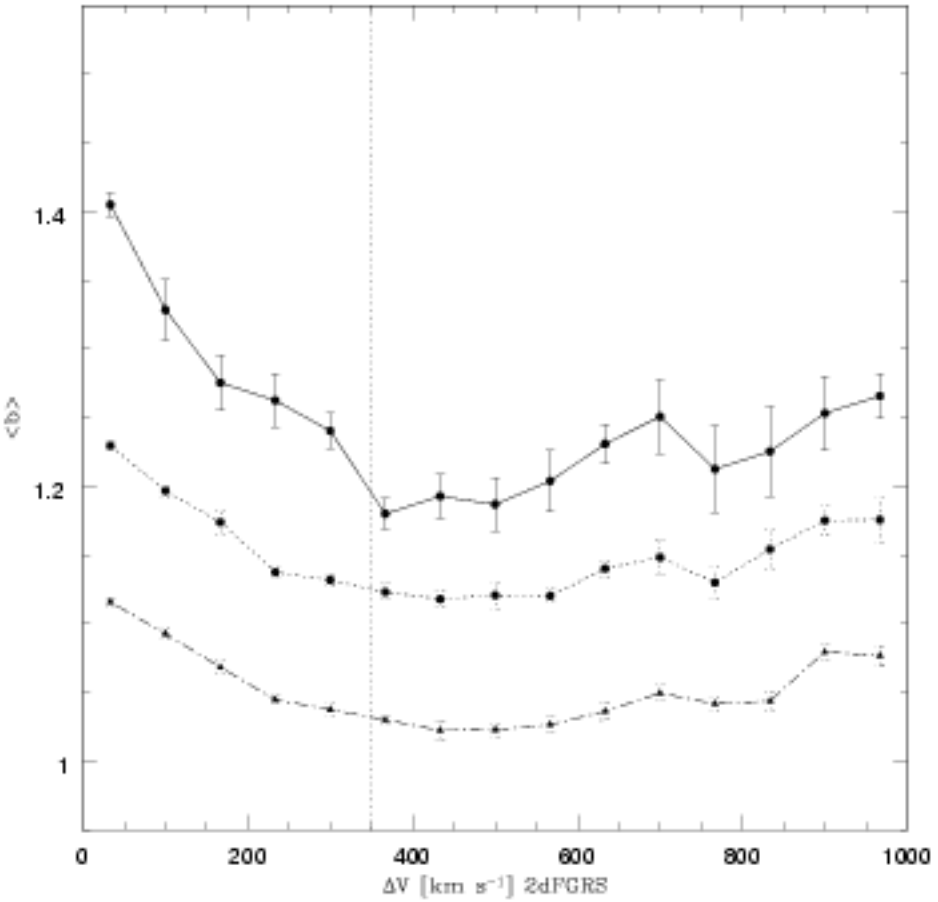

Fig. 2.8: Mean birthrate star formation parameter $\langle b \rangle$ of galaxies as a function of relative velocity to the target: $\eta > 3.5$ (solid line), $\eta > -1.4$ (dotted line) and no η restriction (dotted-dashed line) targets are shown. The dotted vertical line depicts the relative radial velocity threshold for galaxy pair identification.

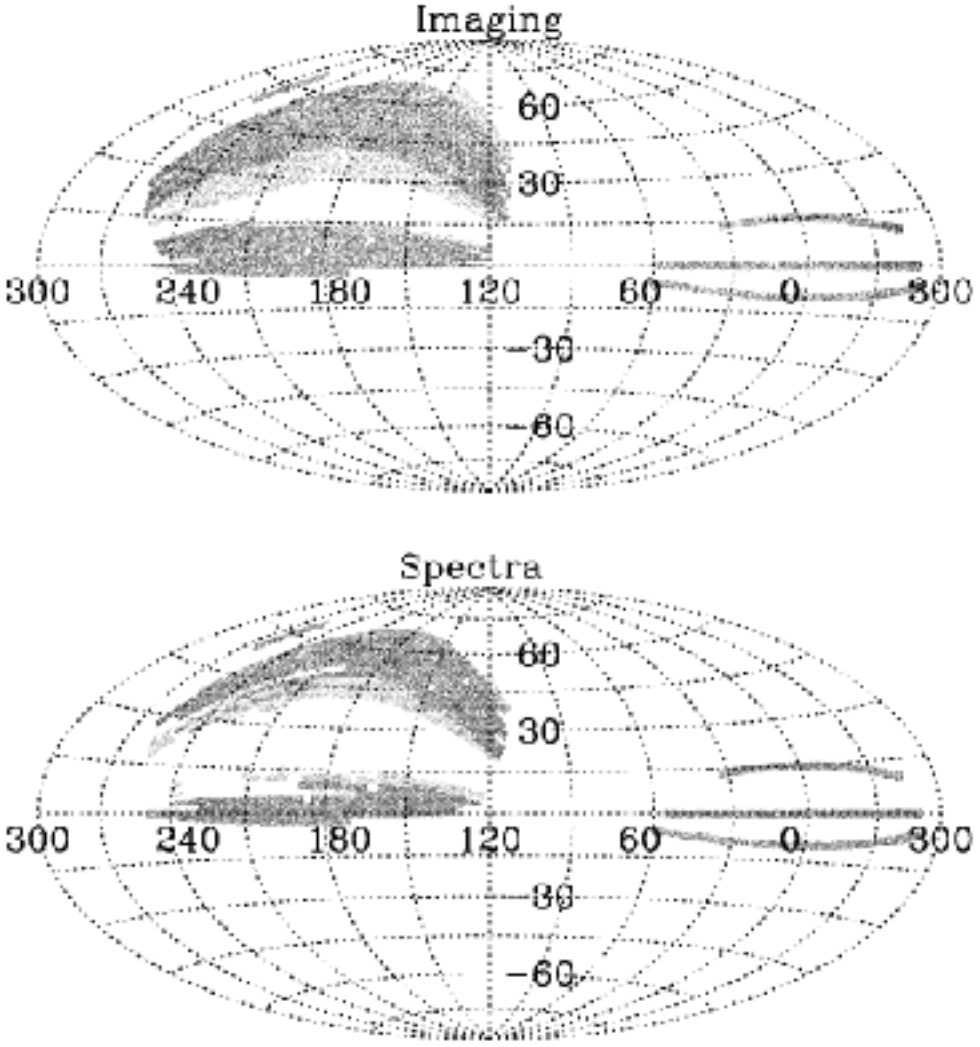

Fig. 2.9: The distribution on the sky of SDSS imaging (upper panel) and spectroscopy (lower panel) included in DR4, shown in J2000 equatorial coordinates. These cover 6670 and 4783 deg^2, respectively. The regions of sky that are new to DR4 are shaded more lightly.

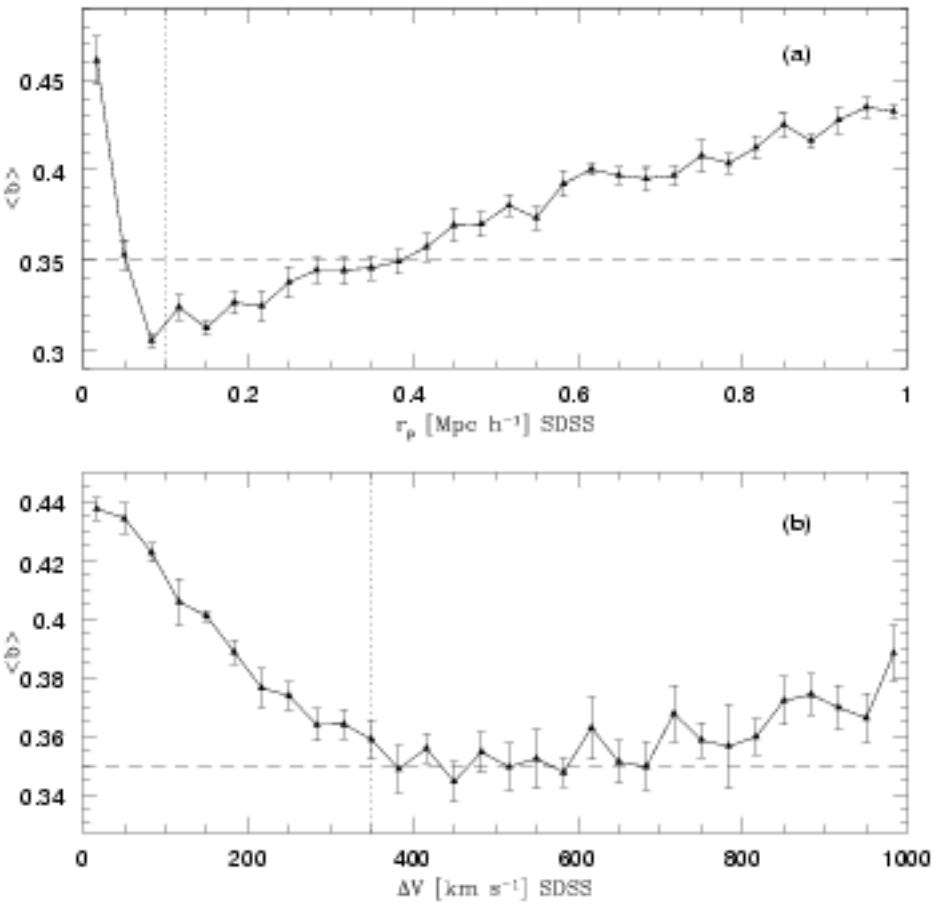

Fig. 2.10: Mean birthrate parameter $\langle b \rangle$ as a function of projected separation r_p (a) and relative velocity ΔV (b) for SDSS neighbours. The dotted vertical lines depict the projected separation and relative velocity thresholds used for the identification of galaxy pairs. The dashed horizontal lines correspond to the mean stellar birthrate parameter value of the total SDSS survey, $\langle b \rangle = 0.35$. Error bars correspond to uncertainties derived from the Bootstrap resampling technique.

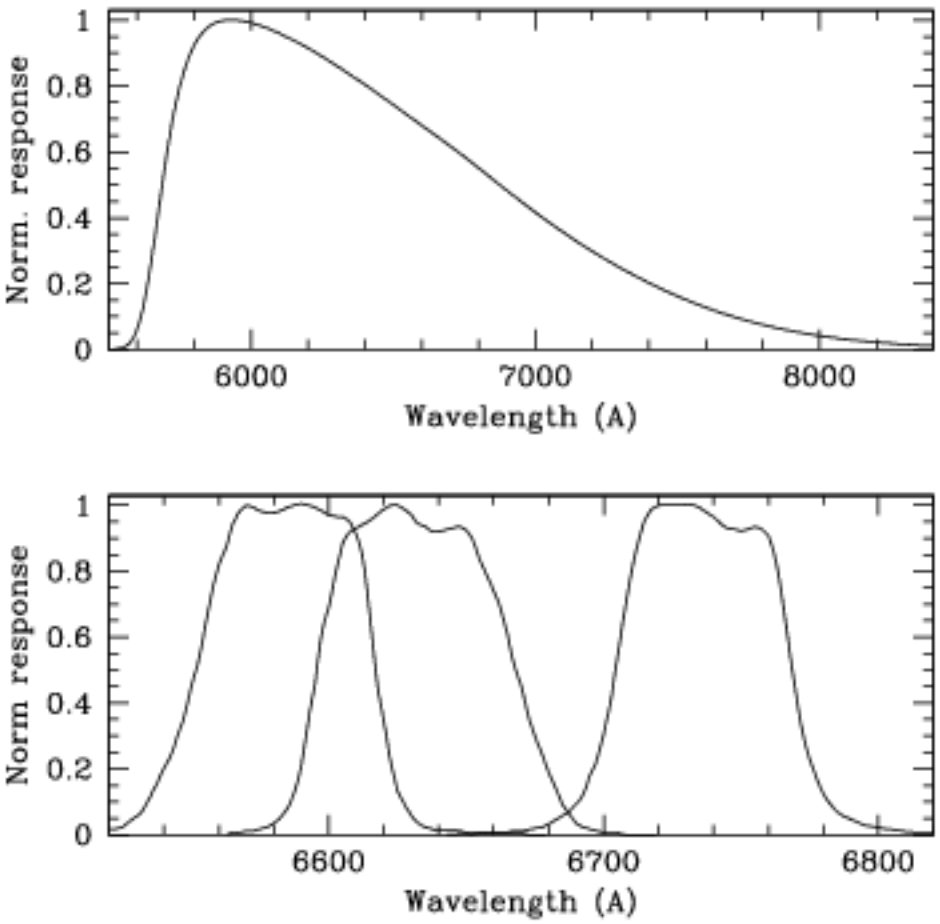

Fig. 2.11: Normalized response of the R broad band filter (*top*), and the three narrow band filters (*bottom*) used during the observations presented in this work.

Tab. 2.2: Log of the observations

Galaxy	Epoch	t_R (s)	$t_{H\alpha}$ (s)	FWHM R	FWHM $H\alpha$	Cal. star	Hα Filter
NGC 488c	Dec 2001	1200	3x1800	2.2	1.8	BD+75 325	663
NGC 772b	Dec 2001	1200	3x1800	1.5	1.6	BD+75 325	663
NGC 772c	Dec 2001	1200	3x1800	1.3	1.7	GD 50	663
NGC 1517a	Dec 2001	900	3x1800	1.6	1.8	BD+75 325	663
NGC 1620a	Dec 2001	180	3x1800	1.6	2.1	BD+75 325	663
NGC 1961a	Dec 2001	900	3x1800	1.6	1.6	G193-74	663
NGC 1961b	Dec 2001	1200	3x1800	1.7	1.4	BD+75 325	663
NGC 1961c	Dec 2001	1200	3x1800	1.1	1.2	BD+75 325	663
NGC 2424b	Dec 2001	1200	3x1800	1.6	1.6	—	663
NGC 2718a	May 2002	900	3x1800	1.5	1.1	Feige 34	663
NGC 2718b	May 2002	900	3x1800	1.5	1.1	Feige 34	663
NGC 2775a	Dec 2001	300	3x1800	1.2	1.5	BD+75 325	658
NGC 2775c	Dec 2001	1200	3x1800	1.3	1.4	BD+75 325	658
NGC 2916a	Dec 2001	1200	3x1800	1.7	1.5	BD+75 325	663
NGC 3043a	Dec 2001	1200	3x1800	1.6	1.2	BD+75 325	663
NGC 3154a	Dec 2001	1200	3x1800	1.1	1.1	BD+75 325	673
NGC 3735a	Dec 2001	1200	3x1800	1.2	1.4	BD+75 325	663
NGC 4030b	May 2002	1200	3x1800	1.4	1.7	Feige 66	658
NGC 4541a	May 2002	1200	3x1800	1.6	1.6	Feige 34	673
NGC 4541b	May 2002	1200	3x1800	1.6	1.6	Feige 34	673
NGC 4541e	May 2002	1200	3x1800	1.6	1.6	Feige 34	673
NGC 4725a	May 2002	1200	3x1800	1.2	1.3	BD+33 2642	658
NGC 5248a	May 2002	1200	3x1800	1.1	1.2	BD+33 2642	658
NGC 5248b	May 2002	600	3x1800	1.8	1.7	Hz 44	658
NGC 5899a	May 2002	1800	3x1800	1.4	1.4	BD+33 2642	663
NGC 5962d	May 2002	1200	3x1800	1.1	1.3	BD+33 2642	663
NGC 5965a_1	May 2002	600	3x1800	1.4	1.2	BD+33 2642	663
NGC 5965a_2	May 2002	600	3x1800	1.4	1.2	BD+33 2642	663
NGC 6181a	May 2002	600	3x1800	1.2	1.2	BD+33 2642	663
NGC 7137a	Dec 2002	500	3x1200	2.2	2.3	—	658
NGC 7678a	Dec 2001	1200	3x1800	1.4	1.6	BD+75 325	663

Note: t_R and $t_{H\alpha}$: exposure times in both filters, R and $H\alpha$; FWHM R and FWHM $H\alpha$: full width half maximun in both filters; Cal. star: spectrophotometric standar stars.

CHAPTER 3

EFFECTS OF INTERACTIONS IN THE FIELD

3.1 Abstract

In this Chaptet, we study field galaxy pairs selected from the 2dF Galaxy Pair Catalog (2dFGPC) described in Chapter 2. Our analysis provides a well defined sample of 2732 pairs, a large database suitable for statistical studies of galaxy interactions in the local universe, $z \leq 0.1$. We have excluded pairs in high density regions by removing galaxies in groups and clusters and we analyze the star formation activity in the pairs as a function of both projected distance (r_p) and relative radial velocity (ΔV). We find power-law relations for the mean star formation birth parameter and equivalent widths of the galaxies in pairs as a function of r_p and ΔV. We find that star formation in galaxy pairs is significantly enhanced over that of isolated galaxies with similar redshifts in the field for $r_p < 25$ kpc h^{-1} and $\Delta V < 100$ km s^{-1}. We found that when compared to isolated galaxies of similar luminosity and redshift distribution, the effects of having a companion are more significant on the star formation activity of bright galaxies in pairs, unless the pairs are formed by similar luminosity galaxies. In this case, the star formation is enhanced in both components. We found that about fifty percent of galaxy pairs do not show signs of important star formation activity (independently of their luminosities) supporting the hypothesis that the internal properties of the galaxies play a crucial role in the triggering of star formation by interactions.

3.2 Introduction

In this Chapter, we focus on an analysis of interacting galaxies in relative isolation. For this purpose, we consider galaxy pairs in the field taken from the total 2dF Galaxy Pair Cata-

log (see details in Chapter 2) and analyze their properties in comparison to galaxies without companions. For this purpose we will exclude those galaxies that belong to groups as defined by Merchán & Zandivarez (2002, hereafter MZ02). Pairs in high density environments will be analyzed in Chapter 4. Here, we aim at answering questions such as: which type of galaxies are preferentially found in pairs, how does star formation vary among them according to their luminosities, etc.

A control sample sharing the same selection effects will be constructed, focusing the analysis on the statistical differences between galaxies in pairs and isolated ones in the 2dFGRS. We stress that this is a useful procedure to unveil the effects of galaxy interactions on the star formation process.

In Section 3.3 we define the field galaxy pair catalog and the comparison sample. Section 3.4 is focused on the analysis of the star formation properties of galaxies in pairs and Section 3.5 summarizes the main conclusions.

3.3 Field Galaxy Pair Catalog (FGPC)

From the previous analysis (Fig 2.7 and Fig 2.8, Chapter 2) we found that a projected distance of 100 kpc h^{-1} and a relative radial velocity of 350 km s^{-1} are reliable limits to select pairs with high probability of being an interacting system with enhanced specific star formation activity. Galaxies at larger distances and with greater velocity differences do not show statistically significant signs of enhanced SF with respect to the background. And since we are interested in studying those pairs that belong to the field (pairs in groups will be discussed in the next Chapter), we matched the total galaxy pair catalog and galaxies belonging to 2dF groups (MZ02). The resulting Field Galaxy Pair Catalog (FGPC) excludes those galaxies members of groups/clusters, comprising 2732 pairs with $z \leq 0.1$ in relative isolation.

In order to properly assess the significance of the results obtained from the FGP catalog we have defined a field control sample (FCS) from the 2dF catalog using a Monte Carlo algorithm that selects, for each galaxy pair in the FGP catalog, two galaxies in the field (i.e. not included in the FGP catalog and not members of the MZ group catalog) within the same redshift range of the galaxy pair. Thus, the procedure followed to construct this control catalog assures that it will have the same selection effects than the FGP catalog, and consequently, it can be used to estimate the actual difference between galaxies in pairs and isolated galaxies, in the field, unveiling the effects of the interactions.

For analyzing the spectral type composition of the FGPs in comparison with that of general galaxies in the field we defined five combined categories (C_i) according to the combina-

tion of spectral type η (see Chapter 2) of the galaxies in the pairs. The first four correspond to galaxy pairs that have equal spectral type: $C1 = (1,1)$, $C2 = (2,2)$, $C3 = (3,3)$ and $C4 = (4,4)$. The last spectral category corresponds to pairs composed of galaxies with different spectral types (Table 3.1).

Tab. 3.1: Spectral composition of galaxy pairs: Percentages of spectral type categories.

Catalog	$C1$	$C2$	$C3$	$C4$	$C5$
FGP	22	7	6	5	59
FCS	7	10	6	3	74
FGP/FCS	3.14	0.7	1	1.7	0.80

Note: FGP: Field Galaxy Pairs; FCS: Field Control Sample.

In Fig. 3.1a we have plotted the fraction of FGPs in the first four spectral categories normalized to those obtained from the control sample. We see that there is an excess of C1 and C4 spectral category pairs with respect to the control sample, suggesting a trend for FGPs to be composed of two galaxies with similar spectral characteristics, both non star forming or both with significant star formation (see Table 3.1).

Also, we have estimated the mean luminosities $\langle (L_1 + L_2)/2 \rangle$, ($L_1$ and L_2 refer to the luminosities of the two members of a pair) of each category pair and that corresponding to the control sample. In Fig. 3.1b we show the corresponding ratios of these two samples. We can see in this figure that on average, galaxies in C3 and C4 pair categories are significantly more luminous than their isolated counterparts.

3.4 Star Formation in Galaxy Pairs

The FGP catalog allows a detailed study of the possible effects of the interactions. For these galaxies, we have estimated the mean values of the birthrate parameter $\langle b \rangle$ as a function of r_p and ΔV.

Fig. 3.2 shows $\langle b \rangle$ in bins of r_p where it can be seen that the star formation efficiency is larger for closer galaxy pairs. A similar behaviour is found for the relative radial velocity (Fig. 3.3). Power laws provide good fits to both sets of data. The following relations for the mean b parameter and the equivalent width have been obtained from these fittings:

$$\langle EW \rangle = (4.10 \pm 0.50) r_p^{-0.40 \pm 0.02} \tag{3.1}$$

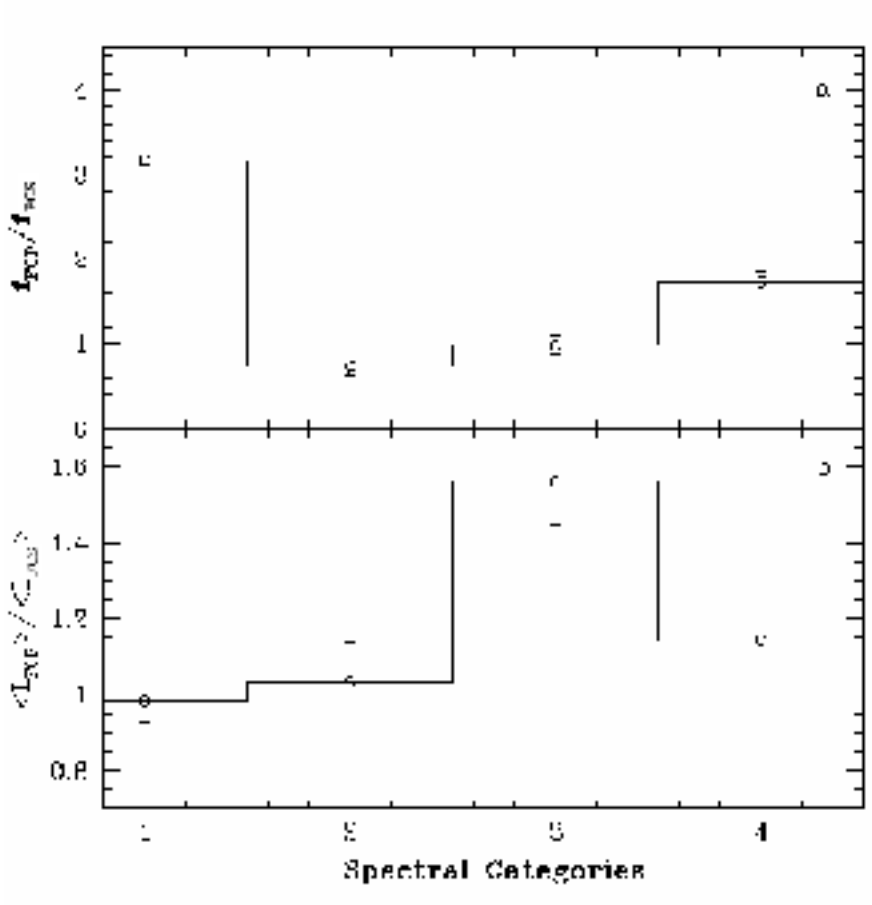

Fig. 3.1: a) Frequency of spectral type combinations of field galaxy pairs (FGPs) and b) Ratio between the mean luminosities of galaxies in pairs and the corresponding to the control sample as a function of their spectral categories. In both cases, the relations have been normalized by using the corresponding parameters determined from the control catalog. Error bars correspond to standard Poisson deviations.

$$\langle EW \rangle = (1.30 \pm 0.50)\Delta V^{-0.30\pm0.16} \tag{3.2}$$

$$\langle b \rangle = (0.63 \pm 0.01) r_p^{-0.23\pm0.02} \tag{3.3}$$

$$\langle b \rangle = (0.40 \pm 0.31)\Delta V^{-0.14\pm0.09} \tag{3.4}$$

where r_p and ΔV are given in Mpc h^{-1} and km s^{-1}, and EW in Angstrom. Uncertainties are estimated by applying the bootstrap technique (100 random samples). Note that the

dependence on the projected distance is more significant than that on the relative velocity separation.

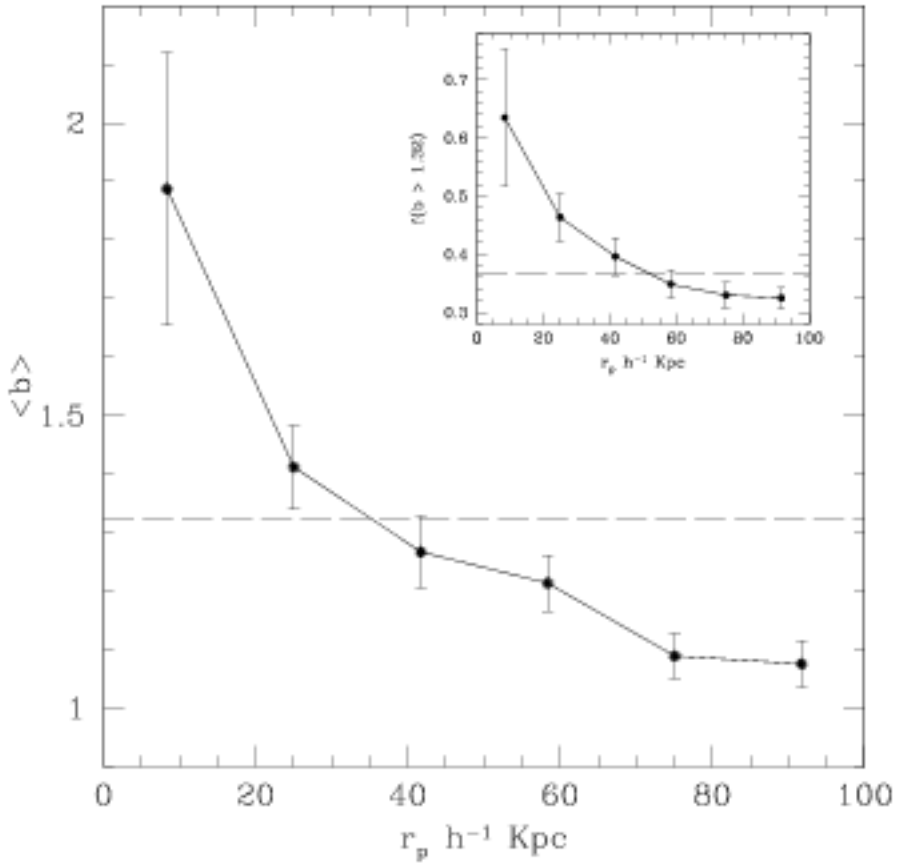

Fig. 3.2: Mean b parameters estimated in projected distance bins for galaxies in interacting pairs. The dashed horizontal lines represent the mean b parameter for the control sample. The small box corresponds to the fraction f^* of galaxies with $b > \bar{b}$.

In order to assess the importance of interactions on SF activity compared to isolated galaxies, we have computed the mean b parameter for the galaxy pair control sample (FCS), $\bar{b} = 1.32$. This value has been depicted in Fig. 3.2 and in Fig. 3.3 (dashed lines) where it can be appreciated that only galaxies in very close pairs in projection show significantly higher mean star formation activity than that of isolated galaxies in the field.

Complications related to the physical interpretation of redshift space identified pairs where r_p and ΔV provide only lower limits for the true galaxy separations should be always considered. Also, interlopers and interactions which have not undergone a close approximation difficult a straightforward interpretation of the mean values of the starbirth rate

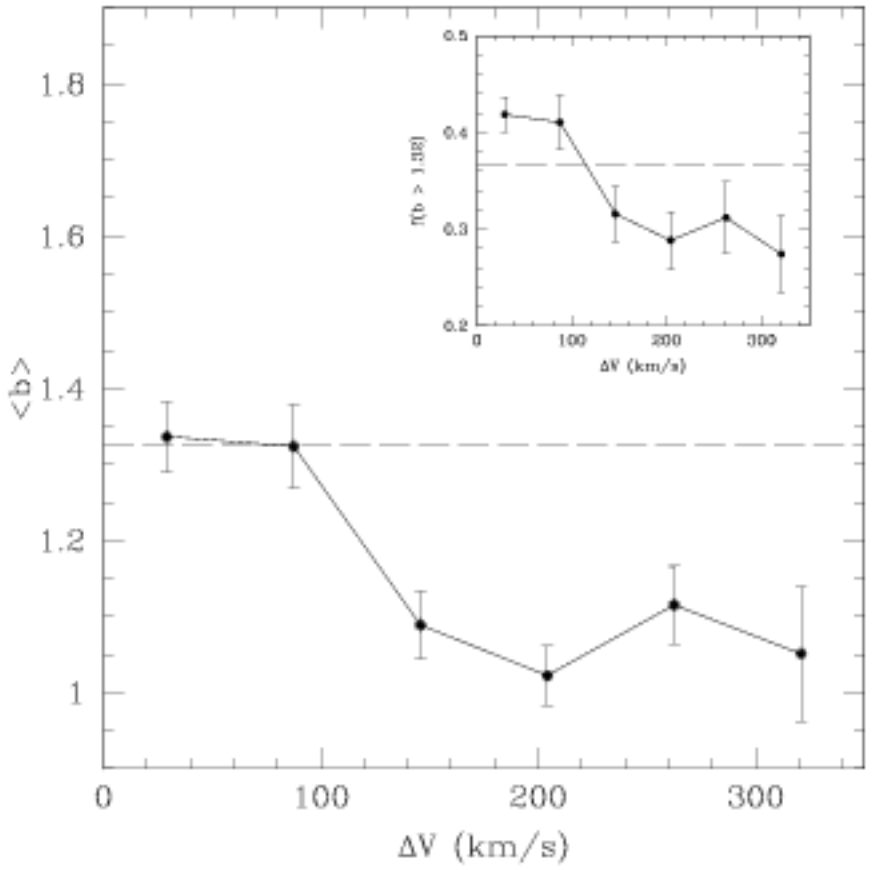

Fig. 3.3: Mean b parametets estimated in relative radial velocity bins for galaxies in interacting pairs. The dashed horizontal lines represent the mean b parameter for the control sample. The small box corresponds to the fraction f^* of galaxies with $b > \bar{b}$.

parametet. Taking into account these caveats, we have calculated the fraction f^* of star forming galaxies with $b > \bar{b}$, and we show them in the small windows of Fig. 3.2 and in Fig. 3.3. The dashed lines represent the corresponding fractions for the control sample. As it can be appreciated, the proximity in velocity and projected distance correlates with an increase in the fractions of galaxies undergoing strong star formation activity until they exceed the mean fraction of the control sample.

The weaker dependence of the mean birthrate parameter $\langle b \rangle$ on relative velocity may have several sources. Firstly, an overall rms uncertainty in radial velocity determination of $\simeq 85$ km s^{-1} is derived by repeated observations in the 2dF survey and by comparison with other redshift catalogs. This large scatter implies a large observational error in the relative velocity of a pair of galaxies in the catalog $\simeq 120$ km s^{-1}. Therefore, this observational

uncertainty should be considered as the main cause of the weaker dependence on relative velocity compared to r_p since the precision in coordinates has negligible uncertainties. There are, however, other issues to be considered, since there can be several pairs with large spatial separations but with small radial velocity differences. Hence, for a given relative velocity bin, contributions of pairs with different orbital position are canceled out. In the case of projected separation bins, there is also a contamination by small r_p and large ΔV although the enhancement of star formation with spatial separation is strong enough to override this contamination.

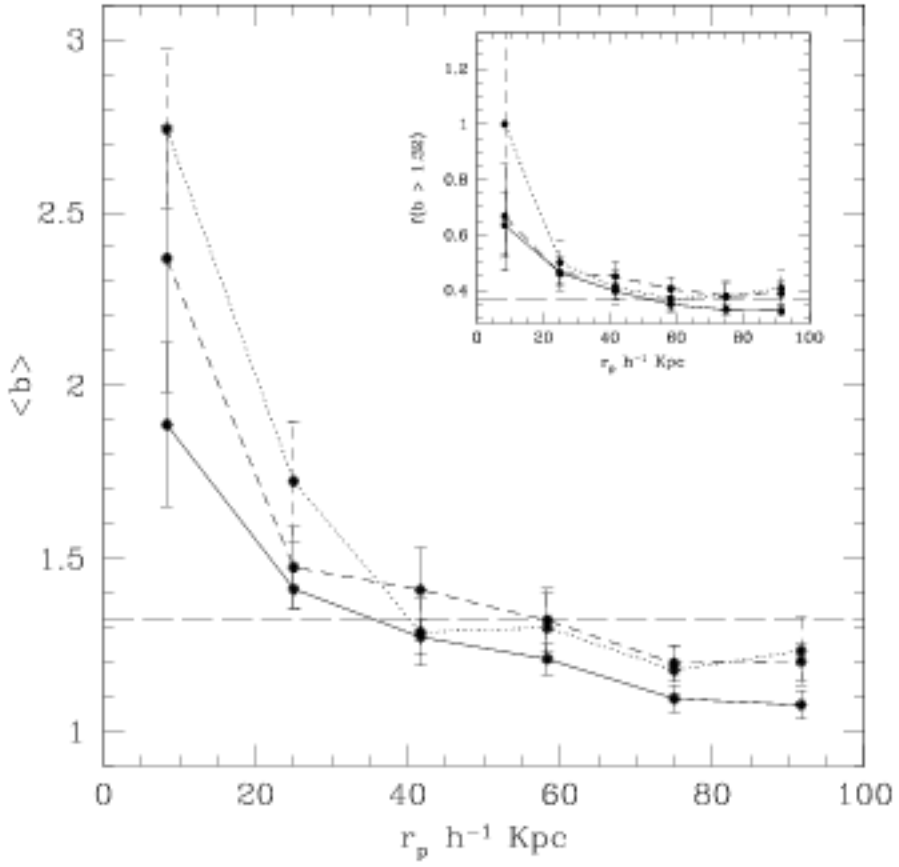

Fig. 3.4: Mean b parameters estimated in projected distance bins for galaxies in the FGP catalog for three different maximum relative radial velocity limits: $\Delta V < 350$ km s^{-1} (solid line), $\Delta V < 100$ km s^{-1} (long-dashed line) and $\Delta V < 50$ km s^{-1} (dotted line). The dashed horizontal line represents the mean b parameter for the control sample. The small box corresponds to the fraction f^* of galaxies with $b > \bar{b}$.

In order to visualize how $\langle b \rangle$ depends on the combination of r_p and ΔV we have esti-

mated b as a function of r_p by considering pairs by different velocity separations (Fig. 3.4). As it can be clearly seen the signal increases as pairs with larger ΔV are excluded from the calculations. A similar behavior is observed for the fractions (f^*). Those are systems with large relative distance observed with a small projected separation. From this figure we may infer that as the galaxies orbit into each other or experience a close encounter, the star formation activity of the system increases. In spite of the uncertainty in ΔV due to measurement errors, we note that the larger star formation activity for pairs with quoted values as small as $\Delta V < 50$ km s^{-1}.

The most significant difference between the star formation activity of galaxies in pairs and those of the control sample is obtained when the analysis is restricted to pairs with $r_p \leq 25$ kpc h^{-1}. This sub-sample shows the strongest signal of enhanced SF as illustrated in Fig. 3.5 where we have plotted the b parameters as a function of the relative radial velocity. The dashed lines depict the mean $\langle b \rangle$ and f^* for the corresponding control sample. Confronting this figure with Fig. 3.3 we can conclude that pairs with small r_p have a statistically significant increase of their star formation rate when restricted to small relative velocities. In consequence, we define a subsample of close pairs by imposing the restrictions: $r_p < 25$ kpc h^{-1} and $\Delta V < 100$ km s^{-1}, hereafter Field Close Galaxy Pair (FCGP) sample (Table 3.2). This set of galaxies exhibits the highest star formation efficiency.

Tab. 3.2: Field Catalogs

Catalogs	Number of galaxies	r_p (kpc h^{-1})	ΔV (km s^{-1})
FGPC	2732 galaxy pairs	< 100	< 350
FCGPC	328 galaxy pairs	< 25	< 100
FCS	5464 isolated galaxies	> 100	> 350

Note: FGPC: Field Galaxy Pair Catalog; FCGPC: Field Close Galaxy Pair Catalog; FCS: Field Control Sample.

3.4.1 Dependence on Luminosity

An analysis of the dependence of the SF activity on the luminosity of the galaxies in pairs could help to understand how SF activity is regulated between pair members. Several observational works have found evidence that in an interacting pair, the fainter galaxy seems to be more affected (e.g. Donzelli & Pastoriza 1997). Also, Colina et al. (2001) found that Ultra Luminous Infrared Galaxies could be related to mergers of different luminosities in the

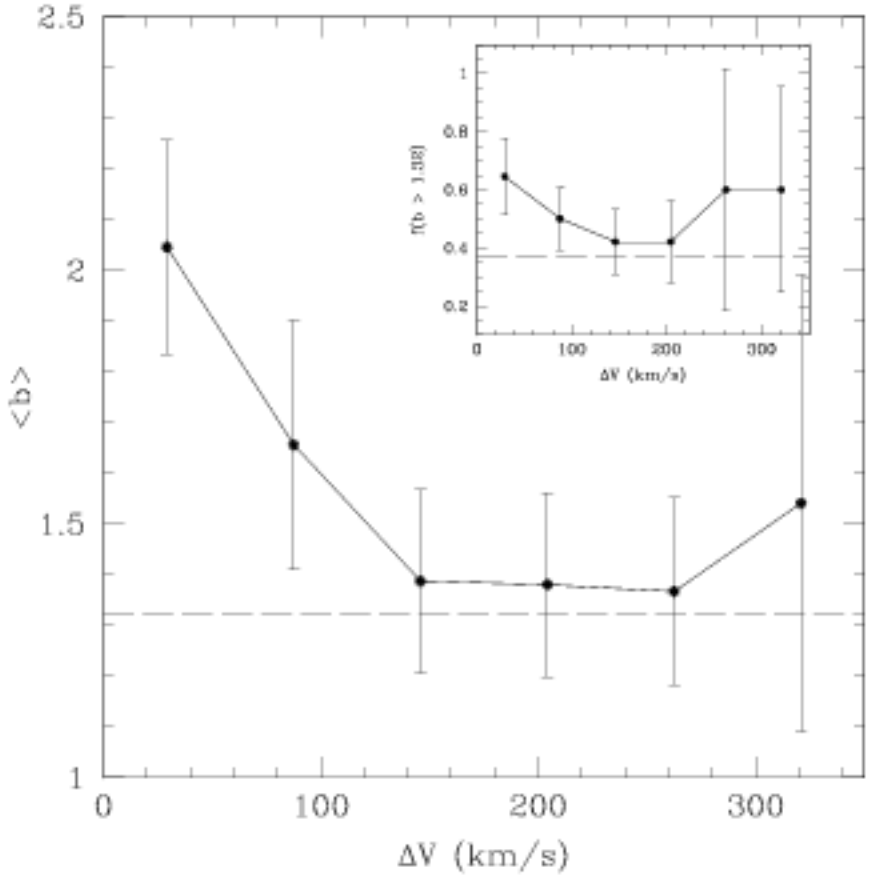

Fig. 3.5: Mean b parameters in bins of relative radial velocity for galaxies in close pairs ($r_p < 25$ kpc h^{-1}). The dashed horizontal line represents the mean b parameter for galaxies in the control sample. The small box shows the fraction f^* of strong star forming galaxies in the samples.

range $0.3 - 2L^*$. Arguments related to the stability properties of the galaxies have been used to explain these observations. Numerical simulations show that disc galaxies with a small (or with a lack of) bulge component (Mihos & Hernquist 1996; Tissera et al. 2002) tend to be more susceptible to the effects of tidal interactions which can trigger gas inflows and star formation. According to Tissera et al. (2002) these systems would be in early stages of evolution where their bulges are being built up, and consequently, on average, they would be smaller (or fainter).

We can use this large galaxy pair catalog for investigating this point on a firmer statistical basis. For this purpose we estimate the mean birthrate parameter in luminosity bins for galaxies in the FGP catalog and those in the control sample. We then define the star formation

excess β as the ratio between these two b parameters. Hence, β yields the excess of star formation in pair galaxies with respect to any isolated galaxy in the field with the same selection effects and redshift distribution.

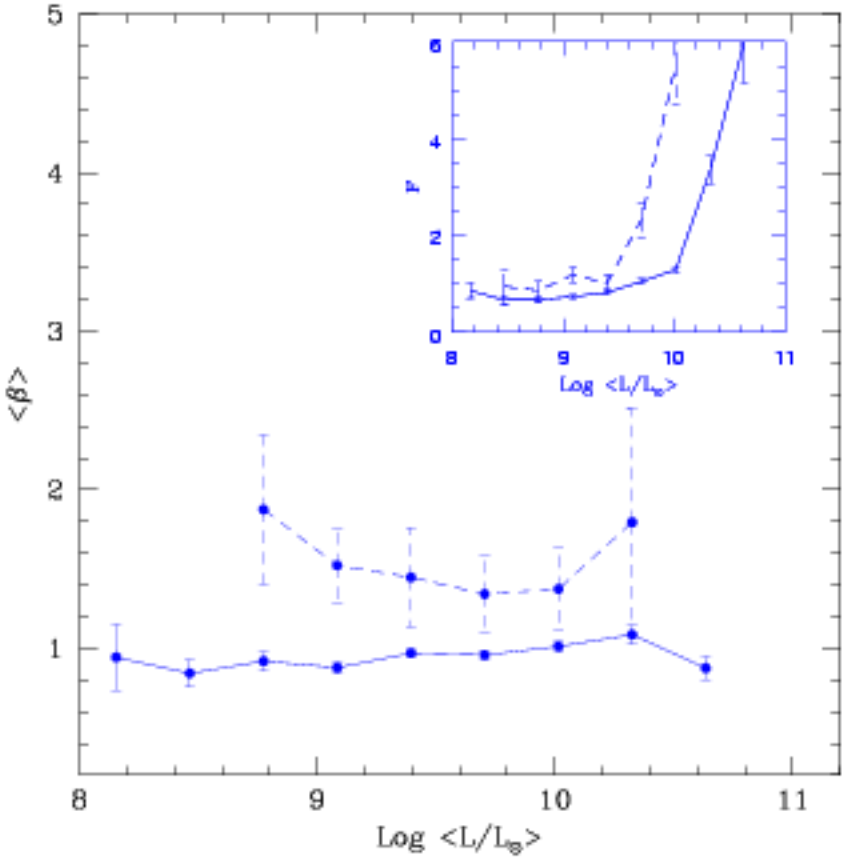

Fig. 3.6: Mean star formation excess parametets β for the FGPs (solid lines) and FCGPs with projected distance r_p <25 kpc h^{-1} and ΔV < 100 km s^{-1} (dashed lines). The small box shows the fraction F^* of strong star formation.

In Fig. 3.6 we show $\langle\beta\rangle$ vs log $\langle L/L_\odot\rangle$ for the FGP and the FCGP samples (r < 100 kpc h^{-1}, ΔV < 350 km s^{-1} and r < 25 kpc h^{-1}, ΔV < 100 km s^{-1}, respectively). As it can be seen the total FGP sample shows the same level of SF activity than isolated galaxies in the field ($\beta \approx 1$), while the FCGP sample has a star formation enhancement with respect to isolated galaxies ($\beta \geq 1.5$). In the small box, we show the relative fraction of galaxies (F^*) that are experiencing larger SF activity than the corresponding mean in the control sample, in each luminosity interval, for both the complete and the close galaxy pair samples, normalized to the corresponding fractions of the control sample. It can be appreciated from this box a

significant increase in the fraction of star forming galaxies in pairs with respect to isolated ones as a function of luminosity. This trend is washed out when mean b values are estimated since there is a large percentage of non star-forming galaxies in pairs. Owing to the fact that the larger difference between the star formation of galaxies in pairs and that of isolated ones is detected for bright galaxies, we have to consider the possible presence of AGN as well as starbursts associated to interactions. This will be consider in Chapter 5 for the SDSS catalog.

3.4.2 Pairs Formed by Similar and Different Luminosity Galaxies

In this section we analyse FGPs according to the relative luminosity of their member galaxies. For FGPs and galaxies in the control sample, we estimate the ratio of luminosities L_2/L_1 of the faint over the bright member. As shown in Fig. 3.7, we found that FGPs are composed of galaxies with relative luminosities similar to those of any isolated pair of galaxies in the field (with the same redshift distribution), except for a weak tendency for some excess of pairs of galaxies composed with different luminosities. The bootstrap error analysis indicates that this excess has a statistical significance. This is likely due to the effects of the interaction, and we may argue for truncated star formation due to the tidal perturbation of the more massive companion.

We define two sub-samples according to the relative luminosity of galaxies (L_2, L_1) in pairs. We adopt $L_2/L_1 = 0.5$ as a threshold to split the FGP catalog into two subsamples of dissimilar ($L_2/L_1 < 0.5$) and similar ($L_2/L_1 \geq 0.5$) galaxy luminosities in pairs (this choice divides the sample into subsamples with roughly the same number of members). Assuming that all interacting pairs might eventually give origin to a merger event, this luminosity ratio can be also interpreted as a threshold to split the data into major and minor interactions subsamples. We then calculated the $\langle\beta\rangle$ parameter as a function of luminosity for these two sub-samples restricted to the subsample of field close galaxy pairs (FCGP: $r_p < 25$ kpc h^{-1} and $\Delta V < 100$ km s^{-1}). While for the minor interactions sub-sample we found no excess, a mean value $\beta \approx 2$ is detected for the major merger candidates. However, in both cases, we found no dependence on luminosity.

In order to further clarify on the importance of galaxy luminosity and the strength of the interaction we have also investigated the dependence of the SF excess on projected distance for the fainter and brighter galaxy members in minor interactions ($L_2/L_1 < 0.5$). For this purpose we have estimated the $\langle\beta\rangle$ parameter as a function of r_p for the faint and bright components of galaxy pairs as shown in Fig. 3.8. It can be appreciated from this figure the similar behavior of the mean SF enhancement with respect to the control sample of the two

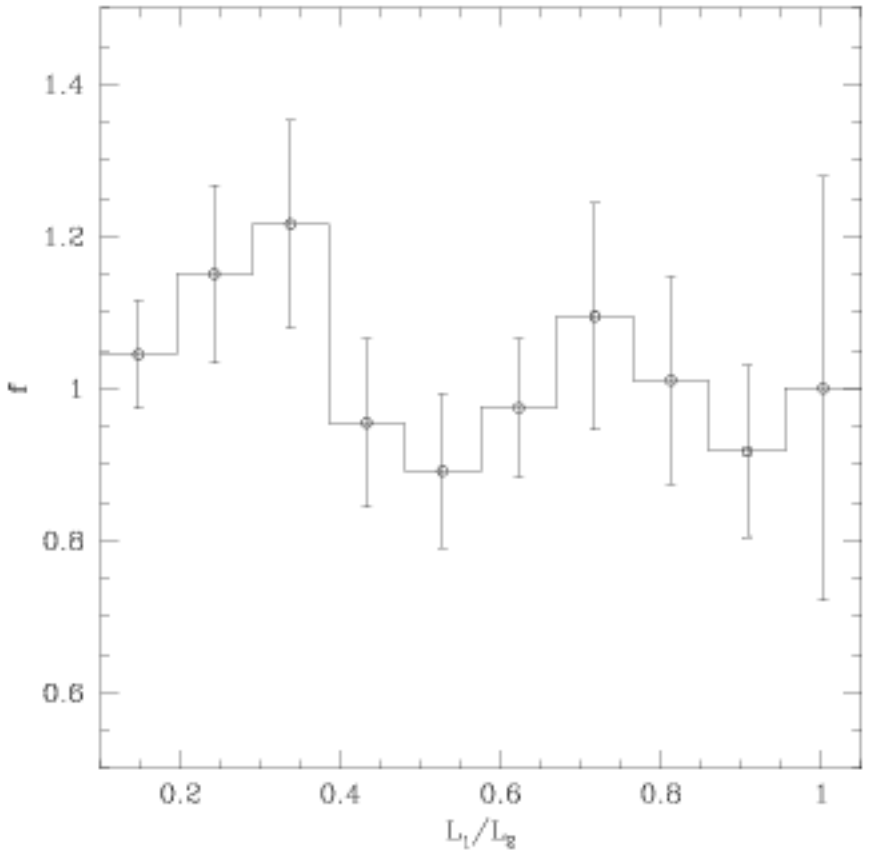

Fig. 3.7: Histogram of the luminosity ratio between the bright and the faint galaxy member of pairs normalized to that estimated for the control sample.

components. However, when fractions are estimated for the bright (dashed) and faint (solid) components we found that the former shows a clear excess. At a given luminosity, brighter components of dissimilar luminosity pairs have a larger probability to have enhanced SF when compared to isolated galaxies and from larger projected distances.

A similar analysis was performed for the major interactions sub-sample. In this case in order to classify them in bright and faint luminosity pairs we estimated the mean luminosity of the pair and adopted a threshold of $\log\,(L_1 + L_2)/2 = 9.5$ (solar units). For these two sets, we estimated $\langle\beta\rangle$ as a function of projected distance. The results are plotted in Fig. 3.9 from where it can be appreciated that the two samples exhibit a similar trend in mean SF enhancement as a function of r_p, which is found to be higher than that of minor interactions. The small box shows the fraction of galaxies with $b > \bar{b}$ normalized to the values of the control sample. In this case, we found that both components of major interactions have a

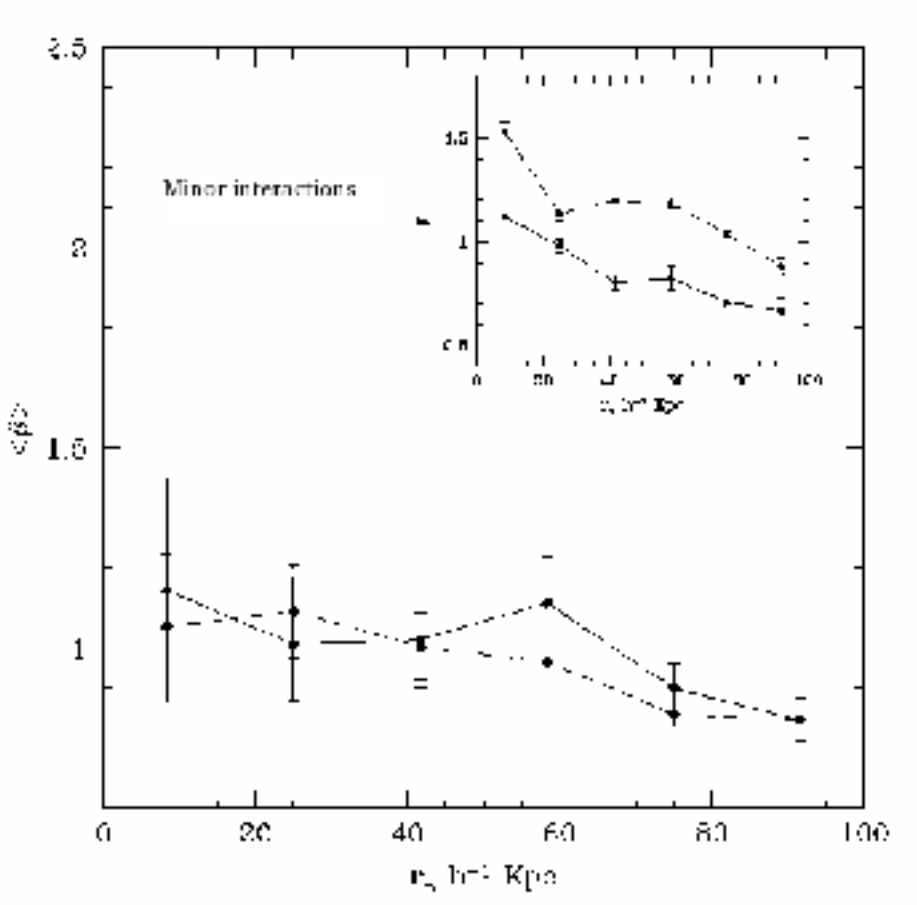

Fig. 3.8: Mean SF excess parametet $\langle\beta\rangle$ versus projected distance for the bright (dashed lines) and the faint (solid lines) membets of galaxy pairs classified as minor interactions (i.e., pairs formed by different luminosity galaxies, $L_1 >> L_2$). The small box shows the fraction F^* for the brighter (dashed lines) and the fainter (solid lines) member.

similar probability to have enhanced SF activity. However, we note that the fractions are larger than those of the corresponding control sample only for close encounters ($r_p \leq 25$ kpc h^{-1}).

This analysis suggests that the effects of interactions on the SF activity is relatively more important in the brighter components of pairs with different luminosities. For galaxies with a similar luminosity companion, both objects show a larger star formation activity than isolated galaxies.

It should be stressed that these results do not contradict observations where the faint member of interacting pairs has on average a larger star formation activity, since these studies lack a proper confrontation to galaxies without companions (see Bergvall et al. 2003 for the

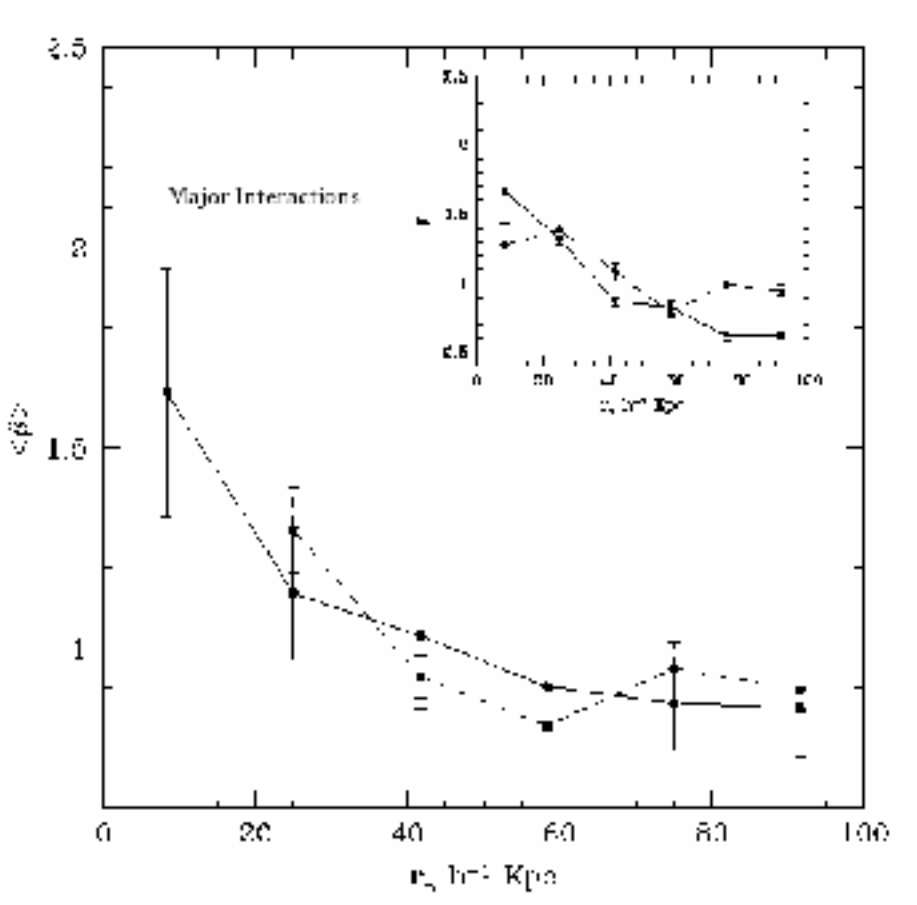

Fig. 3.9: Mean SF excess parametet $\langle \beta \rangle$ versus projected distance for the bright (dashed lines) and the faint (solid lines) galaxy pairs classified as major interactions (i.e., pairs formed by similar luminosity galaxies, $L_1 \sim L_2$). The small box shows the fraction F^* for the bright (dashed lines) and the faint (solid lines) member.

first observational works that used this approach).

3.5 Summary

We have carried out a statistical analysis of 2732 galaxy pairs in the field restricted to $z \leq 0.1$ selected from the 2dFGRS. Our study is centred on the star formation enhancement of the pair members with respect to isolated galaxies in the field with the same redshift distribution and luminosities.

We can summarize our results in the following main conclusions.

1. We detect a significant correlation between the starbirth rate parameter $\langle b \rangle$ and both, projected spatial separation r_p and relative radial velocity ΔV for galaxy pairs. For $r_p <$

25 kpc h^{-1} and $\Delta V < 100$ km s^{-1} we obtain a substantial star formation enhancement with respect to the isolated control sample. The ΔV dependence is less pronounced although we find a systematic increase of star formation activity for decreasing relative velocity.

2. There is not an overall dependence of the mean star formation enhancement $\langle \beta \rangle$ on luminosity for galaxy pairs at $z \leq 0.10$. A nearly constant value $\langle \beta \rangle \simeq 1.2$ for the total FGP catalog and $\langle \beta \rangle \simeq 2$ for the field close galaxy pair subsample have been measured. However, the fractions of galaxies in pairs that have a higher SF activity than the corresponding average one of isolated galaxies, show a clear excess for the bright members.

3. We divide the field close pair sample in minor ($L_2/L_1 < 0.5$) and major ($L_2/L_1 > 0.5$) interactions according to their relative luminosities. We found that bright components in minor interactions show higher probability to have enhanced SF by tidal interactions than isolated galaxies and from larger projected distances than the faint components. In the case of major interactions both components show comparable star formation enhancements and with a similar projected distance dependence.

CHAPTER 4

EFFECTS OF INTERACTIONS ON STAR FORMATION IN GROUPS AND CLUSTERS

4.1 Abstract

We assess the effects of galaxy-galaxy interactions on star formation by analysing pairs in groups and clusters of galaxies with virial masses in the range $10^{13} - 10^{15} M_{\odot}$ extracted from the 2dFGRS (Merchán & Zandivarez 2002). We find that only galaxy pairs with relative separation as small as $r_p < 15$ kpc h^{-1} show significant star formation activity in comparison to other group member galaxies. In Chapter 3, similar results were found for galaxy pairs in the field but for a larger threshold ($r_p < 25$ kpc h^{-1}) so that the nature of star formation driven by galaxy interactions is nearly independent of environment in spite of the general lower level of star formation activity in systems of galaxies. The above results reflect, on one hand, the local nature of star formation induced by tidal interactions and, on the other, the role played by the internal properties of galaxies. By using a 2dFGRS mock catalog we estimate the contamination by spurious pairs, finding that our statistics are dominated by real pairs, in particular for close relative separations, for which our study indicates significant star formation activity. We obtain a similar radial and relative velocity distribution of the pairs with respect to the group centre compared to those of other typical group members, so that galaxy pairs have no particular location and dynamics within groups.

4.2 Introduction

It is well known that galaxies in groups and clusters have significantly reduced star formation with respect to that in the field (e.g. Dressler 1980, Martínez et al. 2002). Domínguez et al. (2002) also obtained that the distribution of star-formation rates is correlated with both the

distance from the cluster centre and the local projected density. However, it is still uncertain how relevant is the global environment in the regulation of star formation in galaxies.

Taking into account these results, in this Chapter we focus on the analysis of galaxy-galaxy interactions within groups and clusters with the aim at assessing if this physical mechanism plays a significant role in star formation triggering in dense virialized systems. For this purpose we constructed the hitherto largest sample of interacting pairs in groups and clusters from the 2dFGRS. By means of spectroscopy analysis, we explore the dependence of the star formation in galaxy pairs on relative projected separation, radial velocity and groupcentric distance.

4.3 Data and Analysis

4.3.1 Pairs in Groups in the 2dFGRS

We constructed a catalog of pairs in groups using the cross-correlate of the total galaxy pairs catalog (2dFGPC) defined by a projected distance $r_p < 100$ kpc h^{-1} and a relative radial velocity $\Delta V < 350$ km s^{-1} with the 2dFGRS group catalog obtained by Merchán & Zandivarez (2002), performed in Chapter 3. These authors identified groups by using a slightly modified version of the group finding algorithm developed by Huchra & Geller, with a minimum number of 4 members, an outer number density enhancement of 80 and a linking radial cutoff of 200 km s^{-1}. The sample comprises 6076 groups spanning over the redshift range of $0.003 \leq z \leq 0.25$ with a mean redshift $z \simeq 0.1$. As a result of this cross-correlation we obtain a sample with 4658 pairs of galaxies in groups. For the analysis we use those pairs with $z < 0.1$ (a total of 3335 galaxy pairs in groups (i.e. 6670 galaxies forming pairs), hereafter Group Galaxy Pair Catalog: GGPC).

Following the procedure outlined in Chapter 3, we focus our attention on the effects of interactions on star formation by comparing with a suitable control sample which differs from the GGP catalog only on the fact that galaxies in groups in the latter have a close companion. Using a Monte Carlo algorithm we select, for each galaxy pair, two other members of the 2dFGRS group catalog. Therefore, in this study, the group control sample (GCS) corresponds to 6670 galaxies in groups and clusters which do not have a companion within $r_p < 100$ kpc h^{-1} and $\Delta V < 350$ km s^{-1}. We stress the fact that this comparison sample of galaxies in groups shares the same environment and has the same redshift distributions than the GGP sample of galaxy pairs in groups. A Kolmogorov-Smirnov test yields that the null hypothesis is true at a 95% confidence level for the redshift and absolute magnitude

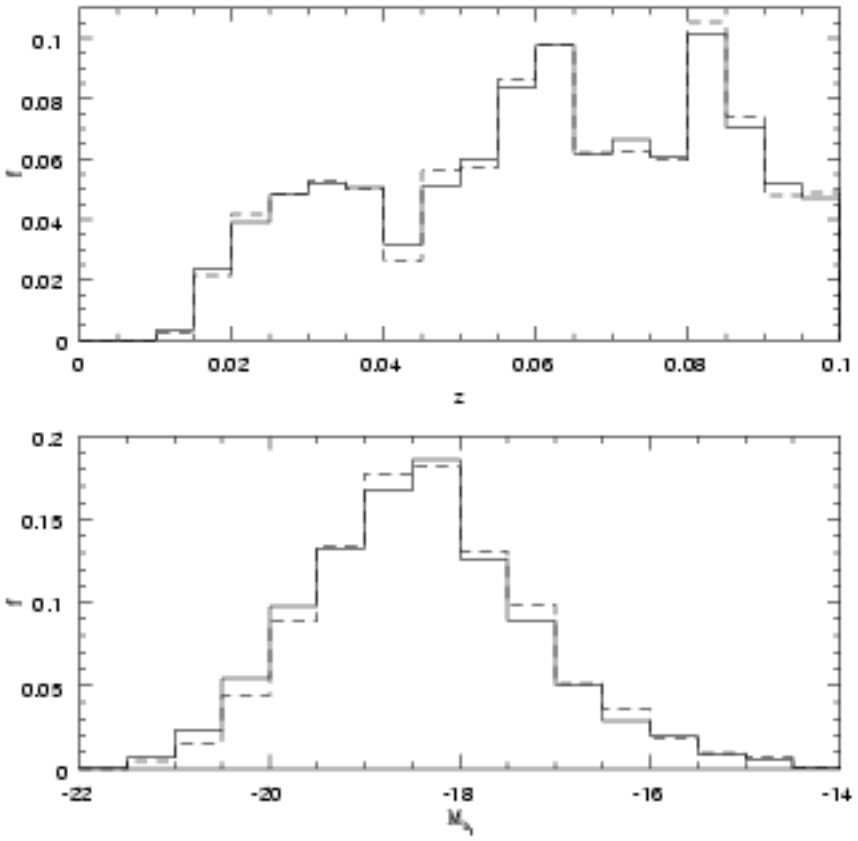

Fig. 4.1: Distributions of redshift and absolute magnitude M_{b_J} of galaxy pairs (solid line) and the control sample (dashed line).

distributions. Hence, the pair and the control samples can be reliably considered similar and appropriate for our analysis (see Fig. 4.1).

Testing the effects of spurious galaxy pairs

The selection of galaxy pairs by using relative velocity differences (ΔV) and projected separation (r_p) has the drawback that spurious pairs can be included. The use of cut-offs for both variables helps to diminish the problem, although they do not solve it completely. In particular, the effects of spurious pairs are expected to be stronger in high density regions (Mamon 1986; 1987), as is the case in this Chapter.

In order to assess the effects of spurious pairs in our observational analysis, we have used the 2dFGRS mock catalog constructed by Merchán and Zandivarez (2002) from a gravitational numerical simulation of the concordance Λ cold dark matter universe ($\Omega_m = 0.3, \Omega_\gamma =$

0.7, $H = 70$ km s$^{-1}Mpc^{-3}$ and $\sigma_8 = 0.9$). The authors performed this simulation by using the HYDRA N-body code developed by Couchman, Thomas & Pearce (1995) with 128^3 particles in a cubic comoving volume of 180 Mpc h^{-1} per side, starting at $z = 50$. From this mock catalog, a mock galaxy pair catalog was constructed by applying the same observational cut-offs defined previously ($r_p < 100$ kpc h^{-1} and $\Delta V < 350$ km s^{-1}). The orbital parameters such as major semi-axis, eccentricities, binding energy, etc., were estimated for both mock pair catalogs by assuming a two-body problem scenario. We adopted $e < 1$ and negative binding energy to distinguish between real and spurious pairs.

We found that for the mock pair catalog $\approx 70\%$ were real pairs. We also imposed the condition of an extra neighbour within $r_p < 400$ kpc h^{-1} and $\Delta V < 500$ km s^{-1} in order to segregate pairs according to environment. For galaxy pairs in these denser regions, we found a similar fraction so we conclude that although spurious pairs are present in our sample, real binary systems clearly dominate the statistics. Nevertheless, we have included estimations of the effects of spurious pairs along this Chapter that can help to further assess their impact on the results.

4.3.2 Position and Velocity Distribution of Galaxy Pairs in Groups

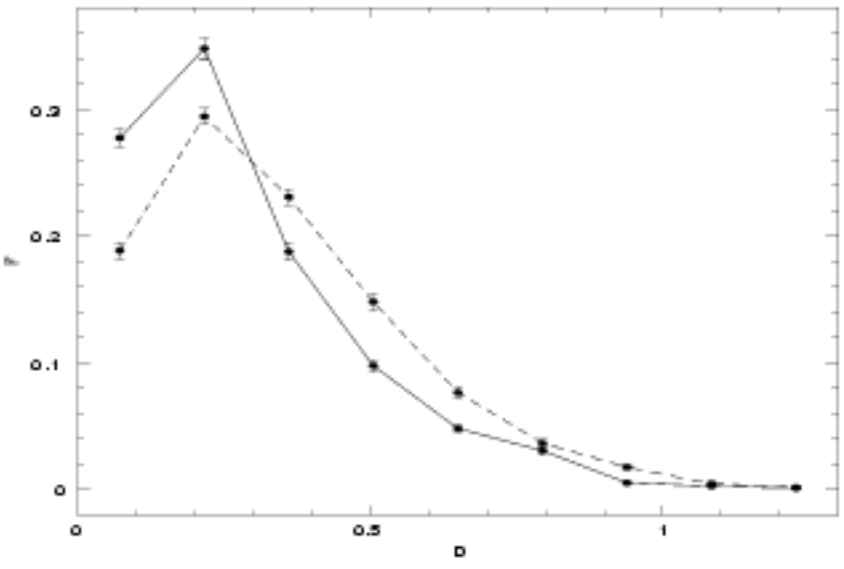

Fig. 4.2: Distribution of normalized group-centric distances D for galaxy pairs (solid line) and the control sample (dashed line).

We first investigate whether galaxy pairs have a particular radial location in groups with

respect to the control sample. For this purpose, we have analysed the distribution of projected radial distance, R_D, and relative velocity, V_{Group} , of pairs with respect to the host group centre normalized to the group virial radius (R_{Vir}) and group mean velocity dispersion (σ), respectively ($D = R_D/R_{Vir}$ and $v = (V - V_{Group})/\sigma$). We restrict the analysis to groups with more than 10 members for the purpose of avoiding large uncertainties in the determination of group centre, mean velocity and velocity dispersion owing to small number statistics. The resulting distributions of the pair and the control samples are shown in Fig.4.2 and Fig. 4.3, from where it can be appreciated that galaxy pairs have a similar concentration to the other group members and have a comparable relative velocity distribution with respect to the host group centre, although we notice that pairs are somewhat more concentrated and have smaller velocity dispersions than other group members.

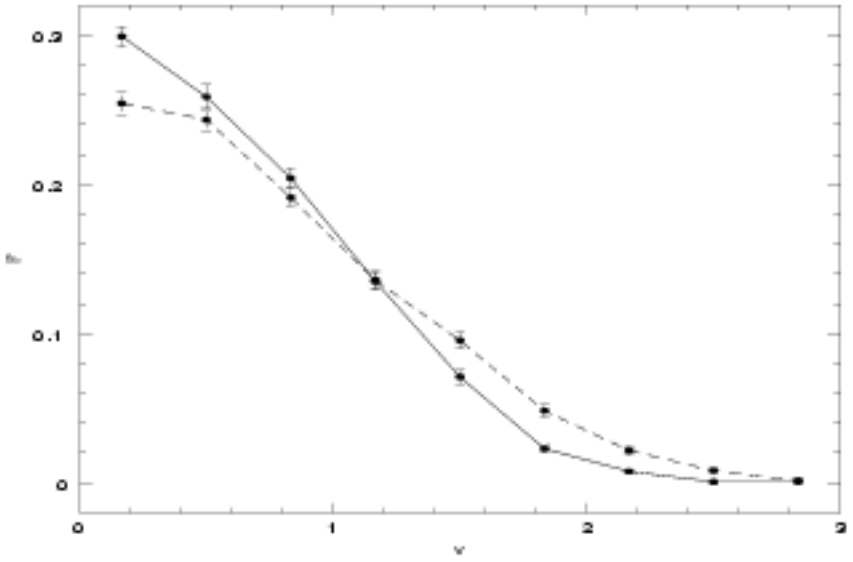

Fig. 4.3: Distribution of normalized radial velocities v for galaxy pairs (solid line) and the control sample (dashed line).

4.3.3 Star Formation in Galaxy Pairs and in the Control Sample

We have also computed the mean star formation birthrate parameter $b = SFR/\langle SFR \rangle$ (see Chapter 2) for different bins of normalized group-centric distance D for the group galaxy pair and the control samples.

The results displayed in Fig.4.4 show clearly that star formation in the galaxy pairs and in the control samples strongly increases for larger group-centric distances, approaching the

mean value for field galaxies in the outskirts. The similarity of these trends in both samples shows that, on average, the environment has the same effects in all group members.

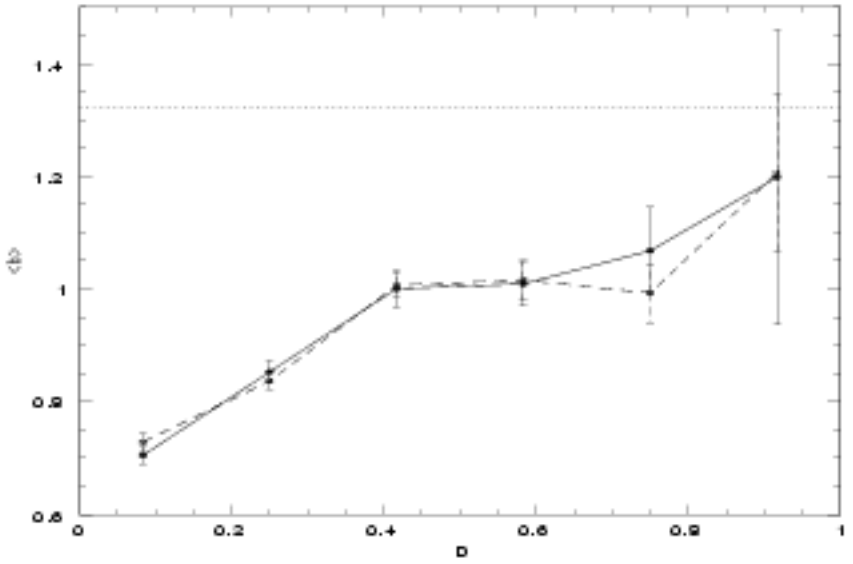

Fig. 4.4: Mean b parameter versus normalized group-centric distance (D) for galaxy pairs (solid line) and the control sample (dashed line) in groups. The dotted line corresponds to the mean b value obtained in Chapter 3 for field galaxies.

Star formation as a function of projected separation and relative radial velocity

We analyse the dependence of star formation as a function of r_p and ΔV by estimating mean values $\langle b \rangle$ as a function of r_p and ΔV for our sample of galaxy pairs in groups. The results are shown in Fig. 4.5 and Fig. 4.6.

From Fig.4.5, it can be seen that the star formation activity is significantly enhanced over the control sample for $r_p < 15$ kpc h^{-1}. We define a subsample of group close pairs by imposing the restriction: $r_p < 15$ kpc h^{-1}, hereafter Group Close Galaxy Pair (GCGP) sample (Table 4.1). Similar results are found for pairs in the field but for $r_p < 25$ kpc h^{-1} (Chapter 3). On the other hand, pairs with smaller relative radial velocity differences have larger mean b values, although redshift measurement uncertainties ($\delta\Delta V \approx 120$ km s^{-1}) may have diluted the true signal. This behaviour indicates that the physics of star formation induced by pair interactions operates in a similar fashion in high density environments, although with a lower general level of star formation activity.

Given the reduced star formation activity of pairs in the central regions of groups as

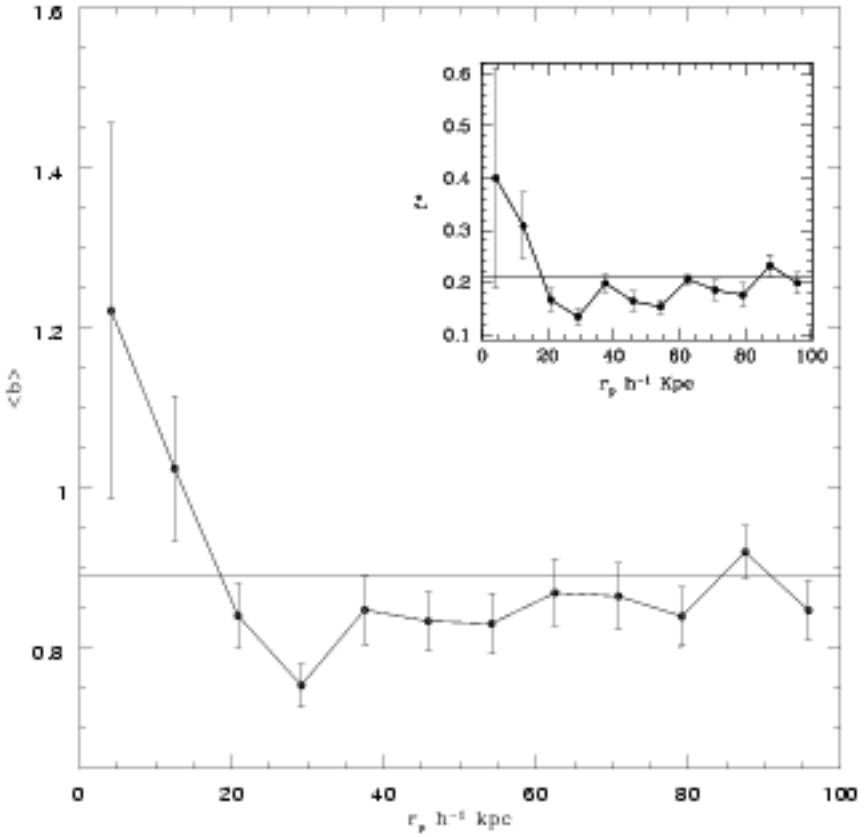

Fig. 4.5: Mean b parameter versus projected distance for galaxy pairs in groups. The horizontal line corresponds to the mean b value obtained from the control sample. The small box corresponds to the fraction f^* of galaxies with $b > 1.34$.

shown in Fig. 4.4, we have estimated the mean b for close galaxy pairs in two D bins limited at $R_D/R_{Vir} = 0.5$ in order to assess if the environment plays a role on the star formation activity of a close pair of galaxies. We found that for the GGP and the control sample, the star formation activity at $D > 0.5$ is 33% higher than at the central region. For GCGP we measure a 100% increase in the star formation activity in pairs at $D > 0.5$ with respect to the centrally located ones, suggesting that tidally induced star formation is more efficient in the outskirt of groups.

We measure the ratio between the mean star formation birthrate parameter of close galaxy pairs in the field and the corresponding mean value of the control sample (1.43 ± 0.14), which is larger than the corresponding ratio for galaxy pairs in groups (1.09 ± 0.01). This trend, together with the smaller spatial separation required for star formation enhancement,

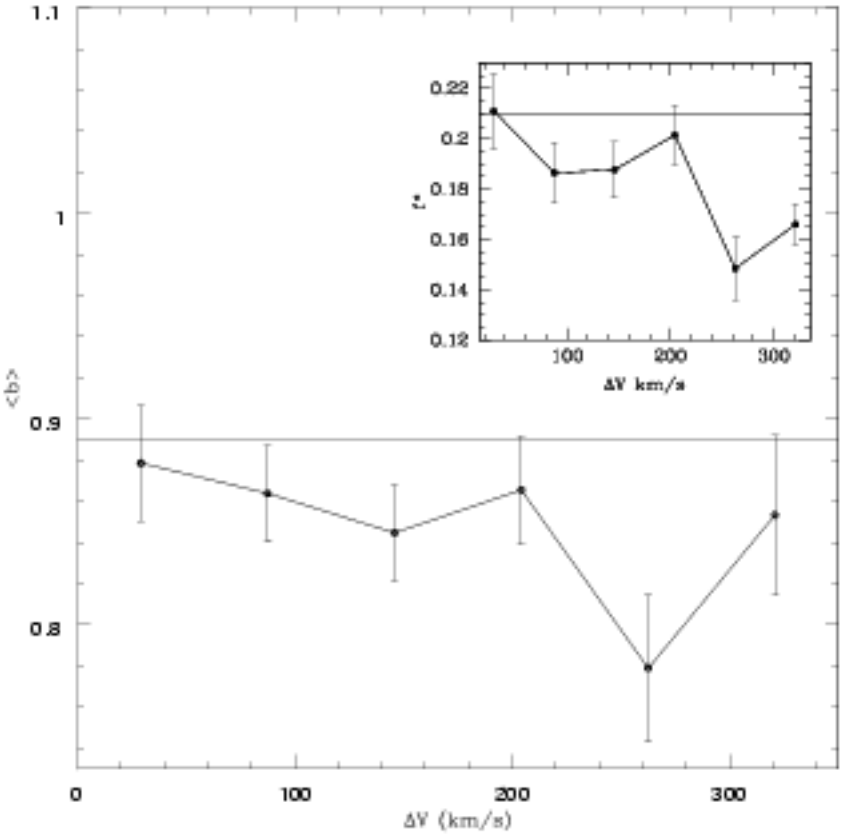

Fig. 4.6: Mean b parameter versus relative velocity for galaxies in interacting pairs in groups. The small box shows the fraction f^* of strong star forming galaxies in the sample.

suggests that tidal torques generated by interactions could be less efficient in pair systems (with similar r_p and ΔV) in high density regions. The fact that densest regions are populated by early type galaxies may indicate that the different response could be due to differences in the internal dynamics of the galaxies in pairs and the gas reservoir available to form stars in these systems.

We should also discuss further the possibility that spurious galaxy pairs, which are more probable in denser regions, can affect the trends. In fact, because of simple probabilistic arguments based on contamination by interlopers (typically 10 members within 0.5 Mpc h^{-1} in 2dF groups) would be approximately 63% at $r_p \approx 100$ kpc h^{-1}, in agreement with the analysis of the simulations. These arguments indicate that the probability of interlopers for the close pair sample would be only $\sim 9\%$ at $r_p \approx 15$ kpc h^{-1} so that our detection of star formation triggering at small separations is not likely to be strongly influenced by interlopers.

Tab. 4.1: Group Catalogs

Catalogs	Number of galaxies	r_p (kpc h^{-1})	ΔV (km s^{-1})
GGPC	3335 pairs	< 100	< 350
GCGPC	228 pairs	< 15	< 350
GCS	6670 galaxies	> 100	> 350

Note: GGPC: Group Galaxy Pair Catalog; GCGPC: Group Close Galaxy Pair Catalog; GCS: Group Control Sample.

Similarly to the analysis described previously we define a close 2dF mock catalog in groups by requiring $r_p < 15$ kpc h^{-1}. In this case we found that 83 % are real pairs in agreement with the probabilistic estimations. As we note from Fig. 4.5 , galaxies in pairs with $r_p > 15$ kpc h^{-1} have mean b values systematically lower than the mean ones for the control sample. Random interlopers should have, on average, a mean b value similar to the control sample one and contribute to take the mean star formation parameter of pairs closer to that of the control sample. The fact that we actually detect lower mean values for $r_p > 15$ kpc h^{-1} indicates that true galaxy pairs have low enough star formation activity to still overcome the effects of interlopers which contribute to push their mean b values up, closer to the one of the control sample. We argue that the galaxy pair sample comprises galaxies with lower star formation than the mean of other member galaxies of groups unless the pair members are very close. This behaviour is similar to field pairs, where again star formation activity is lower than that of the control sample, except for close pairs where there is a significant enhancement.

In order to improve our understanding of the star formation properties of galaxies in pairs, we have calculated the fraction of strong star forming galaxies, $f^* = N(b > 1.34)$. We expect that such a fraction would better reflect the effects of interactions than averages and, moreover, be less sensible to contamination by other member galaxies which are expected to have low b values. The birthrate parameter threshold $b = 1.34$ corresponds to spectral types 3 and 4 ($\eta > 1.1$) reported by Madgwick et al. (2002). As we can appreciate from the small boxes in Fig.4.5 and in Fig.4.6, proximity (in both r_p and ΔV) correlates with an increase in the fraction of galaxies with strong star formation activity. In Fig. 4.7 we show the histograms corresponding to the b parameters for the GCGP sample and the GCS where it can be appreciated that the star formation activity is significantly enhanced for pairs with small relative separations. In order to quantify the results shown in these histograms we estimated the expected number of close pairs with $b \geq 1.34$ to be 40 galaxies if the

distribution were consistent with that of the control sample. Instead, we obtain 54 galaxies in close pairs which represents 8% excess at a 2σ level.

From this analysis, we find indications for an environmental dependence of the relative separation and velocity thresholds for star formation activity induced by tidal torques. Our results also suggest a decrease in the efficiency of tidal torques to induce SF as we move to denser environments (see also Section 4.3.4).

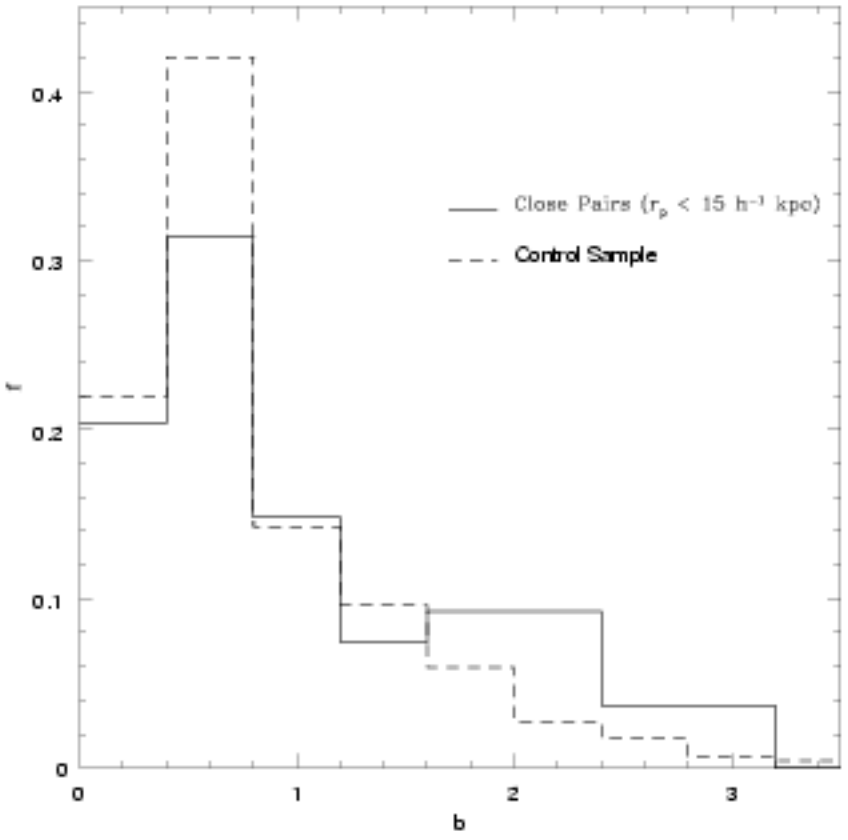

Fig. 4.7: Birthrate parameter b distributions for galaxies in close pairs, $r_p < 15$ kpc h^{-1} (solid line) and in the control sample (dashed lines).

4.3.4 Results Restricted to Rich and Poor Group Subsamples

Important observational evidence shows that dense environments can affect many galaxy properties, in particular the star formation rate (Dressler et. al 1985). Domínguez et al. (2002) found a clear distinction between high and low virial mass groups (adopting a mass

limit of $10^{13.5} M_{\odot}$) in the 2dF Group Galaxy Catalog constructed by Merchán & Zandivarez (2002). These authors found that massive groups have a significant dependence of the relative fraction of low star formation galaxies on local galaxy density and group-centric radius, while low virial mass groups show no significant trends.

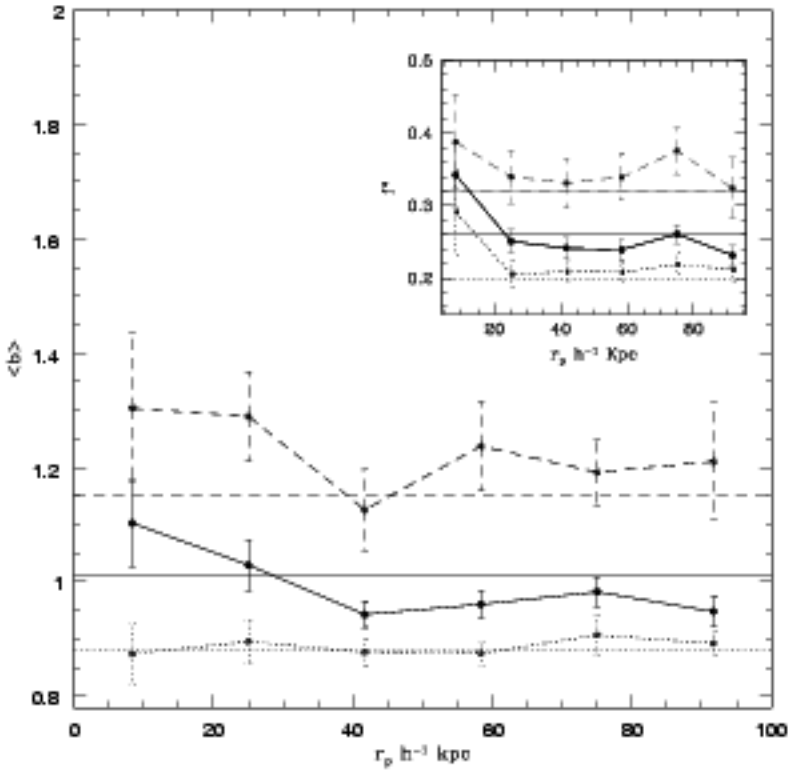

Fig. 4.8: Mean b parameter versus projected distance for galaxy pairs in all groups (solid line) and in the rich and poor subsamples (dotted and dashed lines, respectively). The small box shows the fraction f^* of galaxies with $b > 1.34$ in the different subsamples (same code line). Horizontal lines represent the mean $\langle b \rangle$ values of the corresponding control samples.

In this subsection, and in order to have a sufficiently large number of pairs, we have modified the 10 minimum number member condition to 4 members. This enlarged group sample is divided into a poor and rich group subsamples at $M_{\rm Vir} = 10^{13} M_{\odot}$.

In Fig. 4.8 we show that, as expected, galaxy pairs in rich groups show a weaker star formation activity than pairs in the total sample. Conversely, pairs in poor groups have a higher star formation activity. A similar behaviour is present in b vs ΔV as shown in Fig. 4.9. We also computed the fractions of star forming galaxies with $b > 1.34$ which show a similar trend for rich and poor group sub-samples. At small relative separations there is

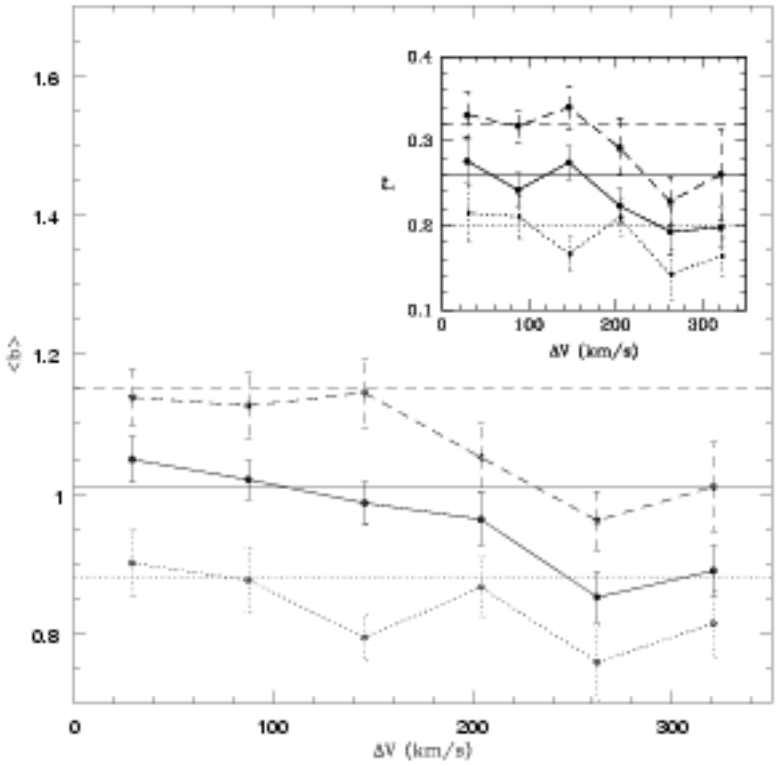

Fig. 4.9: Mean b parameter versus relative velocity for galaxy pairs in all groups (solid line) and in the rich and poor subsamples (dotted and dashed lines, respectively). The small box shows the fraction f^* of galaxies with $b > 1.34$ in the different subsamples (same code line).

a systematic increase of star formation activity irrespectively of environment. The central regions of clusters are mostly populated by early type galaxies. These objects are dominated by a central stellar spheroid which can provide stability to the system against tidal torques (e.g., Binney & Tremaine 1987; Mihos & Hernquist 1996; Tissera et al. 2002). Hence, in these systems, tidal fields are not expected to be that effective to drive gas inflows and trigger starbursts even if there were gas available.

Fig. 4.10 shows the relation between mean b of galaxies in pairs and host group virial mass. We also display the results for the control sample. These trends show that in rich groups, galaxies in pairs have a present-day lower star formation activity than galaxies without close companion. Although effects by spurious pairs should be always taken into account, we argue this result is robust against spurious pairs on the basis of previous discussions (Sections 4.3.1 and 4.3.3). We stress the fact that these results are not dominated by close pairs which show the opposite trend although with large dispersion owing to low number

statistics.

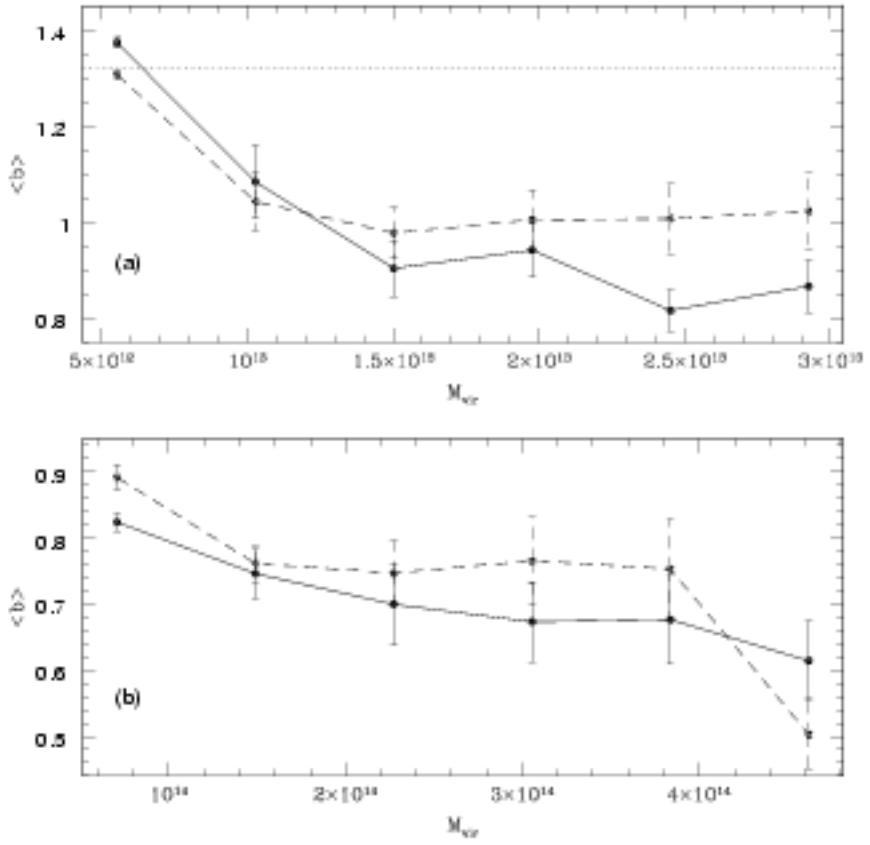

Fig. 4.10: Mean b parameter versus group virial masses for galaxy pairs (solid line) and control sample (dashed line) in groups of low and high mass (a and b respectively). The dotted line represents the mean b parameter of isolated galaxies in the field (see Chapter 3).

4.4 Summary

We have analysed properties of pairs of galaxy systems corresponding to groups and clusters of galaxies with virial masses $10^{13}-10^{15}M_{\odot}$. We stress the fact that the analysis discussed in this Chapter is based on the comparison between two galaxy samples which differed between each other only on the fact that one sample comprises galaxies with close companions, and the other, does not. Hence, we are always estimating the statistical differences in the properties of galaxies introduced by the presence of a companion. The analysis of a mock catalog of galaxy pairs derived from numerical simulations to mimic the 2dFGRS catalog showed

that the statistics are not dominated by spurious pairs.

The main conclusions can be summarized as follows:

- We find that the radial and relative velocity distributions of pairs, normalized to the group virial radius and group mean velocity dispersion, with respect to the group centres are similar (although slightly more concentrated) to those of group members with no companions.
- We find a closer relative projected threshold, $r_p \sim 15$ kpc h^{-1}, for star formation to be significantly enhanced with respect to that of the control sample when compared to that found for galaxy pairs in the field: $r_p \sim 25$ kpc h^{-1} (Chapter 3).
- The general lower efficiency of star formation in dense environments is accompanied by a lower enhancement of the star formation induced by interactions.
- We find that star formation strongly increases for larger group-centric distance for both, pairs and the control sample, in a similar fashion.
- Galaxy pairs in groups have a systematically lower present-day star formation activity than galaxies in the control sample except for very small relative separations were star formation is enhanced.

CHAPTER 5

GALAXY INTERACTIONS IN DIFFERENT ENVIRONMENTS

5.1 Abstract

In this Chapter we analyse star formation rates and colours of galaxy pairs in different environments using the 2dF Galaxy Pair and the Sloan Galaxy Pair Catalogs (defined in Chapter 2). We use the projected galaxy density derived from the fifth brightest neighbour, Σ, for each galaxy, with a convenient luminosity threshold to characterise environment in both surveys in a consistent way. Star formation activity is derived through the η parameter in 2dFGRS and through the star formation rate normalised to the total mass in stars, SFR/M^*, given by Brinchmann et al. (2004) in SDSS, which have been calibrated using common galaxies in the two surveys. For both galaxy pair catalogs, the star formation birthrate parameter is a strong function of the global environment and r_p, ΔV values. We observe that galaxy interactions are more effective at triggering important star formation activity in low and moderate density environments with respect to the control sample of galaxies without a close companion. Although close pairs have a larger fraction of actively star-forming galaxies, they also exhibit a greater fraction of red galaxies with respect to those systems without a close companion, an effect that may indicate that dust stirred up during encounters could affect colours and, partially, obscure tidally-induced star formation.

5.2 Introduction

In previous Chapters (3 and 4), we analysed the star formation activity in galaxy pairs in two well differentiated environments: field and groups/clusters, respectively. In Chapter 3, we analysed statistically a large field galaxy pair catalog, showing the effects of interactions

on the star formation activity, based on a comparative analysis of the properties of isolated galaxies and galaxies in pairs selected from the 2dFGRS. Then, in Chapter 4, we extended these investigations to high density environments: groups and clusters. The results indicated that pairs in groups were systematically redder and with a lower present-day star formation activity than other galaxy members, except for galaxy pairs with relative separation $r_p < 15$ kpc h^{-1} which showed significantly higher star formation activity in comparison to galaxy members without a close companion.

It is interesting to further investigate the effects of environment on star formation in pairs of galaxies, using a continuous variable from low density regions to very high ones.

In this Chapter, we use the samples of pairs, 2dFGP and SDSSGP catalogs, obtained in Chapter 2, from the 2dFGRS and SDSS, respectively. We focus on the statistical study of the effects of the presence of a close companion on colours and star formation activity of galaxies in different environments. We use the projected galaxy density parameter, Σ, derived from the fifth brightest neighbour of each galaxy, with a convenient luminosity threshold to characterise environment in both surveys in a consistent way. This Chapter is structured as follows: Section 5.3 describes the catalogs, control samples and the characterization of environment. Section 5.4 discusses the dependence of star formation on projected separation, relative velocity and environment. Section 5.5 deals with colour distributions as a function of environment. In Section 5.6 we summarize the main findings.

5.3 Observational Data and Galaxy Pair Catalogs

In this Chapter we will make use of the 2dFGP and SDSSGP catalogs to assess the effects of interactions on star formation in different environments.

In Chapter 2, we deduced a linear correlation between b and spectral-type index η which allowed the estimation of the b parameters for these galaxies. However, in order to estimate a birthrate parameter for galaxies in the 2dFGRS which can be compared to that obtained for SDSS, we will use pair galaxies in common in both catalogs to correlate the b parameter derived by SFR/M^* values in SDSS with the η index in 2dFGRS. For these common pairs we find that $b(SFR/M^*)$ and η define a linear correlation of the form:

$$b(\eta) = (0.25 \times \eta) + 0.71.$$

In all our analysis, we have therefore adopted this $b(\eta)$ relation for 2dFGRS galaxies (see

Fig.5.1a). We acknowledge the presence of several objects with low values of b in SDSS spanning the range $-3.5 < \eta < -2.0$ in Fig.5.1a so that this statistical relation is likely to work for active star forming galaxies.

5.3.1 Control Samples

In order to unveil the effects of interactions in different environments we constructed control samples for the 2dFGP and SDSSGP catalogs defined by galaxies without a close companion within the adopted separation and velocity thresholds. By using a Monte Carlo algorithm, for each galaxy pair, we selected two other galaxies without a companion within $r_p < 100$ kpc h^{-1} and $\Delta V < 350$ km s^{-1}. Moreover, these galaxies were also required to match the observed redshift and luminosity distributions of the corresponding pair sample. In this way they will also share incompleteness effects and any other selection bias which may depend on redshift and luminosity. We did not impose other restriction since the purpose of the control sample is to take into account any possible redshift and luminosity bias while allowing a confrontation of other physical parameters such as colours and star formation activity as a function of redshift.

In Fig.5.1 (panels *b* and *c*) we show the redshift distributions for SSDSGP and 2dFGP catalogs (solid lines) and their corresponding control samples, hereafter SDSS control sample (SDSSCS) and 2dF control sample (2dFCS) (dashed lines). Similarly, panels *d* and *e* show the M_r and M_{b_j} distributions from SDSS and 2dFGRS. It can be appreciated that luminosities and redshift for both pairs and control samples are similarly behaved in SDSS and 2dFGRS surveys with small Poisson errors.

5.3.2 Characterizing Environment in 2dFGRS and SDSS Surveys

The characterization of the local environment of galaxies is attained by defining a projected local density parameter, Σ. This parameter is calculated through the projected distance d to the 5^{th} nearest neighbour,

$$\Sigma = 5/(\pi(d_5)^2).$$

For completeness neighbours are chosen with luminosities above a certain threshold and with a radial velocity difference lower than 1000 km s^{-1}. In a similar way as Balogh et al. (2004), we imposed the condition $M_r < -20.5$ to select neighbours in SDSS. For the

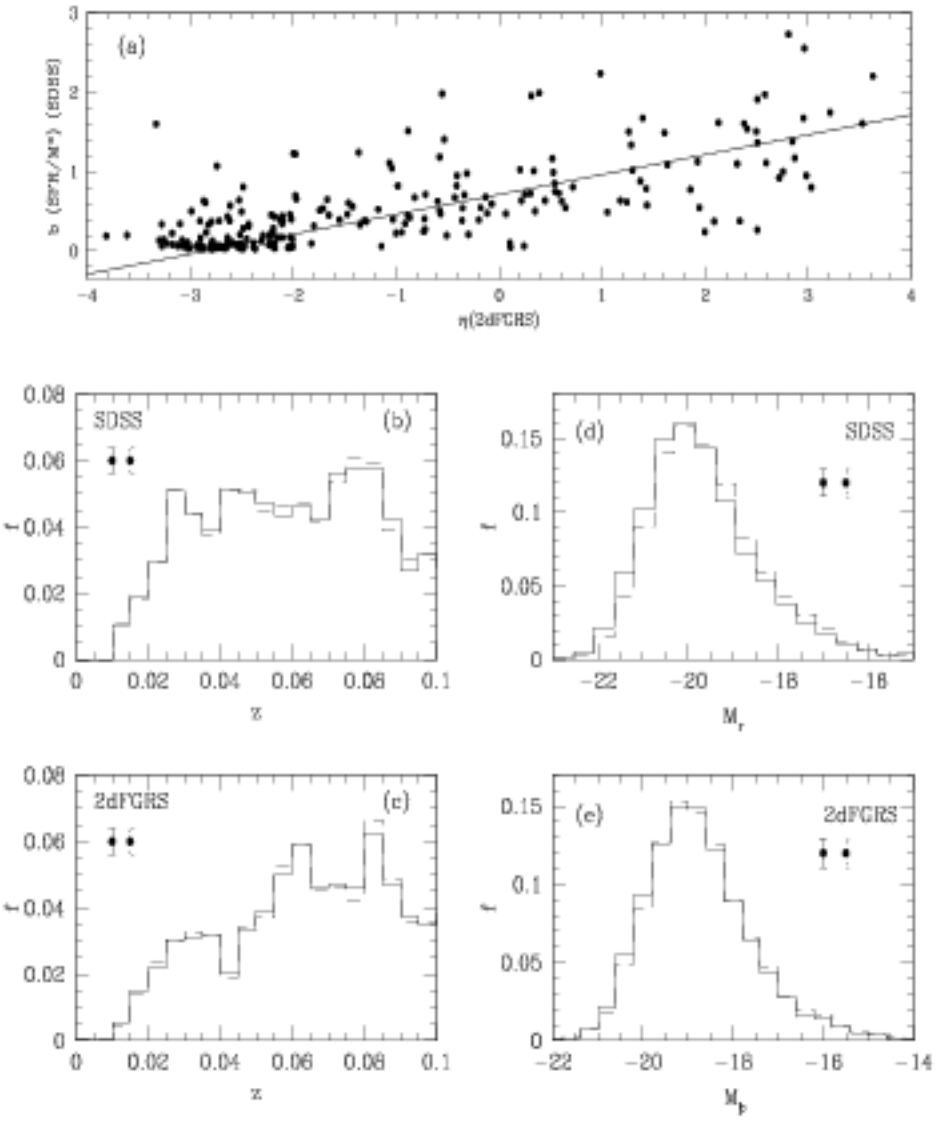

Fig. 5.1: Panel a: $b(SFR/M^*)$ versus η for pair galaxies in common from both catalogs. The solid line represent the linear correlation of the form $b(\eta) = (0.25 * \eta + 0.71)$. Panels (b) and (c) show the redshift distributions and panels (d) and (e) the M_r and M_{b_J} distributions in SDSS and 2dFGRS catalogs, respectively. The solid lines correspond to galaxies in pairs and dashed lines correspond to galaxies in the control samples. Error bars denote the mean Poisson errors.

2dFGRS catalog we estimated a corresponding magnitude limit of $M_b = -19.3$ by requiring that galaxy pairs in the common region with the SDSS had a similar density parameter Σ in both catalogs. This behaviour is illustrated in Fig.5.2(a,b), where we show the distribution of the derived values of Σ for both pair catalogs.

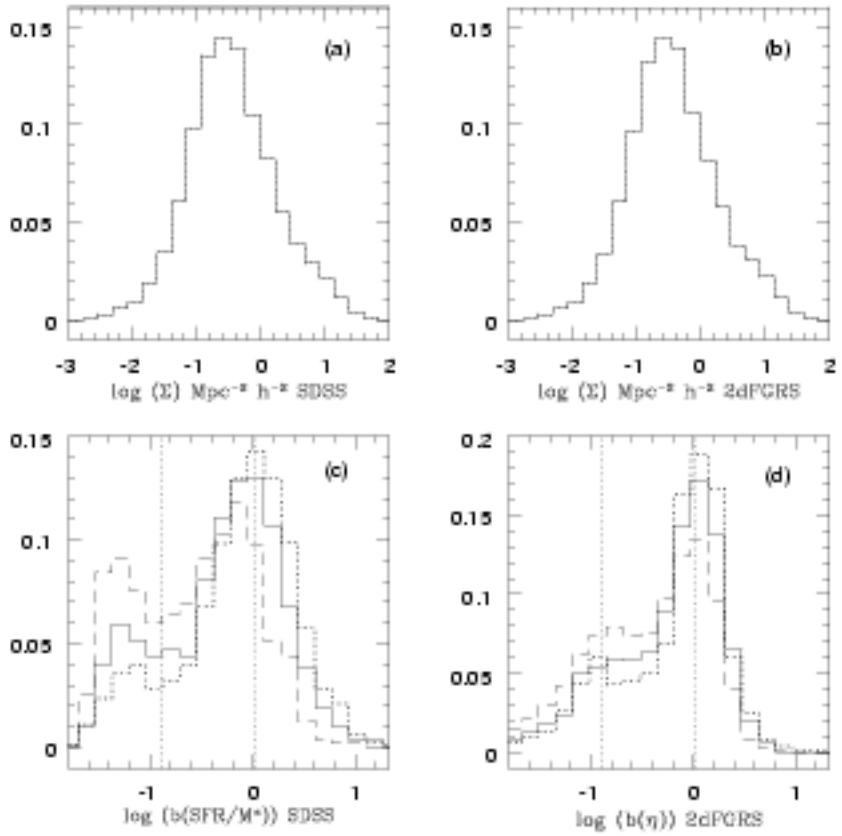

Fig. 5.2: Distribution of $log\ (\Sigma)$ for galaxy pairs in the SDSS (a) and 2dFGRS (b) surveys. Distribution of $log(b(SFR/M^*))$ and $log(b(\eta))$ for pair galaxies in SDSS (c) and 2dFGRS (d) catalogs in different environments: $log\ \Sigma > 0.05$ (dashed lines), -0.57 $< log\ \Sigma <$ 0.05 (solid lines) and $log\ \Sigma <$ -0.57 (dotted lines).

We explored if the results obtained in this analysis could depend on our particular choice of local density estimator. For that purpose, we also used the local densities given by Kauffmann et al. (2004). These authors estimated the local density by counting galaxies within cylinders of 2 Mpc h^{-1} in projected radius and $\pm$ 500 km s^{-1} in depth, in a complete sample of galaxies from SDSS. We found a good correlation signal between both density estimators indicating that these two definitions are adequate to characterize the environment of galaxies.

Also, this comparison has proven that incompleteness effects in our sample are not significantly affecting our Σ estimations. The results discussed in the following section have been checked to be robust against the particular definition of local environment. Hence we claim, that it is environment, and not a particular way of characterizing it, what determines the observed trends found in our work.

In order to analyse into more detail the dependence of star formation on environment, in Fig.5.2(c,d) we show the histograms corresponding to the birthrate parameter, $log(b)$, obtained from SFR/M^* for pairs in the SDSS and from η for pairs the 2dFGRS surveys. We also define three environment classes: low, medium and high, by selecting three suitable ranges of Σ values in order to have equal number of galaxies in each class. These density thresholds are shown in Table 5.1. In order to assess the significance of Σ thresholds, we have computed this parameter for galaxies in 2dF galaxy groups of Merchán & Zandivarez (2002), finding $log\ \Sigma$ values in the range 0.04 to 2.02 in consistency with our present definition of high density environment class ($log\ \Sigma > 0.05$) .

Tab. 5.1: Local Density Ranges

Environment	Σ Ranges ($Mpc^{-2}\ h^{-2}$)	d_5 ($Mpc\ h^{-1}$)
Low ($\approx$ field)	$log(\Sigma) < -0.57$	2.4
Medium ($\approx$ poor groups)	$-0.57 < log(\Sigma) < 0.05$	$2.4 < d < 1.2$
High ($\approx$ groups/clusters)	$log(\Sigma) > 0.05$	1.2

d_5: averaged distance to the 5^{th} nearest neighbour

In Fig.5.2 (c,d) we plot the distributions of birthrate parameter for both galaxy pair catalogs segregated in the three defined environment classes. As it can be clearly appreciated, strong star-forming galaxies tend to avoid high density regions. From this figure, the reader can judge how similarly the star formation activity as a function of the local density behaves for both pair catalogs. We claim that this agreement is good enough to provide a suitable joint analysis of the two data sets.

5.4 *Dependence of Star Formation on Projected Separation, Relative Radial Velocity and Environment*

In Chapter 3 and Chapter 4 we analysed the star formation activity in pairs in two well-segregated environments: field and groups, finding that galaxies in close pairs always exhibited enhanced star formation with respect to galaxies without a close companion. It is

interesting to further investigate the effects of environment with a larger sample where environment can now be characterized as a more continuous variable from very low density regions to very high ones. Moreover, the possibility of working with two different catalogs will allow us to test the robustness of the results.

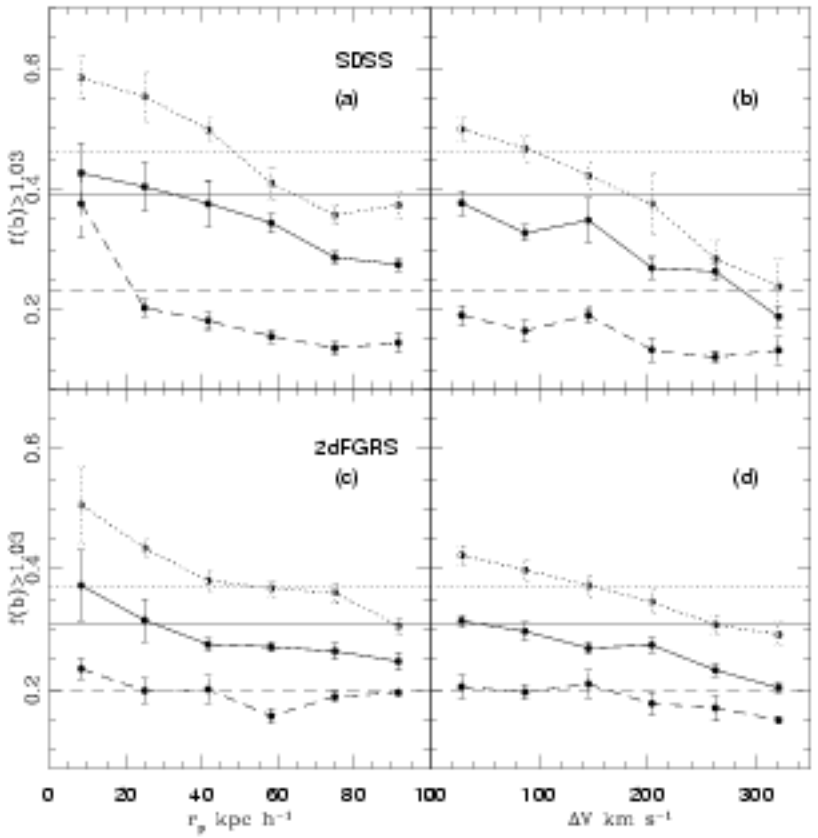

Fig. 5.3: Fraction of strong star-forming galaxies (with $b > 1.03$) in the SDSS (upper panel) and 2dFGRS (lower panel) pair catalogs as a function of the projected distance r_p (a, c) and relative velocity ΔV (b, d) for the three different environmental classes: $log\ \Sigma > 0.05$ (dashed lines), -0.57 $< log\ \Sigma <$ 0.05 (solid lines) and $log\ \Sigma <$ -0.57 (dotted lines). The horizontal lines show the corresponding fractions of the control samples.

We first explored the dependence of the relation between the star formation activity and r_p and ΔV on environment found in Chapter 3 and 4. For this purpose we calculated the fraction of strong star-forming galaxies as a function of r_p and ΔV in pairs and in the control samples in both surveys. We adopted the value $b > 1.03$ for both SDSS and 2dFGRS pair samples since this value define the high star formation peak in Fig.5.2 for the three

defined environmental classes. The results are displayed in Fig.5.3 from where we notice a clear increase of the star formation activity for smaller r_p values, a tendency that is more significant in low density environments. A similar behaviour is observed for the dependence on relative velocity, ΔV, where again star formation is enhanced with respect to the fraction of the corresponding control sample for smaller relative velocities and it is clearly above the value of the control samples only in low density environments. Our results are consistent with those derived in close galaxy pairs by Nikolic et al. (2004), who find the specific star-formation rate to decrease at large relative velocity although this effect is small compared to that observed with relative separation, r_p.

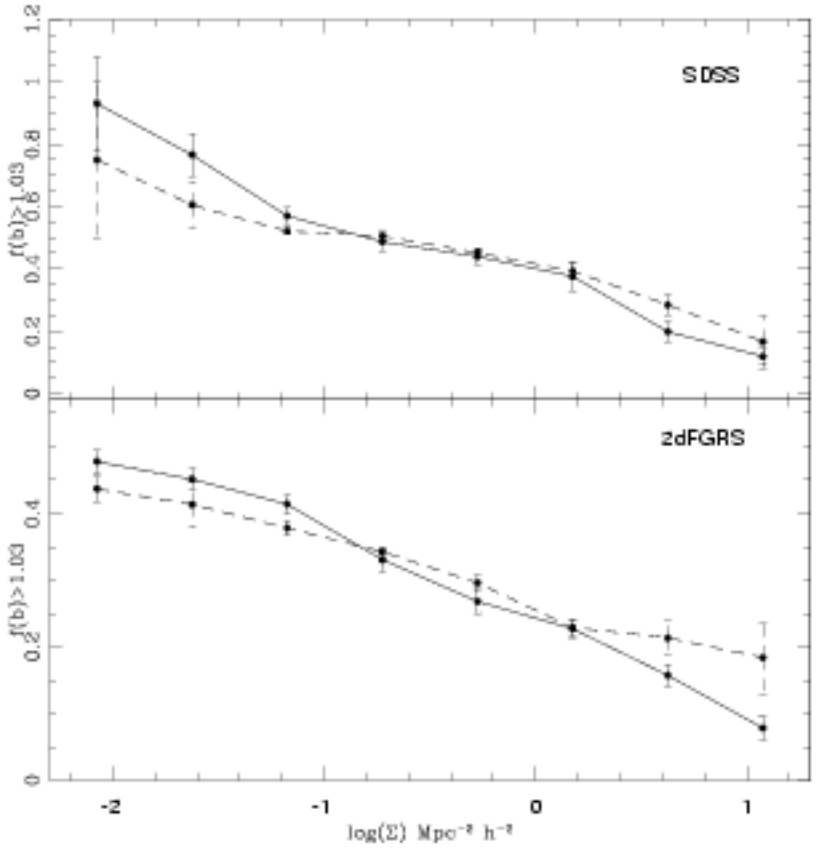

Fig. 5.4: Fraction of strong star-forming galaxies (with $b > 1.03$) as a function of $log(\Sigma)$ in close pairs: $r_p < 50$ kpc h^{-1} $\Delta V < 200$ km s^{-1} (solid lines) and in the control samples (dashed lines) in SDSS (upper panel) and 2dFGRS (lower panel) surveys.

Therefore, from the analysis of Fig.5.3, we deduce that galaxy pairs with $r_p \approx 50$ kpc h^{-1} and $\Delta V \approx 200$ km s^{-1} have a statistically significant enhancement of star formation activity,

regardless of environment. Hence, we define close pair subsamples formed by those systems within such limits, hereafter 2dF close galaxy pair (2dFCGP) and SDSS close galaxy pair (SDSSCGP) catalogs (Table 5.2).

Tab. 5.2: 2dF and SDSS Catalogs

Catalogs	Number of galaxies	r_p (kpc h^{-1})	ΔV (km s^{-1})
2dFGPC	6067 pairs	< 100	< 350
2dFCGPC	1746 pairs	< 50	< 200
2dFCS	12134 galaxies	> 100	> 350
SDSSGPC	11461 pairs	< 100	< 350
SDSSCGPC	3498 pairs	< 50	< 200
SDSSCS	22922 galaxies	> 100	> 350

Note: 2dFGPC: 2dF Galaxy Pair Catalog; 2dFCGPC: 2dF Close Galaxy Pair Catalog; 2dFCS: 2dF Control Sample, SDSSGPC: SDSS Galaxy Pair Catalog; SDSSCGPC: SDSS Close Galaxy Pair Catalog; SDSSCS: SDSS Control Sample.

In order to study into more detail how the fraction of actively star-forming galaxies in close pairs varies with environment, we have computed the fraction of strong star-forming galaxies as a function of projected local density parameter, Σ. The correlation with Σ is illustrated in Fig.5.4. from where we can appreciate a strong dependence of the star formation activity on local density for the close pair samples and their corresponding control ones. It is clear that close pairs show enhanced star formation activity compared to galaxies in the control sample for densities lower than $log\ \Sigma \simeq -1.0$. For $log\ \Sigma > 0$, pairs show a lower star formation activity than galaxies without a close companion, a fact already discussed in Chapter 4. The transition is within $log\ \Sigma \simeq -1$ and $log\ \Sigma \simeq 0$, where the fraction of strong star-forming systems seems to be independent of the presence of a close neighbour. This density range can be associated with that of loose group environments.

As discussed in Chapter 4, interlopers can affect more strongly higher density regions, but the probability to have interlopers is smaller as we take closer pairs. Hence, it is unlikely that the behaviour found in Fig.5.4 can be caused by interlopers.

As we have mentioned in the previous section (5.3.2), we analysed if our results could depend on the particular choice of local density estimator Σ. For that purpose, we explored the results obtained in the two previous figures, using the local densities given by Kauffmann et al. (2004) (*den*) for a sample of galaxies from SDSS. We plotted in Fig. 5.5 the fraction of strong star-forming galaxies (with $b > 1.03$) in the SDSSGPC as a function of the projected distance, r_p, for two different environmental classes, *den*. This figure shows a similar ten-

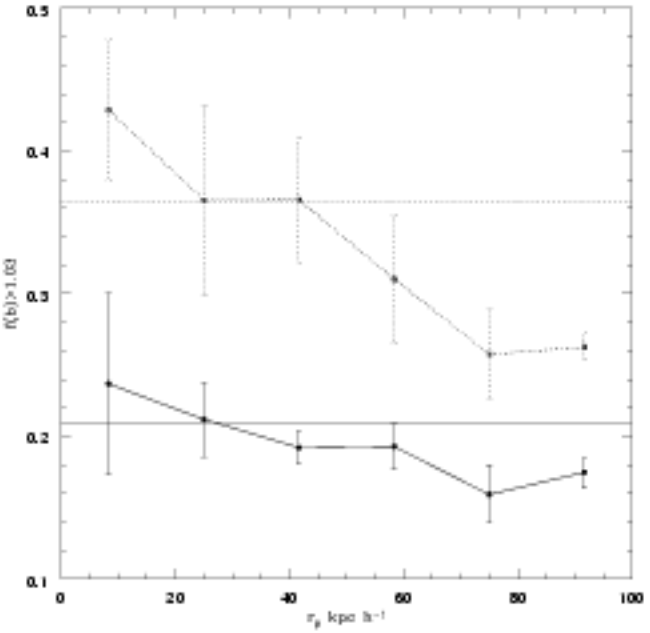

Fig. 5.5: Fraction of strong star-forming galaxies (with $b > 1.03$) in the SDSS pair catalog as a function of the projected distance r_p for two different environmental classes, from the density estimator obtained by Kauffmann et al. (2004). The horizontal lines show the corresponding fractions of the control samples.

dency that we have obtained from Fig.5.3, from Σ. In Fig. 5.6 we show the fraction of strong star-forming galaxies as a function of *den*, in SDSSCGPs ($r_p < 50$ kpc h^{-1} and $\Delta V < 200$ km s^{-1}) and in the SDSSCS. The close galaxy pairs show an enhanced star formation activity compared to galaxies in the control sample for densities lower than $\log(den) \simeq 0.4$. This value corresponds approximately to the value $\log(\Sigma) = -1.0$ (see Fig.5.4). It can be appreciated a good agreement between both density estimators, *den* and Σ, indicating that these two definitions are adequate to characterize the environment of galaxies. We can conclude that it is environment, and not a particular way of characterizing it.

As mentioned in Chapter 2, subsection 2.4.2, in the case of the SDSS survey, incompleteness in the spectroscopic sample could introduce possible systematic bias in our results. In spite of the low fraction of contamination (< 10 %) we have studied the star formation activity for the clean and contaminated subsamples ($m_r \leq 17.5$) from SDSS catalog defined previously. We calculated the fraction of strong star-forming galaxies ($b > 1.03$) as a function of projected distance and relative velocity, in the three different density environments (Table 5.1). The results are shown in Fig.5.7 where it can be seen that the trends are very sim-

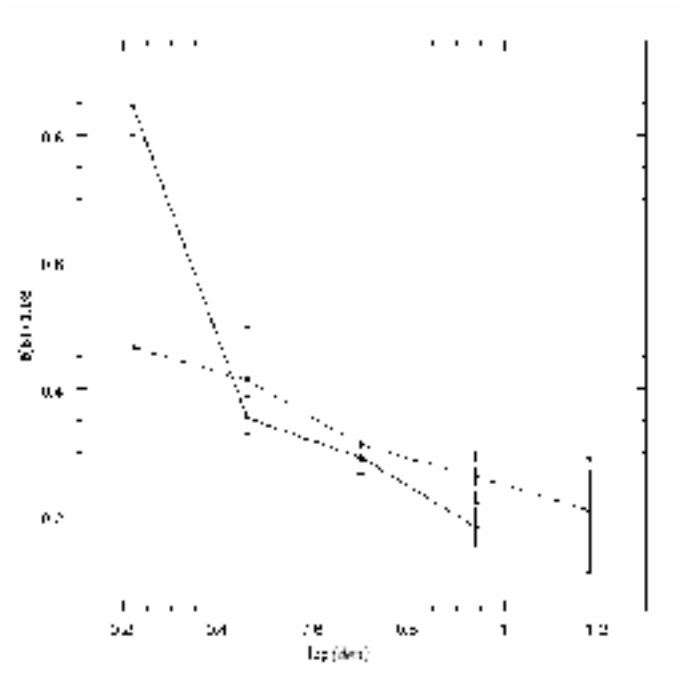

Fig. 5.6: Fraction of strong star-forming galaxies (with $b > 1.03$) as a function of the density estimator obtained by Kauffmann et al. (2004), in SDSSCGPs: $r_p < 50$ kpc h^{-1} and $\Delta V < 200$ km s^{-1} (solid lines) and in the SDSSCS (dashed lines). Log(den) $\sim$ 0.4 corresponds approximately to log(Σ) = -1.

ilar in both samples within the quoted uncertainties. This test indicates that incompleteness in the spectroscopic SDSS survey is not a serious concern for our analysis.

Given the strong dependence of star formation activity on morphological type, we have tested in SDSS if the effects of interactions obtained, depend on the concentration parameter C (ie. is the ratio of Petrosian 90 %- 50% r-band light radii) and on stellar mass M^* given by Kauffmann et al. (2004). Galaxies with a bulge (disc) dominated morphology have $C > 2.5 (C < 2.5)$ values, so we have analysed the fraction of star-forming galaxies in the pair sample as a function of projected separation for these two concentration-type galaxies separately. The results are shown in Fig.5.8 where it can be appreciated the increase of star formation activity at small separations for both disc and bulge dominated galaxies. Of course, disc-dominated galaxies have in general a much larger fraction of star-forming galaxies than bulge-dominated systems. However, regarding the comparison of pair to control samples, the two types of objects behave in a similar fashion under the presence of a close companion. Similarly, galaxies with small mass in stars are more likely to be strong star-forming systems than galaxies with large stellar masses. However, the trend of increasing star formation

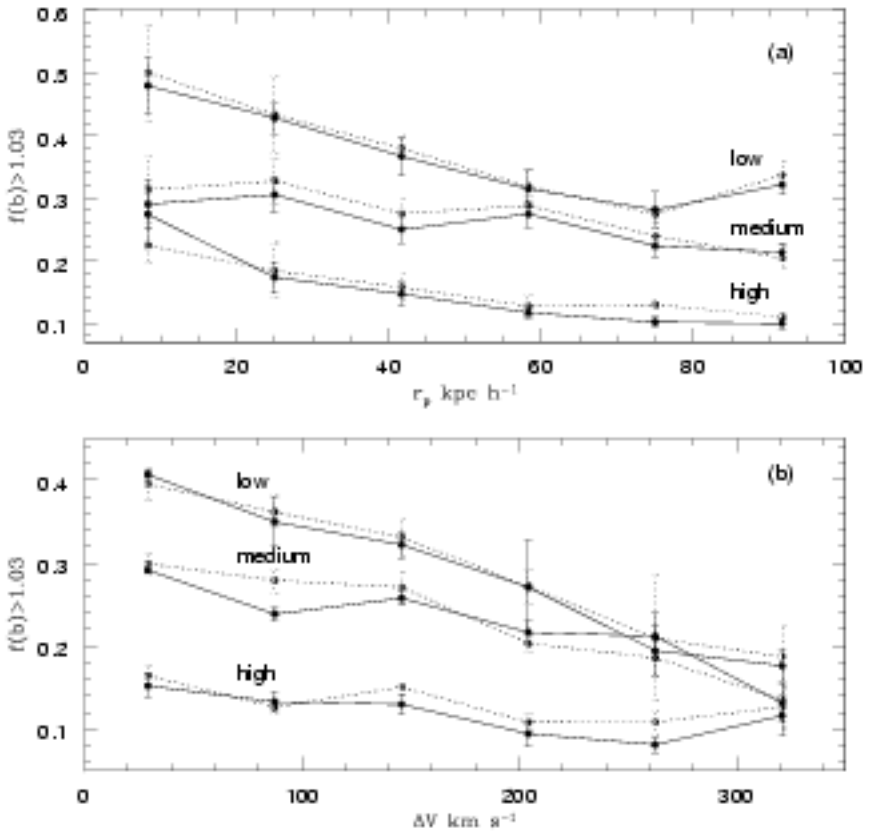

Fig. 5.7: Fraction of galaxies in pairs restricted to $m_r \leq 17.5$ with $b > 1.03$ for the total (solid lines), and clean (dotted lines) samples in SDSS, as a function of r_p (a), and ΔV (b), for high ($log\ \Sigma > 0.05$), medium (-0.57 $< log\ \Sigma <$ 0.05) and low ($log\ \Sigma <$ -0.57) density environments.

activity for close relative separation is observed in a similar fashion for both large and low stellar mass systems.

Hence the fact that we detect lower star formation activity in pairs in the denser regions with respect to galaxies without a close companion in the same kind of environment suggests that galaxy pairs as bound systems could be more evolved than their surrounding loose galaxies.

A comprehensive analysis of these environmental effects requires also a study of extremely low star-forming systems. We calculate the fraction of galaxies with low star formation activity in pairs and in the control samples as those with $b < 0.13$ in both SDSS and 2dFGRS surveys as a function of projected galaxy separation between pair members, r_p, and

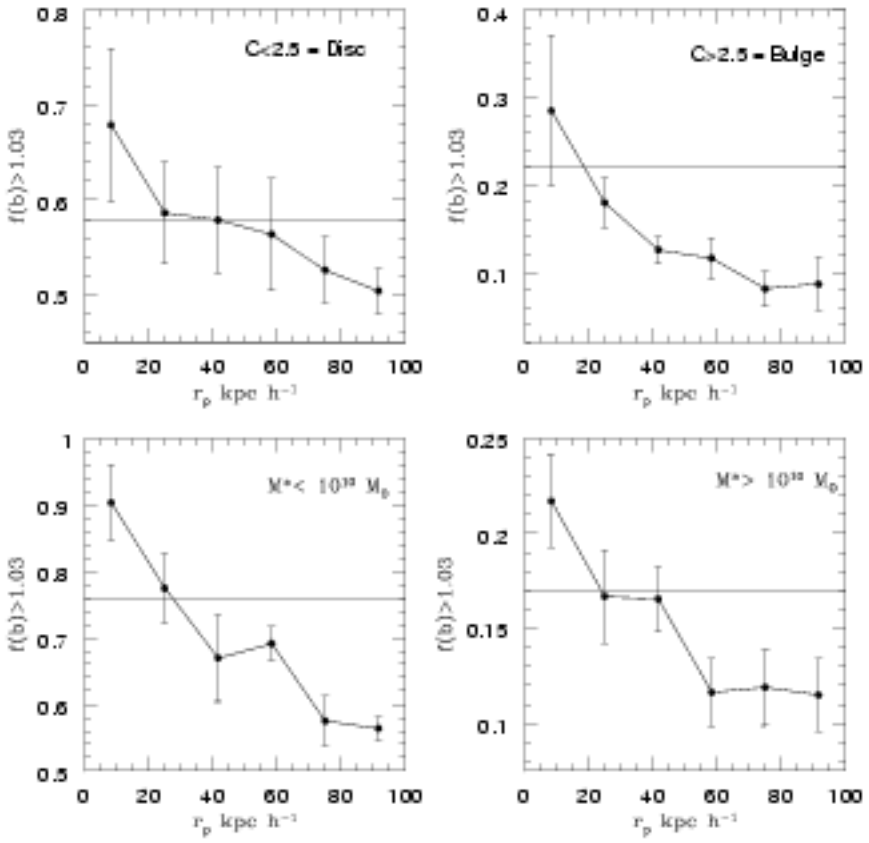

Fig. 5.8: Upper panels: Fraction of galaxies with $b > 1.03$ in the SDSS pair catalog as a function of r_p for low $C < 2.5$ or larger $C > 2.5$ concentration index values corresponding to disc or bulge dominated morphologies, respectively. Lower panels: Same as in upper panels for subsamples with low and high mass in stars ($M^* < 10^{10} M_\odot$ and $M^* > 10^{10} M_\odot$). The horizontal lines in the four panels correspond to the fractions of the control samples.

relative velocity, ΔV, for the same three different environments used in Fig.5.3 (Table 5.1). This $b = 0.13$ value corresponds to approximately the low SFR peak for the SDSS and the 2dFGRS distributions as it can be seen in Fig.5.2.

From Fig.5.9, we can notice a clear increase of the low star-forming galaxy fraction in pairs with larger r_p and ΔV values, a trend that is more significant in high density environments. As we mentioned before, the effects of spurious pairs should be higher for larger relative projected separations and in higher density regions. Hence, part of the trend could, in principle, reflect the effects of interlopers. However, on one hand, for close pairs these effects are not that significant as mentioned before and, on the other, the incorporation of

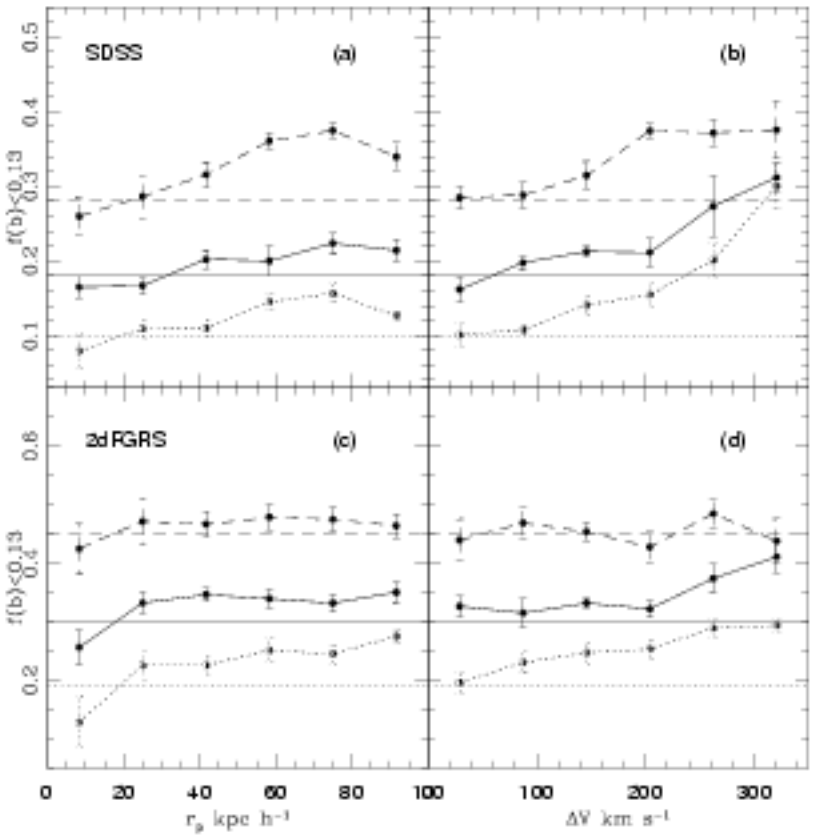

Fig. 5.9: Fraction of low star-forming galaxies (with $b < 0.13$) as a function of projected distance, r_p (a, c), and relative velocity, ΔV (b, d), for three different environmental classes: $log\ \Sigma > 0.05$ (dashed lines), -0.57 $< log\ \Sigma <$ 0.05 (solid lines) and $log\ \Sigma <$-0.57 (dotted lines), in the SDSS (upper panel) and 2dFGRS (lower panel) surveys. The horizontal lines show the fractions of the corresponding control samples.

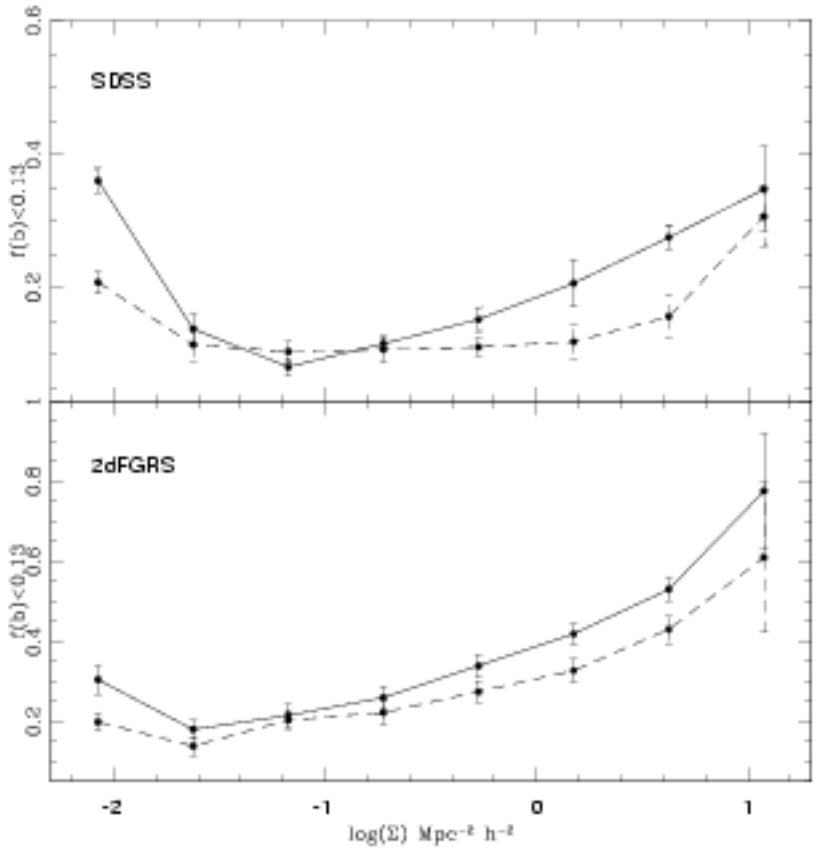

Fig. 5.10: Fraction of low star-forming galaxies (with $b < 0.13$) as a function of $log(\Sigma)$ in close pairs: $r_p < 50$ kpc h^{-1}, $\Delta V < 200$ km s^{-1} (solid lines) and in the control samples (dashed lines) in SDSS (upper panel) and 2dFGRS (lower panel) surveys.

interlopers should push the average of pairs toward that of the control sample while we are actually getting a lower value for close neighbours.

In Fig.5.10 we show the fraction of galaxies with low star-forming activity as a function of the projected local density parameter in close pairs and in the corresponding control samples. From this figure, it can be appreciated the expected dependence on local density for galaxies with and without a close companion so that the fraction of low star-forming systems increases with increasing density. However, we also found an increase of low star-forming galaxies in very low density regions. For close pairs there is a clear excess of low star-forming galaxies in all environments.

5.5 *Colours of Galaxies in Pairs*

In this section, we make use of the galaxy colour information in SDSS using Petrosian magnitudes for each object to further study galaxies in pairs. We calculate the colours with K and extinction corrections following Blanton et el. (2003).

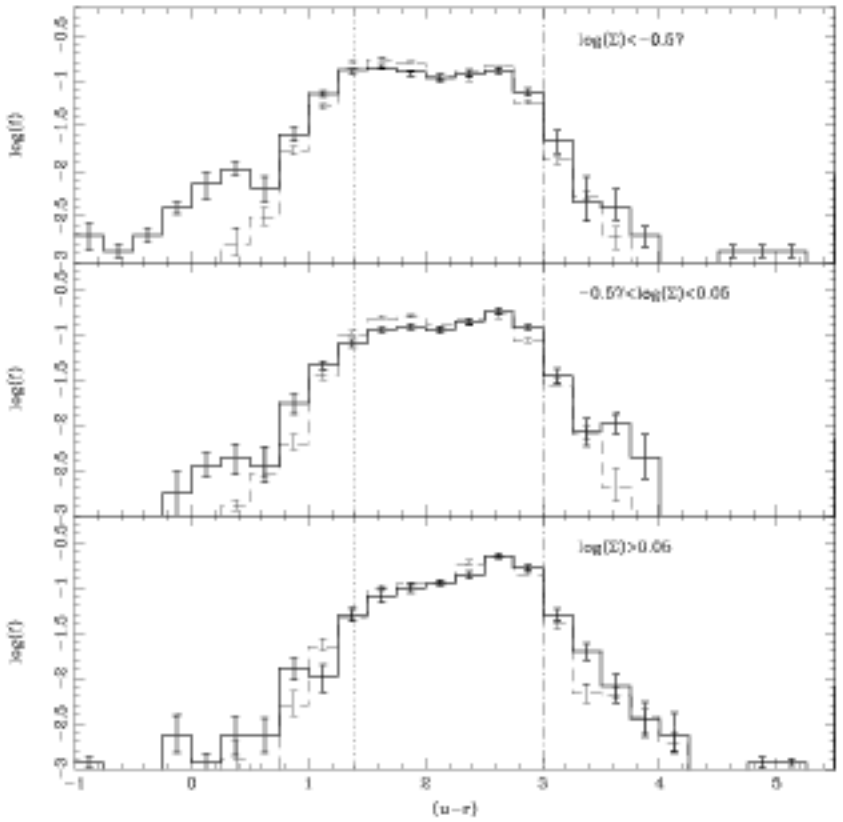

Fig. 5.11: Distribution of $u-r$ colours for galaxies in SDSSCGPs ($r_p < 50\,\mathrm{kpc\ h^{-1}}$, $\Delta V <$ 200 km $\mathrm{s^{-1}}$) (solid line) and in the corresponding SDSSCS (dashed lines), for the three different environmental classes defined in Section 5.3.2. The vertical lines correspond to the adopted blue (dotted) and red (dot-dashed) limits. Error bars correspond to Poisson standard errors. Notice the tail of blue galaxies in pairs in low density environment.

Fig. 5.11 shows the $u-r$ colour distributions for galaxies in close pairs (solid lines) and in the control sample (dashed lines) for the three environmental classes previously defined. From this figure it can be appreciated that close pairs have distributions with an excess of both red and blue galaxy colours with respect to those of the corresponding control sample. This behaviour is more significant in low density environments. Error bars correspond to

Poisson deviations in each colour bin. A more detailed look yields that, regardless of environment, galaxies in pairs populate more densely the colour ranges $u-r<1.4$ (dotted line), corresponding to blue, young stellar populations, and the regions with $u-r>3$ (dot-dashed line) dominated by the more extreme red stellar population, than those of the control samples. A similar analysis for $g-r$ colours yields a comparable trend with the blue and the red extreme defined by $g-r<0.4$ and $g-r>0.95$, respectively. These values are adopted as colour thresholds to define the extreme red and blue populations.

5.5.1 The Extreme Blue and Red Galaxies

Following the analysis of Section 5.4, we also computed the fraction of galaxies with extreme blue and red colour indexes as a function of projected separation and relative velocity, for the same three environmental classes. We use the colour thresholds determined in the previous section: $u-r<1.4$ and $g-r<0.4$.

Fig.5.12 shows an increase of the fraction of extremely blue galaxies for small r_p and ΔV. This behaviour indicates that galaxies in close pairs have an excess of young stellar populations with respect to that of the control sample. This excess is similar for the three environments (approximately a factor 1.5), although, in high density regions, systems have to be closer to reach this excess. The relative separation thresholds vary from $\approx 50\,\mathrm{kpc\,h^{-1}}$ to $\approx 20\,\mathrm{kpc\,h^{-1}}$ from low to high density regions. This behaviour is consistent to that found for the star formation activity as it can be appreciated from Fig.5.3.

In Fig.5.13 we have plotted the fraction of extreme blue galaxies as a function of projected local density parameter, Σ, for systems in both close pairs and control samples. As expected, the global trend with Σ is complementary to that found in Fig.5.4 so that the fraction of extreme blue galaxies in close pairs is higher in low density regions in comparison to the corresponding ones of the control sample. This relation inverses for high densities where we find that this fraction is larger in the control sample. The transition area ocurres in a density range consistent with that found for the fraction of strong star-forming pairs.

We have also explored the dependence of the fraction of extremely red galaxies on projected separation and relative velocity. Fig.5.14 shows an equivalent set of plots to that of the extreme blue fraction displayed in Fig.5.12, for the same range of Σ values. Note that the fractions of red galaxies in the control samples are almost independent of environment and their boostrap errors are ≈ 0.005. For galaxies in pairs there is an increase of this fraction for small r_p and ΔV values, indicating that close pairs have an excess of red objects regardless of the environment. The boostrap error bars for the fractions of the pair and control samples

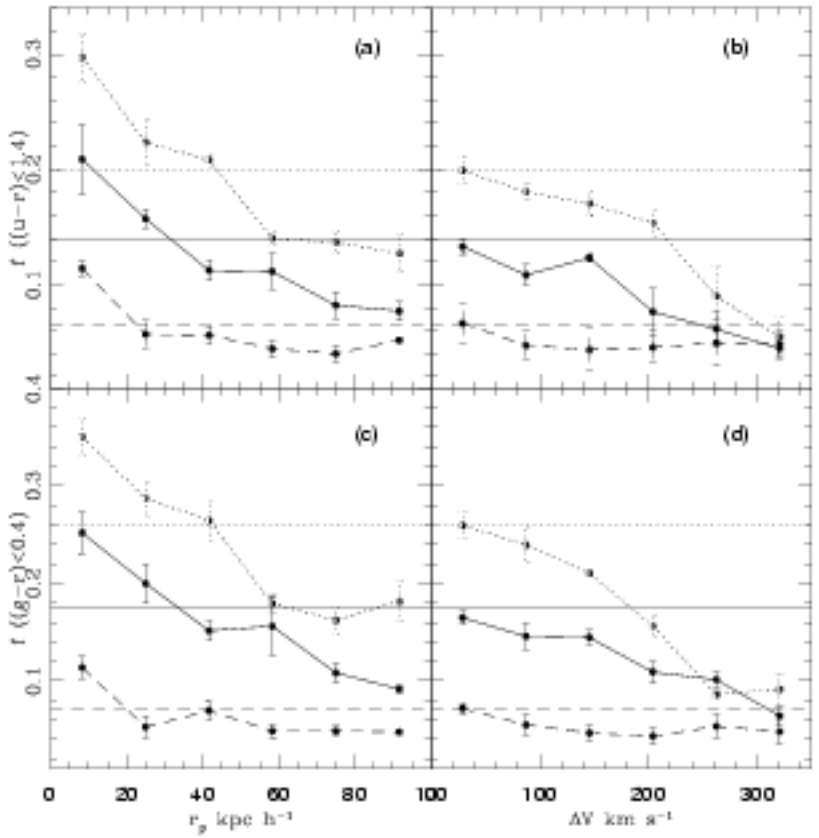

Fig. 5.12: Fraction of galaxies with $(u-r) < 1.4$ and $(g-r) < 0.4$ as a function of projected distance, r_p (a,c) and relative velocity, ΔV (b,d), for the three different environmental classes defined in Fig.5.3 The horizontal lines show to the fractions of the corresponding control samples.

indicate that the signal is statistically meaningful at more than 3σ-level.

One possible interpretation of this trend is that many galaxies in pairs have been very efficient in forming stars at early stages of their evolution so that, currently, they exhibit red colours. However, from Fig.5.9 we can appreciate that the fractions of low star-forming galaxies decrease for smaller relative separation for all environments, while the strong star-forming fractions increase (Fig.5.3). The behaviour of colours and star formation activity suggests that there is an important fraction of galaxies in very close pairs ($r_p < 20$ kpc h^{-1}) which tend to be redder than the rest of the galaxies but have enhanced star formation activity with respect to the control sample. The red colours of these star-forming galaxies in close pairs could be due to obscuration as the result of dust stirred up during the encounter which

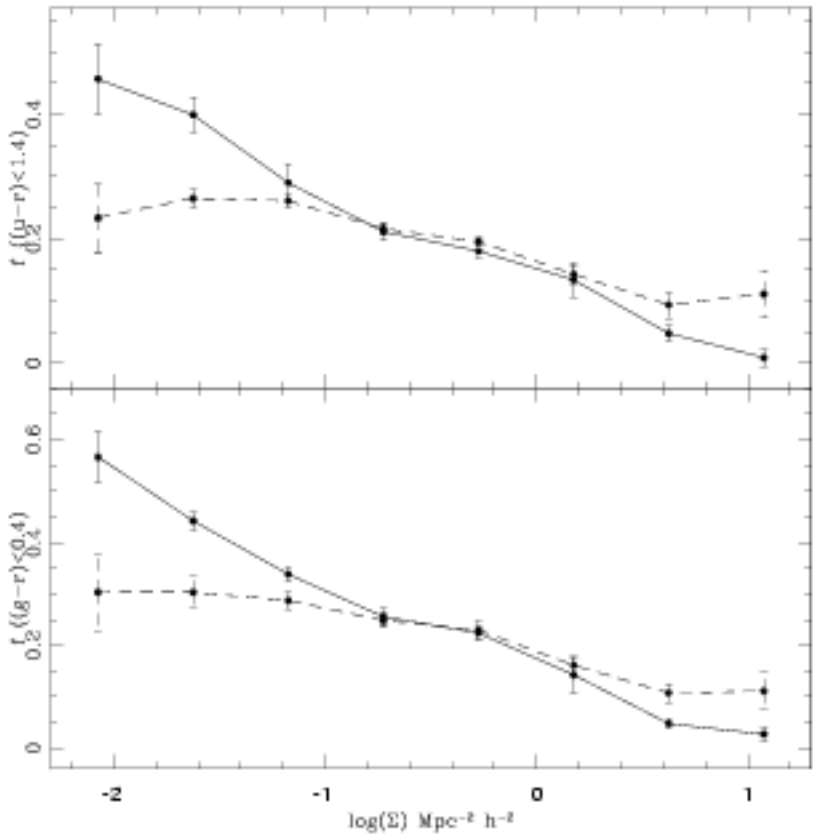

Fig. 5.13: Fraction of galaxies with $u - r < 1.4$ (a) and $g - r < 0.4$ (b) as a function of projected local density, Σ, for close pairs (solid lines) and control sample (dashed lines).

could also hide part of the star formation activity.

In order to further understand the dependence on environment of the fraction of galaxies with red colour indexes in close pairs and in galaxies without a close companion, we have analysed the fraction of extreme red galaxies in close pairs as a function of the local density parameter, Σ. The results are shown in Fig.5.15 from where it can be appreciated that there is an excess of extreme red galaxies in close pairs compared to that of the control sample in all kind of environments. This trend tends to be stronger in high density environments, consistent with the results of low star-forming galaxies discussed in Section 5.4.

We also notice that, at extremely low density environments, galaxies, regardless of the presence of a companion, also show a larger fraction of red objects in comparison with those of transition density region. This feature is consistent with the change in the slope of the relation between the fraction of low star-forming galaxies and Σ detected for $log\ \Sigma \leq -1.2$

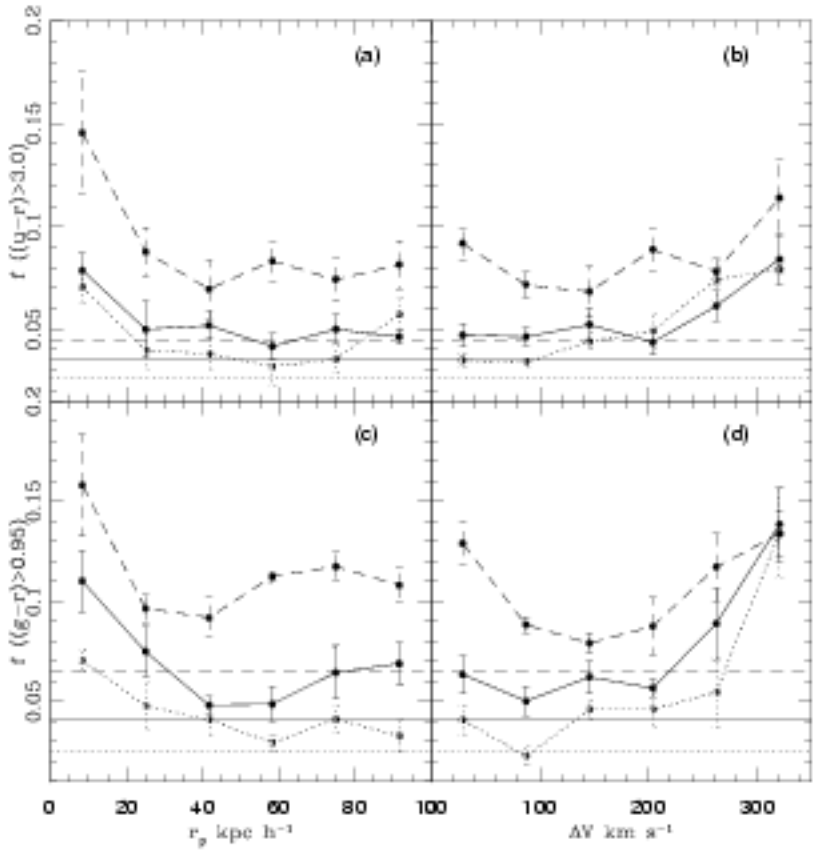

Fig. 5.14: Fraction of galaxies with $(u-r) > 3.0$ and $(g-r) > 0.95$ as a function of projected distance r_p (a,c) and relative velocity ΔV (b,d) for the three different environmental classes defined in Fig.5.9. The horizontal lines show the fractions of the corresponding control samples.

(Fig.5.10). We argue that these trends can be interpreted as the result of the growth of small scale overdensities in global underdense regions, where the subsequent infall of gas should close and as a consequence, the star formation activity is likely to have been strongly reduced at later times. Hence generally, galaxies would be less efficiently feeded by gas infall in this regions, and on top of that, galaxies in pairs would be more efficient at consuming this gas, producing a larger fraction of red and low star-forming systems.

Previous studies of the colour distribution of galaxies showed an important dependence of the fraction of red galaxies with environment and luminosity (Kauffmann et al. 2004; Balogh et al. 2004; Baldry et al. 2004). In particular, Balogh et al. (2004) claimed that the colour distribution is bimodal with only the relative fraction of galaxies in the red and

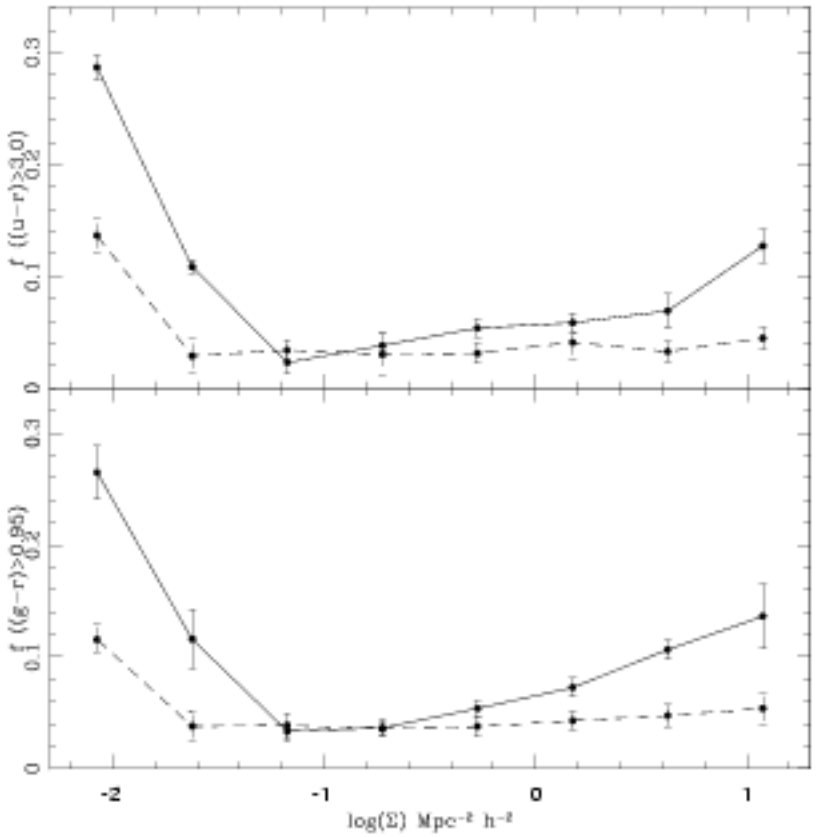

Fig. 5.15: Fraction of galaxies with $u - r > 3.0$ (a) and $g - r > 0.95$ (b) as a function of projected local density, Σ, in close pairs (solid lines) and in the control sample (dashed lines).

blue peaks varying with local density and luminosity. These authors interpreted their results resorting to a rapid change of galaxy colours due to mergers and interactions. Our results support these findings given the strongest dependence of star formation activity and colours of galaxies in pairs on environment with respect to galaxies without a close companion.

5.6 Summary

We have carried out a detailed analysis of photometric and spectroscopic properties of galaxies in pairs at different environments. The galaxy pair catalogs derived from the 2dFGRS and SDSS galaxy surveys available comprise 6067 and 11461 pairs, respectively. In order to characterize environment, we have used a projected galaxy density parameter, Σ, derived

from the fifth bright nearest neighbour of each galaxy. We have adopted $M_r < -20.5$ in SDSS and $M_{b_J} < -19.3$ in 2dFGRS so that the derived projected densities of both surveys are nearly consistent with each other. In agreement with previous Chapters our analysis indicates that, globally, star formation activity obtained from 2dFGRS and SDSS are strong functions of environment, projected separation and radial velocity.

The SDSS galaxy pair catalog has been cleaned of AGNs (see Chapter 2). Conversely, the 2dFGRS may suffer from some contamination by AGNs which can affect the relation. This could explain in part some of the small differences found in the results from both catalogs. Note, nevertheless, that trends are very similar.

Our results found can be summarized as follows:

- There is an increase of star formation in pairs for smaller projected separations and relative velocities in all environments. However, in high density regions galaxies have to be closer to statistically show an enhancement respect to galaxies without a close companion.

- The dependence of extremely blue and actively star-forming fractions of galaxies in close pairs on local density shows a change in behaviour respect to the equivalent fraction of the control sample. In low density environment, blue and star-forming galaxies tend to be in pairs. In high density regions, galaxies without a close companion have a higher contribution to blue and actively star-forming systems. The transition densities correspond to group environments.

- Extremely red and low star-forming galaxies in pairs outnumber those without a close companion in all environments. The fraction of red and low star-forming galaxies without a close companion shows an increase in the lowest density regions analysed. The corresponding fraction of galaxies in pairs increases in both the low and the high density ends. In low density environments, this effect is more pronounced for pair galaxies owing to the combined effects of the expected lack of gas infall in such regions and the high efficiency of galaxies in pairs to use the available gas for new stars at early stages of their evolution.

CHAPTER 6

STAR FORMATION IN SATELLITE GALAXIES

6.1 Abstract

In this Chapter, we present narrow-band observations of the Hα emission in a sample of 31 satellites orbiting isolated giant spiral galaxies. The sample studied spans the range $-19 < M_B < -15$ mag. The Hα emission was detected in all the spiral and irregular objects with fluxes in the range $1.15 - 49.80 \times 10^{-14}$ erg cm^{-2} s^{-1}. The average and maximum values for the current star formation rates are 0.68 and 3.66 M$_\odot$ yr^{-1} respectively. Maps of the spatial distribution of ionized gas are presented. The star-forming regions show a rich structure in which frequently discrete complexes are imposed over more diffuse structures. In general, the current star formation rates are smaller than the mean values in the past obtained from the current stellar content; this probably indicates a declining rhythm with time in the generation of new stars. However, the reserve of gas is enough to continue fueling the current levels of star formation activity for at least another Hubble time. Four of the objects (NGC 2718b, NGC 4541e, NGC 5965a$_1$ and NGC 5965a$_2$) with higher current star formation rates show clear signs of interaction with close companions of comparable brightness at projected distances of 25, 20 and 2 kpc respectively. The only two galaxies in our sample that do not show star formation activity are members of these interacting systems. It is unclear if this is a consequence of intrinsic properties (both are Hubble early types) or if it is related to possible disruption of the external parts due to the interaction. In the case of the pair NGC 2718a-b there are indications of gas transport between both galaxies.

6.2 *Introduction*

Cold dark matter cosmologies predict a hietarchical scenario (e.g., White & Rees 1978) in which small structures are formed first, and then by several processes of merging, accretion, etc., larger structures are generated. Currently, one of the most discussed questions in this field is the so-called "missing satellite problem"; in fact, semi-analytic models (Kauffmann et al. 1993) and numerical simulations (Klypin et al. 1999; Moore et al. 1999) of small structure formation in cold dark matter cosmologies predict a number of satellites in the halos of large galaxies an order of magnitude larger than the observed counts in the Local Group. A possible observational incompleteness of factor up to three of the known population of dwarfs orbiting the Milky Way, as has been evaluated by Willman et al. (2004), is not enough to solve the discrepancy. It has also been proposed that star formation in low-mass structures could be inhibited by a strong photo-ionizing background (Somerville 2002), especially at low redshift (Dijkstra et al. 2004).

Reconstructing the evolutionary history of satellites in galactic halos is, then, essential for validating the main predictions of these models. This requires study of the role of physical processes such as interactions, mass losses, morphological transformation and star formation. Obviously, the best studied are the Milky Way and Andromeda halos, although extending the study to other host galaxies is necessary for studying possible variations from halo to halo, which probably depends on the host mass, the merging history, and the environment. That was our motivation to start an observational program that comprises photometry in optical broad- and narrow-band filters for a sample of satellites orbiting external giant spiral galaxies. In previous articles Gutiérrez et al. (2002) and Gutiérrez & Azzaro (2004) have analysed the morphology and photometry of about 60 such objects. This analysis enabled us to validate and extend the relations found in the satellites of the Local Group.

In this study, we use narrow-band observations in Hα to estimate the current star formation rate of a subsample comprising most of the late type objects. We analyse the evolution of star-forming activity with time, and the relation to morphological type, HI mass, and environment. In Chapter 2 we have presented the observations and data reduction of the satellite galaxies sample that we analyse in this work. This Chapter is organized as follows. Section 6.4 presents the images and qualitatively analises the Hα maps of each object; the star formation rate estimates are presented in Section 6.5; the relation between interactions and star formation, and the cosmological evolution of star formation activity are discussed in Sections 6.6 and 6.7; finally Section 6.8 presents the conclusions.

6.3 Observing Program

6.3.1 The Sample, Observations and Data Reduction

The satellite galaxy sample analysed in this Chapter comprises 31 spirals and irregulars objects spanning a large range in luminosity ($-19 < M_B < -15$), and constituting a sample useful for statistical studies of the population of late-type galaxies present in the halos of large spiral galaxies. The satellites are at least 2.2 magnitudes fainter than their parents, and have projected distances $r_p < 500$ kpc h^{-1} and relative velocities $\Delta V < 500$ km s^{-1} from the primaries.

The observations and data reduction have been explained in Chapter 2.

6.4 Images of the Satellite Galaxies

The R-band and Hα images, after continuum subtraction, are presented in Figures 6.1, 6.2 and 6.3. We have detected Hα emission in all but two galaxies. For most of the galaxies, the Hα emission shows a complex morphology in which it is possible to discern diffuse and discrete structures. A description of these images is presented in Appendix A. The identification of interacting systems is based on spatial proximity and on the presence of features in the R band, such as a bridge in the case of the pair NGC 2718a-b, tidal streams in the pair NGC 4541b-e, and distortion of the outer isophotes in the case of the two components of NGC 5965a. For the other galaxies there is also some evidence of current or past interactions on the basis of the proximity to the parent (NGC 3154a), possible companions with unknown redshift (NGC 3735a, NGC 4030b, NGC 4541a and NGC 6181a), knots differentiated from the main body of the galaxy having strong star formation activity (NGC 1961b, NGC 5899a and NGC 7678a), or the presence of possible tidal galaxies (as in NGC 2775c).

6.5 Hα Luminosities and Star Formation Rates

The Sextractor software (Bertin & Arnouts 1996) was used to carry out the photometry of the galaxies in the broad and narrow-band filters. We considered two possible estimates for the total flux of the galaxies. The first is the integrated flux in a predefined aperture (the same as for the narrow and broad filter) and the second the flux in the automatic aperture computed in Sextractor according to the extrapolation proposed by Kron (1980). In general, we noted that the first method gives more robust values for those galaxies that are more irregular, while the second is more appropriate for objects with a well defined regular profile. In the cases in

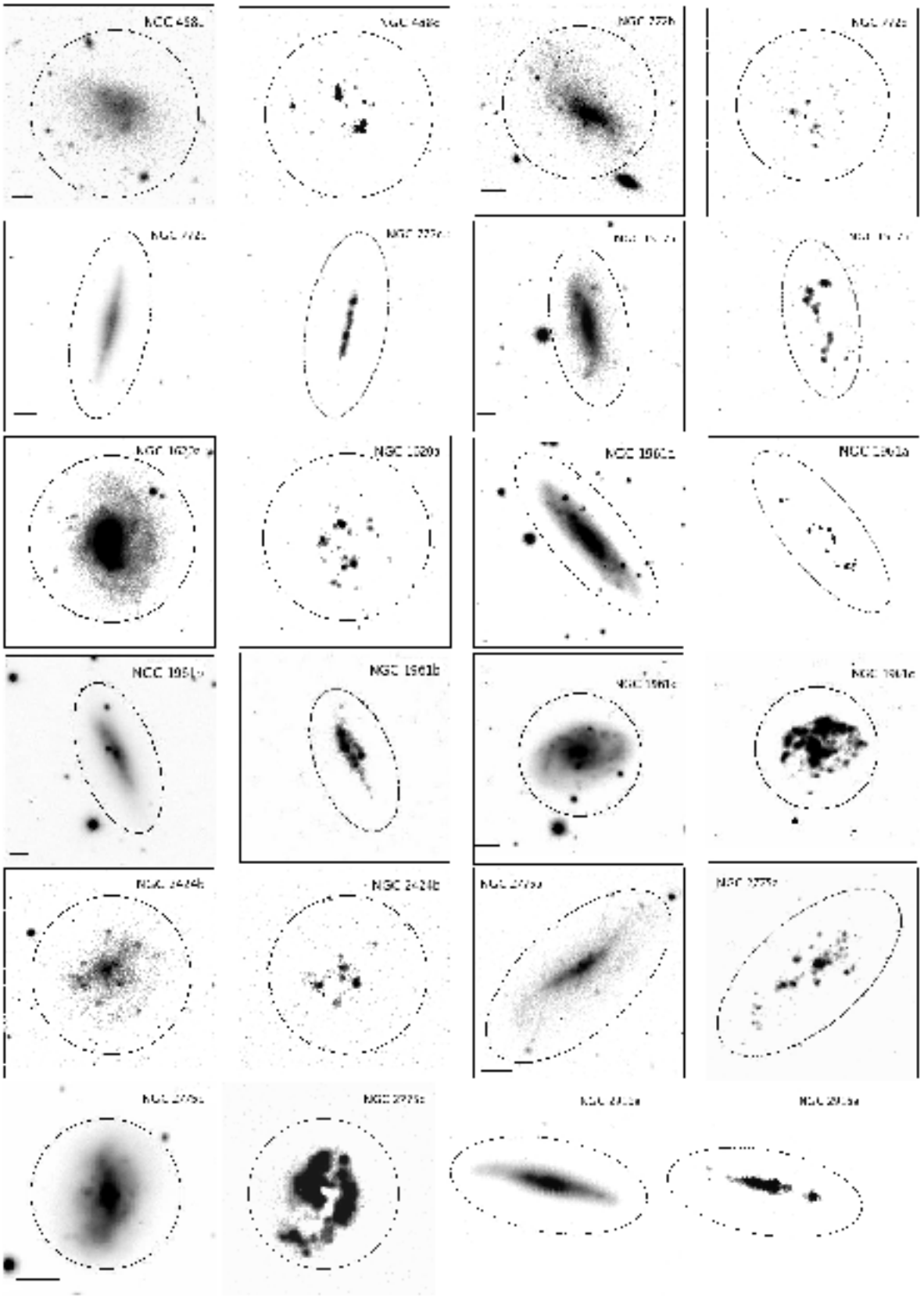

Fig. 6.1: Images of the sample of objects analysed in this work. For each object are ptesented the *R*-band and Hα images after continuum subtraction. North is at the top and East to the left. The small line at the bottom is scaled to an angular size of 10 arcsec.

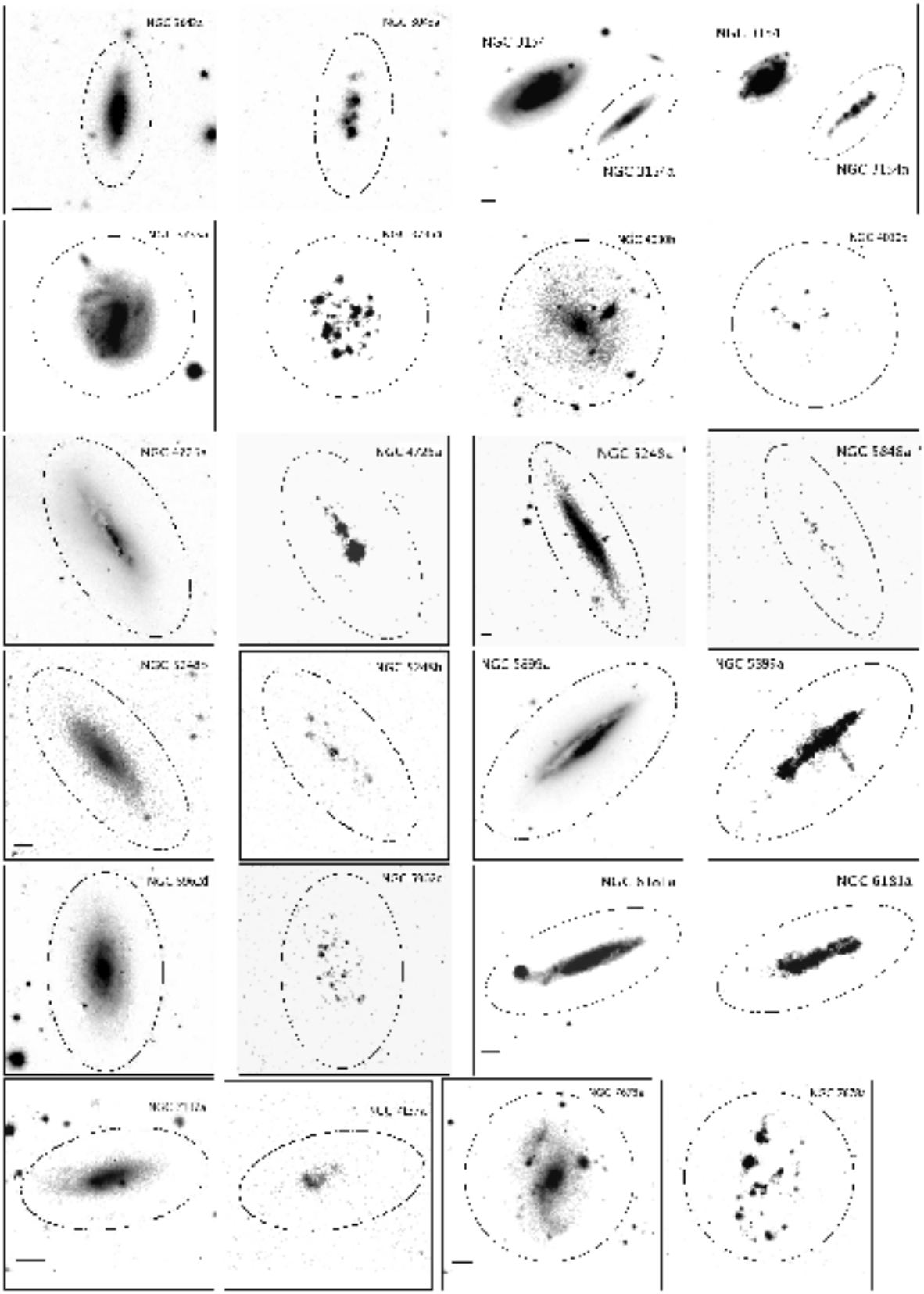

Fig. 6.2: Cont.

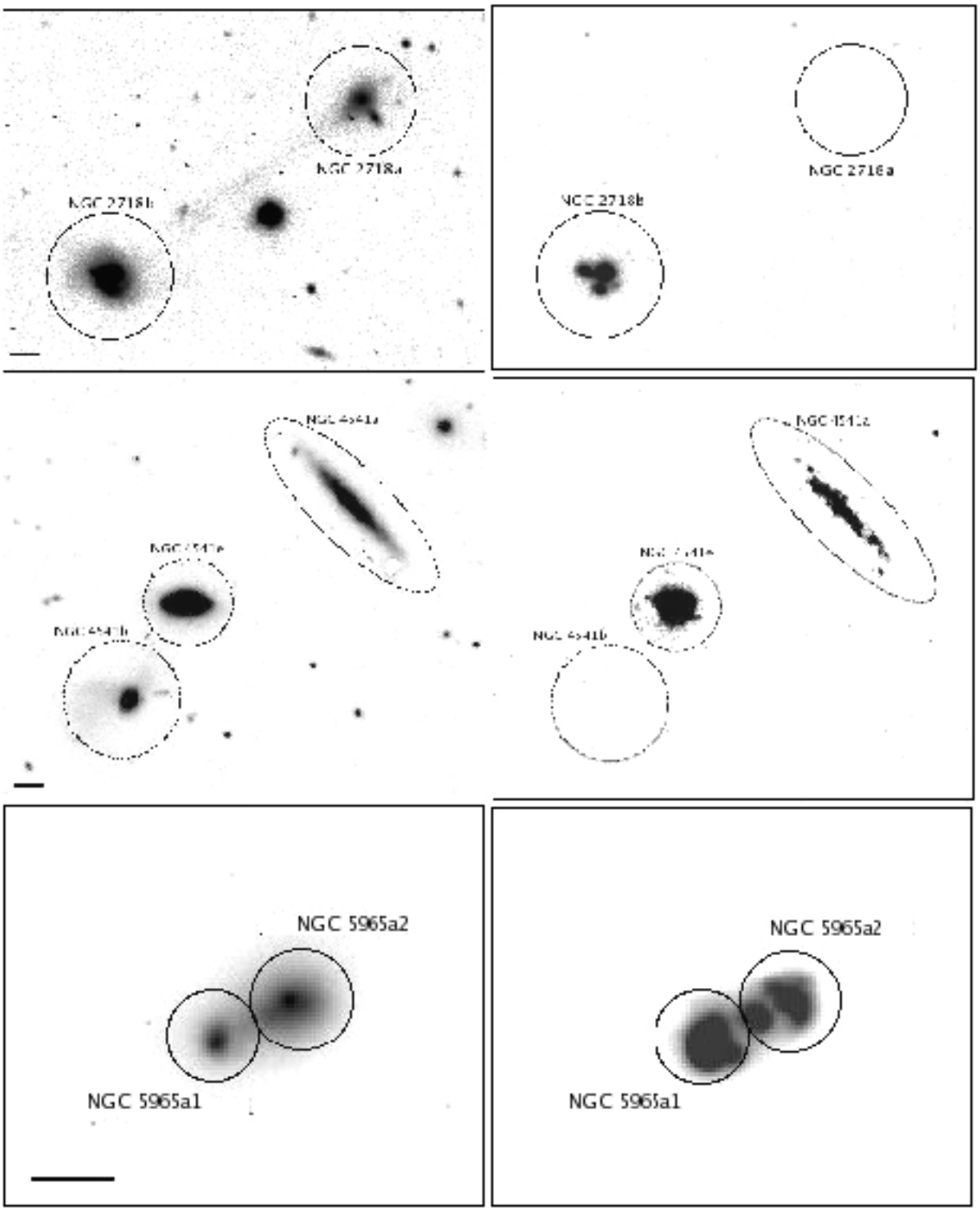

Fig. 6.3: Idem for the three pairs of interacting satellite galaxies: NGC2718a-b, NGC4541a, NGC4541b-e and NGC5965a_1-a_2.

which a fixed aperture was chosen, we checked that the estimated fluxes are similar to those computed with the subroutine PHOT of IRAF. For the absolute calibration and estimation of Hα emission, we followed the procedure detailed in Gil de Paz et al. (2003). Because of the width of our narrow filters, the emission also includes the contribution of [NII] for which an accurate subtraction would require spectroscopic observations.

One of the objects (NGC 4030b) was observed at two epochs (Dec 2001 and May 2002). We think that the $\sim$10% difference between the estimates of Hα fluxes in both observations (1.33 and 1.46 $\times 10^{-14}$ erg cm^{-2} s^{-1} for the observations of December and May respectively) are representative of the statistical uncertainty of our procedure. Another test was to observe the apparently non-interacting early-type galaxy NGC 1620b for which we do not in principle expect significant levels of star-forming activity. For this galaxy we estimate an Hα flux after continuum subtraction of -0.87×10^{-14} erg cm^{-2} s^{-1}, which in absolute value is well below any of the detections of Hα emission. We think that this negative value is not entirely due to the uncertainties in the estimate, but indicates Hα in absorption, as is commonly found in early-type galaxies (Kennicutt 1992).

The Hα equivalent widths (EWs) represent the ratio between the Hα emission and the continuum averaged over the full galaxy. Figure 6.4 shows the relation between the relative flux of the Hα emission and the morphological type. The mean values and 1σ dispersions in Hα EWs are 16.4 $\pm$ 5.1, 24.3 $\pm$ 9.6 and 18.9 $\pm$ 7.7, for types 2 (Irr), 3 (Sb/Sc), and 4 (Sa) respectively. The mean values found for the different morphological types of non-interacting objects are similar, and consequently we do not notice differences in Hα EWs with morphological types as found by other authors (e.g. Kennicutt 1998). The much higher Hα EWs values found for four of the satellites in interaction indicate that their activity is directly related to current interaction processes.

The Hα EWs were converted in fluxes ($f_{\mathrm{H}\alpha}$) following the calibration explained in Chapter 2 (Subsection 2.5.2); $f_{\mathrm{H}\alpha}$ was then converted into absolute luminosity according to $L_{\mathrm{H}\alpha} = 4\pi D^2 f_{\mathrm{H}\alpha}$. To estimate distances, we took the recessional velocity of the respective parent galaxy (the satellite is more affected by the peculiar velocities). In any case, the difference in the estimated luminosity would be relevant for only a few systems at very low redshift and with comparatively large differences in velocity between the parent and the satellite (NGC 4030b is the extreme case). For the Hubble constant we assumed $H_0 = 72$ km s^{-1} Mpc^{-1}. The Hα fluxes and luminosities are presented in Table 6.1. For the galaxies with Hα emission, the luminosities are in the range $\log L_{\mathrm{H}\alpha} = 38.85$-$41.66$ erg s^{-1}. The histogram with the distribution of Hα luminosities is presented in Figure 6.5.

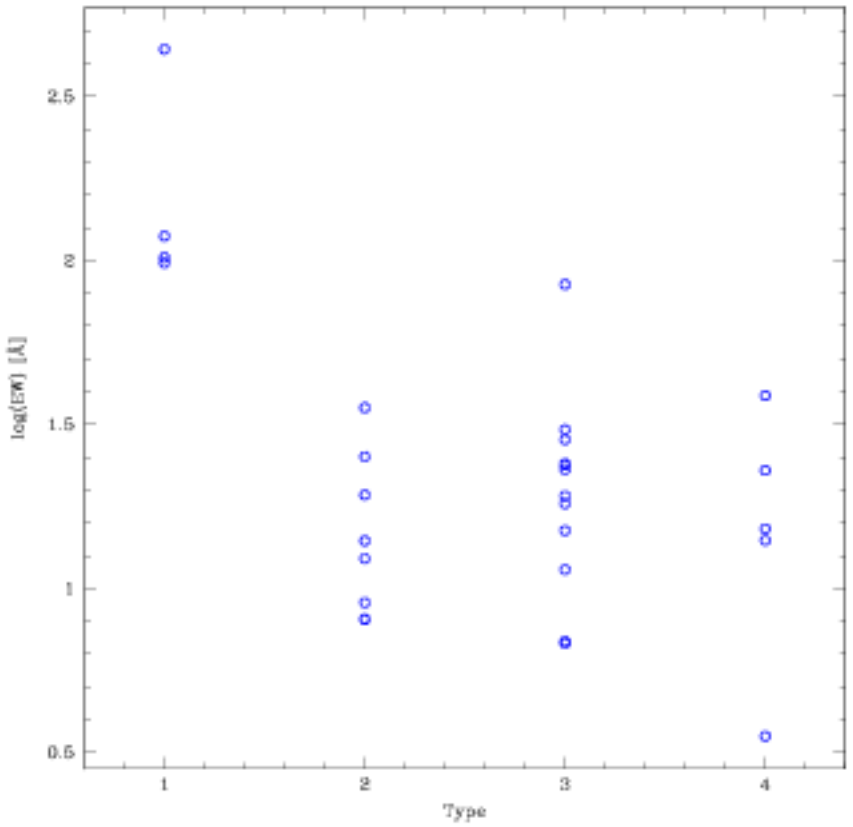

Fig. 6.4: $H\alpha$ equivalent widths as a function of the galactic type: (1) Objects in interaction, (2) Irregular, (3) Sb/Sc and (4) Sa.

To convert $L_{\mathrm{H}\alpha}$ to current star formation rates (SFRs), we use the calibration provided by Kennicutt (1998):

$$\mathrm{SFR}\ (M_{\odot}\ yr^{-1}) = 7.9 \times 10^{-42} L_{\mathrm{H}\alpha}\ \mathrm{erg\,s^{-1}}$$

,which assumes a Salpeter (Salpeter 1955) initial mass function between $10^{-1} - 10^{2}\ M_{\odot}$. Because we do not have observations of other Balmer lines (specifically Hβ) we did not apply any correction for internal extinction. The values obtained for the current SFR are presented in Table 6.2 column 2). Figure 6.6 shows SFR as a function of luminosity in the B band. A significant correlation (although with a large scatter) exists. A similar tendency was found in the sample of blue compact galaxies studied by Kong et al. (2002), and with the much larger sample of $\approx 10^{5}$ SDSS galaxies studied by Brinchmann et al. (2004). Four

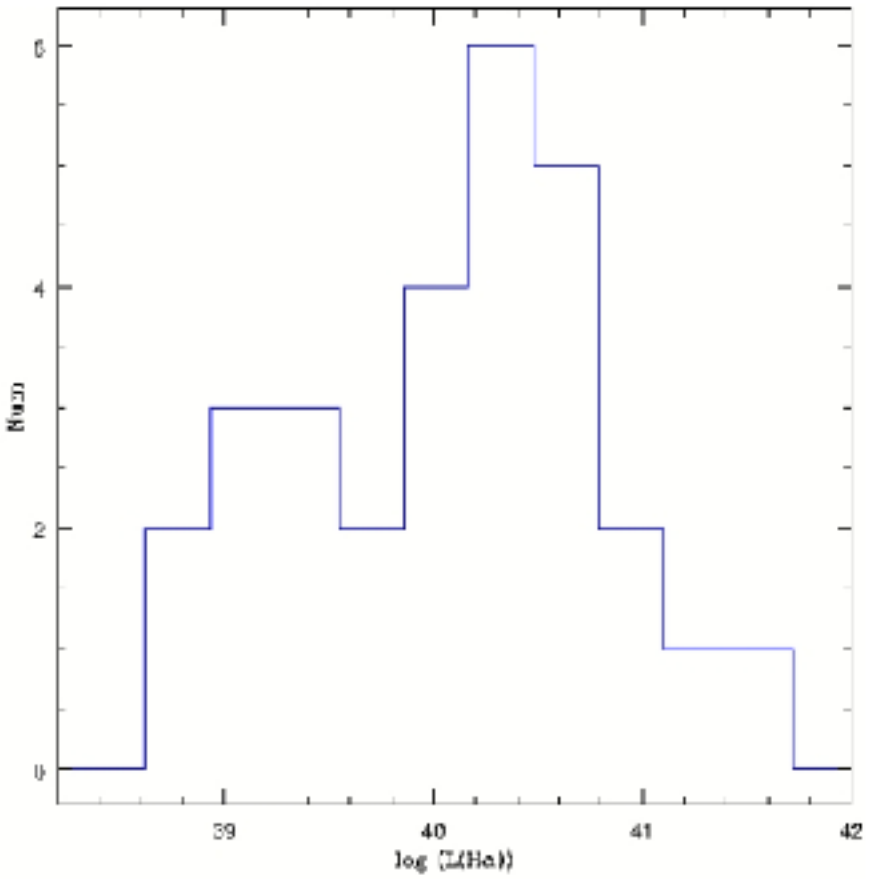

Fig. 6.5: Distribution of $H\alpha$ luminosities for the sample of satellite galaxies.

of the interacting satellite galaxies (indicated by filled circles in the figure) show a similar tendency, although they clearly have higher levels of star formation than non-interacting galaxies with similar luminosities.

6.5.1 Comparison with Previous Star Formation Rates Estimations

SFRs of some of the objects analysed in this research have been previously estimated by other authors. In some cases, their SFRs have been estimated from Hα measurements in narrow-band images or spectroscopy, while in others, SRFs have been obtained from observations in the far-IR or radio. Below we compare our results with these previous studies compiled from the literature.

- NGC 2718a and NGC 2718b: Mendez et al. (1999) have estimated a luminosity of

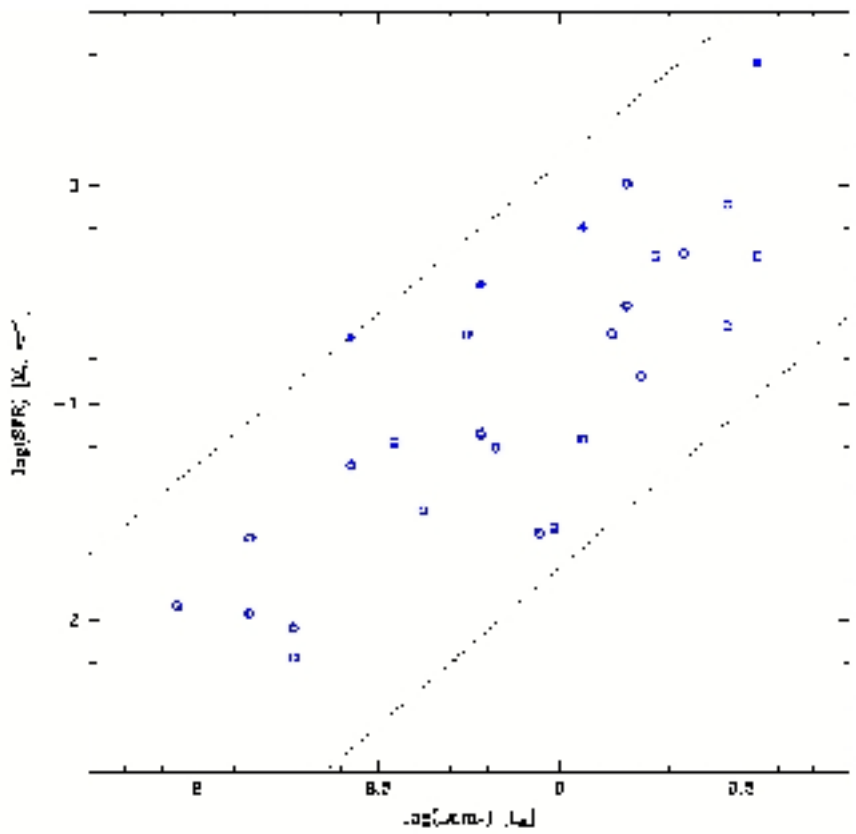

Fig. 6.6: Current star formation rate, SFR, estimated from the $H\alpha$ luminosities, as a function of luminosity in the $B-band$. Objects in interaction have been indicated by a filled circle.

40.87 erg s^{-1} for the component NGC 2718b, which is in agreement with our value of 40.91 erg s^{-1}. However, they derived an EW of 260 Å for the Hα emission of this galaxy, which is a factor $>$ 2 larger than our value. Our estimate of Hα EW for this galaxy is also $\sim$2.5 smaller than that presented by Kong et al. (2002) from long-slit observations. However, our EW and Hα luminosities agree with the estimates by Gil de Paz et al. (2003), 120 Å and 40.85 erg s^{-1} respectively. So, considering only the three measurements based on narrow-band imaging, it seems that the three estimates of the Hα luminosities are in agreement, but they are in clear disagreement with EWs derived from long-slit spectra. Although the reason for this discrepancy between the estimates obtained with each technique is unclear, it could be related to the irregular spatial distribution of the Hα features. This renders the extrapolation of the Hα intensity from the area covered by the long-slit to the whole galaxy inaccurate.

• NGC 5965a_1-a_2: The estimates carried out previously by other authors enclose the Hα flux for the whole system. For this, our estimate of the Hα flux is 27.2×10^{-14} erg s^{-1} cm^{-2}, which agrees well with the value of $30\pm3 \times 10^{-14}$ erg s^{-1} cm^{-2} measured by Gil de Paz et al. (2003). For this pair, Bell (2003) obtained an SFR of 0.8 $M_\odot$ yr^{-1} from radio measurements, while Hopkins et al. (2002) obtained 0.8 and 1.7 $M_\odot$ yr^{-1} from observations at 60 μm and 1.4 GHz respectively. However, these authors used a different distance to the galaxy (53.2 Mpc) instead of the value 47.6 Mpc that we have used. Converting our results to their distance scale, we would obtain SFR = 0.72 $M_\odot$ yr^{-1}, which is within 25% of the value derived by these authors from the luminosity at 60 μm. Given the different uncertainties and assumptions in each of the methods, we consider both estimates to be in very close agreement.

6.6 *Interactions and Star Formation*

In previous Chapters (3, 4 and 5) we have carried out statistical analyses of star formation in the samples of pair galaxies from the 2dFGRS and SDSS surveys, finding that objects with close neighbours tend to have a higher star formation activity than those that are isolated. This tendency is more efficient for pairs situated in low density regions. According to the studies by Sekiguchi & Wolstencroft (1992) and Donzelli & Pastoriza (1997), enhancement of the star formation activity is more likely to take place in both galaxies of the pair but tends to be higher in the fainter component. However, our analysis in Chapter 3, indicates that are the bright components in minor merger candidates those that show higher probability to have enhanced star formation.

Two basic types of interactions can be differentiated in the halos of giant galaxies; those between parent and satellites, and those between satellites. In theory both can produce morphological changes and mass losses, and affect the star formation activity in the interacting objects; for instance Knebe et al. (2005) by using N-body simulations have estimated that interactions between satellites can account for $\sim$30% of the total masses lost through their hectic existence.

Gutiérrez et al. (2002) pointed out two clear cases of interaction (NGC 2718a-b, NGC 4541b-e) between pairs of satellites. An additional pair (the two components of NGC 5965a) was also considered by Gutiérrez & Azzaro (2004). A relatively high fraction of other satellites in our sample show morphological signs that could be attributed to present or recent interaction (see Section 6.4 and Appendix A), but the possible companions have not been accurately identified. Our results confirm that interactions between satellites significantly

affect star formation activity.

According to Gutiérrez & Azzaro (2004) the difference in magnitudes between the two members of the pairs NGC 2718ab, NGC 4541be, and NGC 5965a_1a_2 are $\delta m \sim 1$ mag in the R band. In the first two cases, a high level of Hα emission is detected in just one member of the interacting system, NGC 2718b and NGC 4541e, which are brighter components of their respective pairs. The other two galaxies in these pairs, NGC 2718a and NGC 4541b are the only two members of the sample analysed that do not show Hα emission. These two galaxies are also the only objects in our sample that were classified as early types and have been included only as members of the interacting pairs. The filaments and bridges seen in pairs NGC 2718a-b and NGC 4541b-e do not show Hα emission either. We propose that in the case of NGC 2718a the presence of the bridge connecting this galaxy with the companion, and the comparatively large amount of gas (see next section) in NGC 2718b are signs of mass transfer from one galaxy to the other. This is probably inhibiting galaxy formation in the donor and enhancing it in the accreting galaxy. The stripping suffered by NGC 2718a could also be responsible for its morphological evolution toward early-type objects. The situation is more confusing for the pair NGC4541 b-e, where only one of the two plumes emerging from NGC 4541b seems to point towards NGC 4541e and there are no HI measurements in the literature for any of the two galaxies of the pair.

In the pair NGC 5965a_1-a_2 both members show a high level of star formation, the brighter galaxy (a_1) also being the one that has experienced the more intense SFR activity. In this case, the small projected spatial distance, the absence of tidal streams, or bridges and the elongation of the isophotes through the respective companion seem to indicate that these two galaxies are experiencing the first approximation and the gas is being strongly compressed.[1] We have also computed the Hα emission in an aperture enclosing both galaxies and obtained SFR = 0.576 $M_\odot$ yr^{-1}. This is $\sim$5% higher than the result obtained by just adding the Hα emission estimated for each component. Although compatible with the uncertainties of the method, this excess could also indicate the presence of some Hα residual emission in the intergalactic medium. The fact that in each of the interacting pairs the SFR activity is more intense in the brighter component is in agreement with our previous conclusions obtained in Chapter 3.

Our sample does not contain clear cases of interactions between satellites and parents, so

[1] We consider the two components of NGC 5965a to have velocities of 3357 and 3429 km s^{-1} for NGC 5965a_2 (SBS 1533+574A) and NGC 5965a_1 (SBS 1533+574B) respectively (Izotov, Y. 2005 priv. comm.). Apparently the recessional velocity quoted in the NED database for the component SBS 1533+574B is wrong.

that it is not possible to estimate the relevance of such interactions to star formation activity. We note, however, that NGC 3154a, which is the object in our sample that has the smallest projected distance from its progenitor (19 kpc), is one of the more active satellites forming stars. However, we did not detect special signs of morphological distortion in this satellite.

We can roughly check if the abundance of interacting pairs found is reasonable according to the expectations of numerical simulations in CDM models. Knebe et al. (2004) have estimated that the mean number of satellites that have at least an encounter per orbit with other satellites depends on halo age, and ranges from $\sim$4% (for old halos) to $\sim$58% (for young halos). These encounters tend to be more frequent and faster in the internal parts of halos. The three interacting pairs found in a sample of $\sim$60 satellites studied by Gutiérrez & Azzaro (2004) would then require very low velocity encounters, with interactions lasting $\sim$1/2–1/8 of the orbital period. This seems to contradict the observed differences in radial velocities ($\sim$50–90 km s^{-1}), and projected distances ($\leq$ 20 kpc) between both members of each pair. However, larger statistical samples are needed to make a more robust assessment.

6.7 *Current vs. Past Star Formation Rates*

The star formation history for satellites in CDM halos have been considered by Mayer et al. (2001). These authors show that high and low surface brightness and galaxies (HSB and LSB respectively) react differently to the interaction with the central galaxy. In LSB satellites, bursts of activity occur after each pericentric passage, while in HSB satellites the first burst consumes most of the gas. In both cases the activity is very inhomogeneous over cosmological times. Following the method proposed by van Zee (2001) it is possible to estimate the average star formation rate over the Hubble time from the total mass of stars formed. The resulting $\langle SFR \rangle_{\rm past}$ for the galaxies in our sample are presented in Table 6.2 column 3, and are in the range $\sim$0.04–1.04 M$_\odot$ yr^{-1}. For most of the galaxies, these values are larger than the current star formation rates as estimated from the $H\alpha$ luminosities. The normalized distributions of the current and past SFR are shown in Figure 6.7. It is worth noting that the current SFR spans a large range of values extending the distribution to very low values. The histogram of $\langle SFR \rangle_{\rm past}$ looks sharper and shifted to higher values. The mean value of the birthrate parameter $b = SFR_{\rm current}/\langle SFR \rangle_{\rm past}$ (the ratio between present and average past star formation rates) is largely conditioned by the high values of the starbursting interacting systems, so we consider the median 0.68 as more representative of the general distribution.

The absolute magnitude of each satellite vs. $\log b$ is shown in Figure 6.8. The region with higher values of the b parameter is occupied by the four starbursting interacting galaxies and

by NGC 3154a. The b values for these galaxies are in the range 3–9. We notice a weak trend in the sense that brighter satellites seem to have a comparatively higher current activity; in fact, four of the five brightest galaxies (excluding the interacting systems) have $b \sim 1$, which seems to indicate that these galaxies are still able to maintain now their mean past star formation rate. The global tendency of decline in star formation rate with cosmological time is expected according to simulations by Mayer et al. (2001). The values of b for any of the morphological types (excluding the interacting systems) spread roughly over an order of magnitude, which probably indicates a great variety of star formation histories. The distribution of b (see Figure 6.7) is qualitatively similar to that found by van Zee (2001). We do not notice any clear differences between the different morphological types, but given the small size of the sample we have not tried to quantify this accurately.

Another way to compare the relevant time scales for the star formation evolution is by computing how much time (t_{form}) the galaxy would have needed to form all the stellar content at the current star rate, and what is the maximum time (t_{gas}) that the galaxy can continue forming stars at the current rates. The analysis of this in conjunction with optical luminosities and current star formation allow a first approximation to the evolution of the galaxy over cosmic times. An accurate limit for t_{gas} can be estimated simply dividing the current gas content by the current star formation rate. This of course would correspond to an ideal case in which all the gas would be converted into stars, and no losses or accretion occurred. Using the LEDA database,[2] we have compiled the existing HI measurements as a way to estimate the gas content in each galaxy. These are presented in Table 6.2 column 4. The values of t_{gas} indicate that the current gas content would be enough to fuel the star formation at the current star formation rate at least during another Hubble time. For about one third of the galaxies t_{form} exceeds the Hubble time, so that we conclude again that on average the star formation rate was higher in the past. As expected, the starbursting galaxies NGC 2718b, NGC 4541e and NGC 5965a$_1$, and NGC 5965a$_2$ are among the objects with the lowest formation times (also NGC 3154a, which is the satellite galaxy in our sample closest to their parent).

Previous studies (e.g., Casoli et al. 1996) have shown that star formation rate in spiral galaxies is correlated with the mass of molecular and atomic gas. Our results confirm that relation as illustrated in Figure 6.9. The correlation extends along one and two orders of magnitude in gas mass and star formation rate, respectively. NGC 2718b, one of the interacting galaxies has the largest SFR in the sample and is also one of the galaxies with higher gas content. This seems to reinforce the scenario of significant accretion of gas from NGC 2718a

[2] http://leda.univ-lyon1.fr/

as outlined in a previous section.

Figure 6.10 presents t_{gas} vs. $t_{formation}$, for our sample of satellite galaxies and compares these time scales with those for other four samples taken from the literature: the Sculptor group dIrrs studied by Skillman et al. (2003), the Local Group dIrrs of Mateo (1998), the gas-rich low surface brightness galaxies studied by van Zee et al. (1997), and the isolated dIrrs of van Zee, (2000, 2001). The figure shows a clear, direct correlation between both time scales. The range of magnitudes and the selection effects are different for each sample so that it is difficult to extract statistical conclusions, although all the samples tend to follow common tendencies.

6.8 Summary

We have carried out a detailed analysis of narrow-band observations of the Hα emission in a sample of 31 satellites orbiting isolated giant spiral galaxies. The objects studied span the range $-19 < M_B < -15$ mag. and were selected according to the relative brightness (at least 2.2 magnitudes fainter than their parents), projected distances (< 500 kpc) and relative velocity (< 500 km s^{-1}) from the primaries. We have presented imaging and photometry in a narrow filter band covering the position of the Hα line. The results can be summarized as follows:

- In all the spirals and irregular satellites (29 objects) we detected $H\alpha$ fluxes above 1.15-49.80 x 10^{-14} erg s^{-1} cm^{-2}. The inferred current star formation rates are in the range 0.006–3.66 $M_\odot$ yr^{-1}.

- There are three cases of clear interacting pairs. Four of the galaxies in these pairs are among the objects with higher star-forming activity. In contrast, the only two galaxies of the sample that are not forming stars are also members of these pairs. We do not detect Hα emission in the filaments associated with these interactions.

- The object with a largest current star formation rate (apart from the interacting systems) corresponds to the satellite galaxy NGC 3154a, which has the smallest projected distance from its progenitor (19 kpc) and the SFR could be due to interaction with the parent galaxy.

- The median of the birth parameter b is 0.68, indicating a fall in activity with cosmic time, assuming perfect efficiency, the current gas content of the galaxies is enough to fuel this activity for more than another Hubble time.

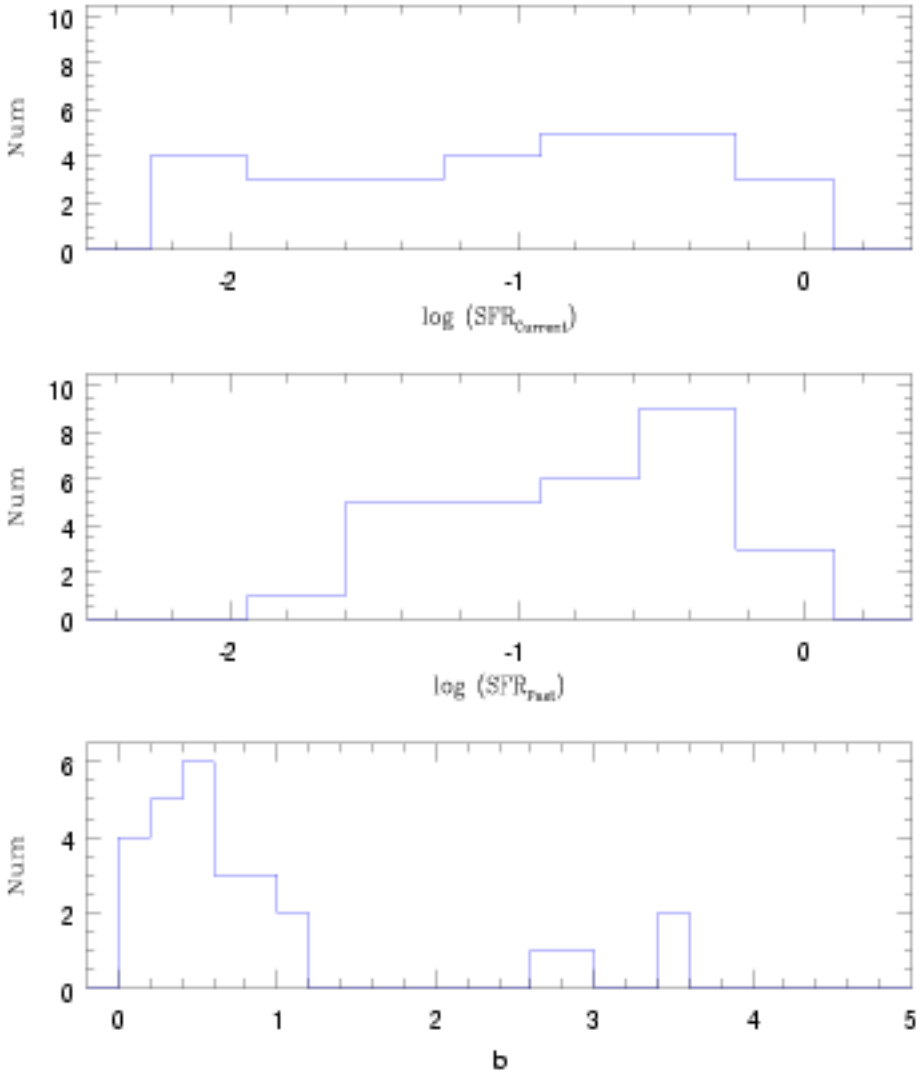

Fig. 6.7: Distribution of current (*top*) and past (*center*) star formation rates, for the sample of satellite galaxies. The bottom box shows the distribution of stellar birthrate parameter, $b = SFR_{Current}/\langle SFR \rangle_{Past}$.

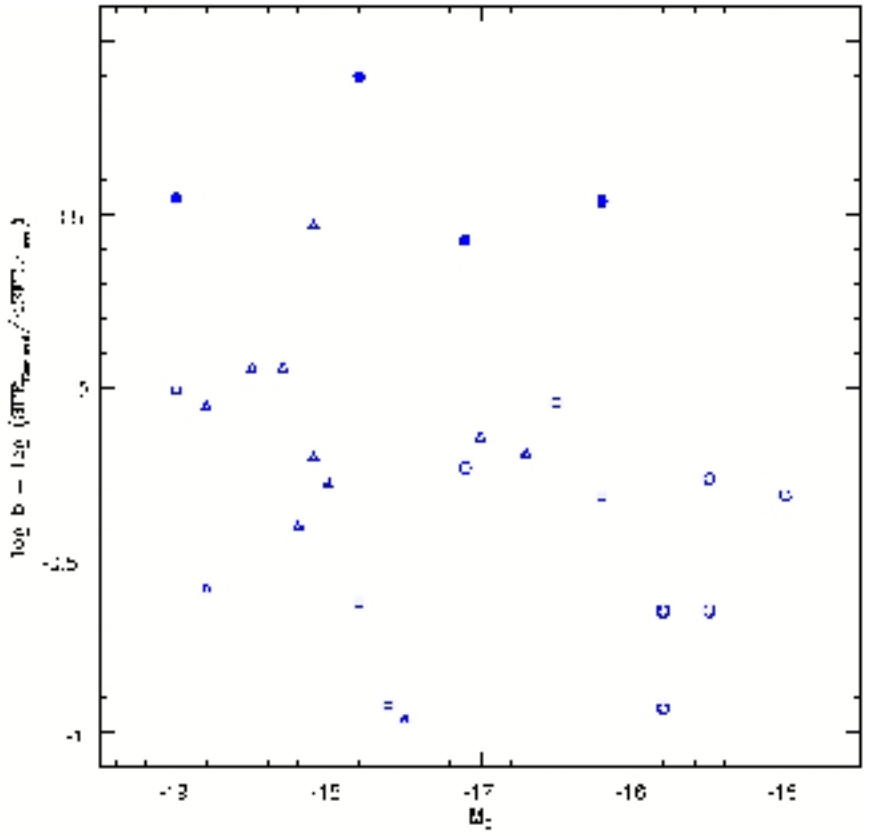

Fig. 6.8: Stellar birthrate parameter as a function of the absolute magnitude (M_B), in satellite galaxies for different Hubble morphological types: Irregulars (*open circles*), Sb/Sc (*open triangles*) and Sa (*open squares*). Interacting galaxies are indicated by filled symbols.

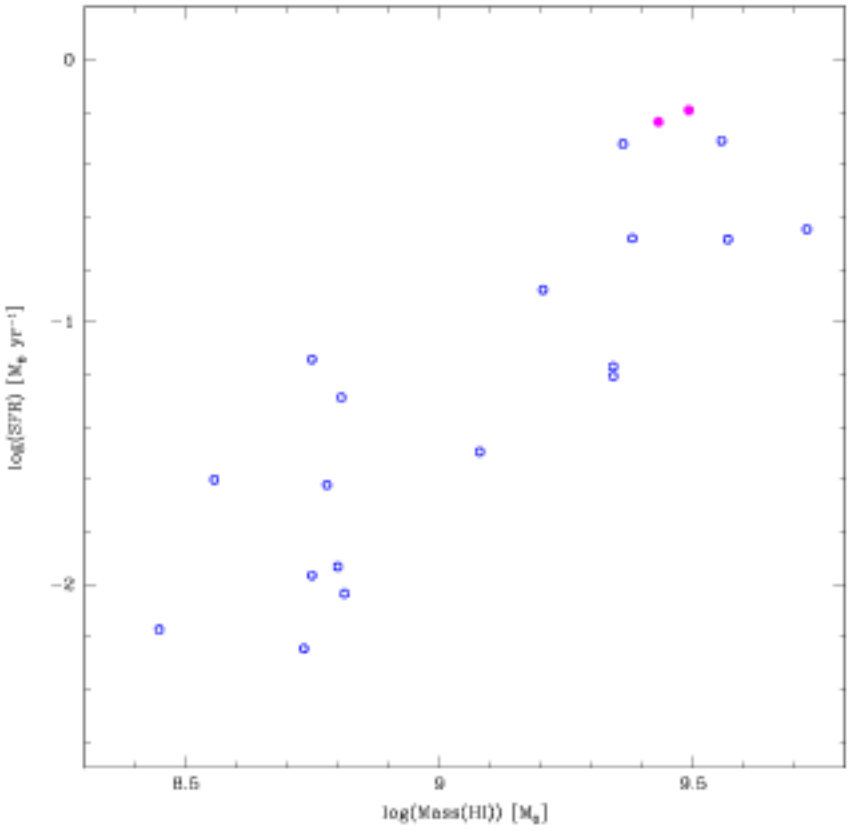

Fig. 6.9: Current star formation rate, SFR, estimated from Hα measurement, vs. HI mass of the gas. Interacting galaxies, NGC 2718b and NGC 5965a (computed in an aperture enclosing both galaxies, NGC 5965a$_1$ and a$_2$), are indicated by filled symbols.

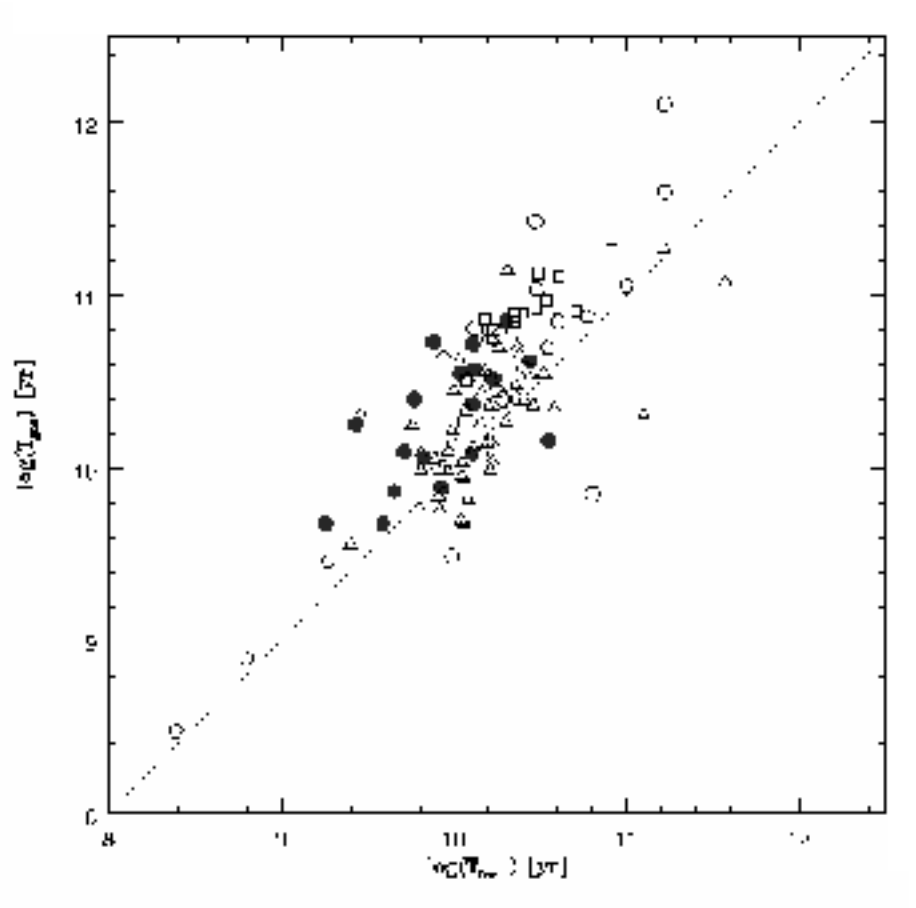

Fig. 6.10: Comparison between the ratio of the gas mass to the current SFR ($T_{\rm gas}$) and the ratio of the luminosity to the current SFR (T_{form}), for the satellite galaxies (filled circles), and four samples taken from the literature: the Sculptor group dIrrs studied by Skillman et al. (2003) (open circles), the Local Group dIrrs of Mateo (1998) (open pentagons), the gas rich low surface brightness galaxies studied by van Zee et al. (1997) (open squares), and the isolated dIrrs of van Zee, (2000, 2001) (open triangles).

Tab. 6.1: $H\alpha$ equivalent width, fluxes and $H\alpha$ luminosities

Galaxy	r_p (kpc)	$EW_{H\alpha}$ (Å)	H_α Flux (10^{-14} ergs cm^{-2} s^{-1})	log L(Hα) (ergs s^{-1})
NGC 488c	116	8.07	1.15	39.13
NGC 772b	390	13.97	2.15	39.48
NGC 772c	429	15.19	4.63	39.81
NGC 1517a	130	23.76	9.33	40.41
NGC 1620a	227	8.03	2.75	39.89
NGC 1961a	214	6.89	7.97	40.45
NGC 1961b	139	15.01	9.90	40.55
NGC 1961c	120	28.42	29.00	41.01
NGC 2424b	182	35.52		
NGC 2718a	102	-11.64		
NGC 2718b	82	118.58	23.80	40.91
NGC 2775a	401	23.99	9.53	39.61
NGC 2775c	64	19.26	21.40	39.96
NGC 2916a	71	14.01	2.66	39.93
NGC 3043a	263	38.72	4.02	39.92
NGC 3154a	19	84.40	13.00	41.11
NGC 3735a	192	3.54	2.01	39.53
NGC 4030b	414	23.03	1.46	38.85
NGC 4541a	193	22.89	5.48	40.78
NGC 4541b	228	-1.29		
NGC 4541e	217	101.22	42.10	41.66
NGC 4725a	132	11.41	49.80	40.22
NGC 5248a	150	9.05	3.78	39.06
NGC 5248b	164	12.33	2.76	38.93
NGC 5899a	106	19.14	40.80	40.79
NGC 5962d	89	6.80	3.58	39.50
NGC 5965a$_1$	532	440.68	16.50	40.64
NGC 5965a$_2$	532	102.03	9.41	40.40
NGC 6181a	257	30.49	46.40	40.78
NGC 7137a	64	25.21	2.24	39.17
NGC 7678a	165	18.15	9.36	40.42

* Observation for NGC 2424a were not taken in photometric conditions.

Tab. 6.2: HI mass, star formation properties and time scales

Galaxy	SFR ($M_\odot$ yr^{-1})	$\langle SFR \rangle_{Past}$ ($M_\odot$ yr^{-1})	log M_{HI} ($M_\odot$)	t_{gas} (Gyr)	t_{form} (Gyr)
NGC 488c	0.011	0.048	8.75	51.9	12.9
NGC 772b	0.024	0.044	8.78	25.1	5.8
NGC 772c	0.051	0.107	8.80	12.4	5.1
NGC 1517a	0.206	0.290	9.57	17.9	2.7
NGC 1620a	0.062	0.149	9.35	35.5	10.7
NGC 1961a	0.225	0.867	9.73	23.5	12.9
NGC 1961b	0.279	0.447			5.5
NGC 1961c	0.817	0.938			3.6
NGC 2424b		0.048	9.05		
NGC 2718a		0.221			
NGC 2718b	0.640	0.081	9.50	4.8	1.8
NGC 2775a	0.032	0.050	9.06	37.6	13.1
NGC 2775c	0.072	0.123	8.74	7.8	8.4
NGC 2916a	0.067	0.285	9.34	32.5	17.2
NGC 3043a	0.066	0.073			
NGC 3154a	1.016	0.347			1.5
NGC 3735a	0.027	0.222			36.1
NGC 4030b	0.006	0.132	8.74	95.0	128.7
NGC 4541a	0.476	0.486			7.3
NGC 4541b		0.382			
NGC 4541e	3.659	1.043			1.0
NGC 4725a	0.132	0.336	9.21	12.0	12.6
NGC 5248a	0.009	0.041	8.82	70.6	19.9
NGC 5248b	0.007	0.057	8.45	41.7	27.3
NGC 5899a	0.489	0.434	9.56	7.3	4.5
NGC 5962d	0.025	0.230	8.56	14.4	35.1
NGC $5965a_1$	0.350	0.132			1.7
NGC $5965a_2$	0.200	0.058			1.3
NGC 6181a	0.476	0.421	9.36	4.8	3.8
NGC 7137a	0.012	0.024	8.80	54.0	7.5
NGC 7678a	0.208	0.400	9.39	11.5	6.7

* HI data were collected from the LEDA catalog

CHAPTER 7

ACTIVE GALACTIC NUCLEI AND GALAXY INTERACTIONS

7.1 Abstract

We perform a statistical analysis of active galactic nuclei (AGN) host characteristics and nuclear activity for AGNs in pairs and without companions. Our study concerns a sample of AGNs derived from the SDSS-DR4 data by Kauffmann et al. and pair galaxies obtained from the same data set in Chapter 2. An eye-ball classification of images of 1607 close pairs (r_p <25 kpc h^{-1}, $\Delta V < 350$ km s^{-1}) according to the evidence of interaction through distorted morphologies and tidal features provides us with a more confident assessment of galaxy interactions from this sample. We notice that, at a given luminosity or stellar mass content, the fraction of AGNs is larger for pair galaxies exhibiting evidence for strong interaction and tidal features which also show sings of strong star formation activity. Nevertheless, this process accounts only for a $\sim 10\%$ increase of the fraction of AGNs. As in previous studies, we find AGN hosts to be redder and with a larger concentration morphological index than non-AGN galaxies. This effect does not depend whether AGN hosts are in pairs or in isolation. The OIII luminosity of AGNs with strong interaction features is found to be significantly larger than that of other AGNs, either in pairs or in isolation. Estimations of the accretion rate, $L[OIII]/M_{BH}$, show that AGNs in merging pairs are actively feeding their black holes, regardless of their stellar masses. We also find that the luminosity of the companion galaxy seems to be a key parameter in the determination of the black hole activity. At a given host luminosity, both the OIII luminosity and the $L[OIII]/M_{BH}$ are significantly larger in AGNs with a bright companion ($M_r < -20$) than otherwise.

7.2 Introduction

We have seen in previous Chapters that, galaxy-galaxy interactions are an effective mechanism to regulate the star formation activity in galaxies. Our studies of galaxies in pairs showed, with high statistical signal that star formation is enhanced by a factor of two in close systems (Chapters 3 and 4).

The physics behind the triggering of star formation activity during galaxy-galaxy interactions have been explained by theoretical (Martinet 1995 and references there in) and numerical analysis (e.g. Toomre & Toomre 1972; Barnes & Hernquist 1992, 1996; Mihos & Hernquist 1996). These studies showed that the starbursts are fueled by gas inflows produced by the tidal torques generating during the encounters. The efficiency of this mechanism depends on the particular internal characteristics of galaxies and their gas reservoir.

By producing gas inflows, galaxy interactions may efficiently feed a central black hole and faster AGN activity (Sanders et al. 1988). The co-evolution of galaxies and black holes is now widely accepted, although many details on how this coexistence works are still understudied (Heckmann et al. 2004). Toomre & Toomre (1972) suggested that collisional disruption and gas dissipation could feed the nuclear activity of galaxies. Other ideas about the fueling of active galaxy nucleus are the disk of barred galaxies generated by internal instabilities which can lead the gas to the centre of galaxies (Schwartz 1981, Shlosman, Begelman & Frank 1990) and the presence of more that one supermassive black hole which seems likely in the nucleus of merger remnants (Begelman, Blanford & Rees 1980).

Certainly, all these processes may provide clues to solve the AGN fueling problem. However, the AGN-galaxy interaction paradigm has been the issue of several studies which aim at determining, for example, the frequency of AGNs in a sample of interacting galaxies, the proximity effects of a close companion on the AGN power, etc. Dahari (1985), in a sample of 167 systems, found that there is an excess of Seyferts among spiral interacting galaxies and also that Seyfert activity and the existence of external tidal forces are interrelated. However, Seyfert nuclei were not found in interacting ellipticals. From a statistical study of companions of Seyfert galaxies, Fuentes-Williams & Stocke (1988) derived that Seyfert galaxies have a marginal excess of comparable size companions and a clear excess of faint companions. However, Keel (1996) found that the presence of AGN does not seem to be related to the type of collisional interaction.

Conversely Schmitt (2001) analysed a sample of different types of active galaxies such as LINERS, transition galaxies, absorption-line galaxies, Seyfert and HII galaxies. This author showed that galaxies of different activity types are similar in percentage of companions to

galaxies of similar morphological types with no nuclear activity. This result suggests that interactions between galaxies are not a necessary condition to trigger the nuclear activity in AGNs. Similar results were found by Kelm, Focardi & Zitelli (2004) by studying a sample of Seyfert in UZC-Compact Groups and by Coldwell & Lambas (2006) who analysed the percentage of close companions of SDSS quasars within the range $r_p < 100$ kpc h^{-1} and $\Delta V < 350\,\mathrm{km\ s^{-1}}$.

An interesting approach to study the role of interactions on the feeding of both star formation and black holes is to study AGN activity in galaxy pairs. In fact, Storchi-Bergmann et al. (2001) found a correlation between active galactic nucleus and star formation activity in interacting galaxies by analyzing 35 Seyfert 2 nuclei. The galaxy spectral information available in large surveys provides unique information and high statistical numbers to study on more robust basis the relation between these processes. In this Chapter, we combine the galaxy pair catalog (SDSSGPC) constructed in Chapter 2, from the Fourth Data Release Sloan Digital Sky Survey (SDSS-DR4) with a sample of 88000 narrow-line AGN selected by Kauffmann et al (2003, hereafter K03) from the SDSS-DR4, which is hitherto the largest sample of AGNs.

In section 7.3, we briefly describe the AGN and pair catalogs. Section 7.4 analyses the properties of hosts of Type-2 AGN galaxies. Section 7.5 provides a comparative statistical analysis of AGNs in pairs and without companions with the aim of unveiling the role of interactions in triggering AGN activity. In section 7.6 we give our main conclusions.

7.3 AGN SDSS-DR4 Data

From SDSS-DR4, K03 have constructed a catalog with a subset of 88178 narrow emission line galaxies that are classified as AGN, within redshift range $0.02 < z < 0.3$.

Considering the unified model (Antonucci 1993), AGNs can be separated into two categories: Type 1 AGN where the black hole and the associated continuum and broad emission-line region is viewed directly and Type 2 AGNs where only the narrow line region can be observed due to the obscuring medium. The Baldwin, Phillips & Terlevich (BPT, 1981) line-ratio diagram allows us to distinguish type 2 AGNs from normal star forming galaxies by considering the intensity ratios of two pairs of relatively strong emission lines. The sample of Type 2 AGN of K03 was selected taking into account the relation between spectral lines, $[OIII]\lambda5007, H\beta$, $[NII]\lambda6583$ and $H\alpha$ luminosities, where an AGN is defined if

$$log([OIII]/H\beta) > 0.61/(log([NII/H\alpha]) - 0.05) + 1.3. \qquad (7.1)$$

We then use 88000 Type 2 AGNs in K03 catalog. The luminosity of $[OIII]\lambda5007$ emission line will be used as a tracer of AGN activity.

7.3.1 SSDS Close Galaxy Pair Catalog

In Chapter 2 we selected galaxies in pairs adopting projected relative distance and relative velocity thresholds: $r_p < 100$ kpc h^{-1} and $\Delta V < 350$ km s^{-1}. We found that these limits are adequate to define galaxy pairs with enhanced star formation activity. In Chapters 3, 4 and 5, we also detected a clear correlation between star formation activity and the proximity to a close neighbour supporting the physical scenario where tidal torques generated during the interactions trigger gas inflows, feeding the star formation activity.

For the purpose of analysing the effects of close interactions, which are known to produce the strongest effects, we selected close pair galaxies by requiring $r_p < 25$ kpc h^{-1} and $\Delta V < 350$ km s^{-1}. With this further restriction to closer relative separations, the effects of interactions are largely increased as shown in Chapter 3. Galaxy pairs are only selected within a redshift range $0.01 < z < 0.10$ in order to avoid strong incompleteness at larger distances as well as significant contributions from peculiar velocities at low redshift. The final close pair catalog in the SDSS comprises 1607 close galaxy pairs. Following the procedure explained in previous Chapters, we constructed a control sample by selecting those galaxies without a close companion within $r_p < 100$ kpc h^{-1} and $\Delta V < 350$ km s^{-1}. The control sample is also required to have the same redshift and magnitude distribution as our close galaxy pair catalog.

As discussed in Chapter 2, the effects of incompleteness or aperture (e.g see also Balogh et al.2004) do not introduce important bias in the galaxy pair catalogs. Regarding incompleteness, by combining the spectroscopic and photometric surveys, we estimated that the spectroscopic catalog has an incompleteness of only $\approx 9.5\%$. Hence, neither effect is expected to have a strong impact on our close galaxy pair catalog.

7.4 The Hosts of Type 2 AGNs in Galaxy Pairs

As a first step, we identified AGN hosts in our close pair catalog (i.e. pairs with $r_p < 25$ kpc h^{-1} and $\Delta V < 350$ km s^{-1}) by cross-correlating it with the AGN catalog. We found 498 galaxy pairs with one member exhibiting AGN activity. This represents $\approx 30\%$ of the total close pair catalog. We also detected that 108 close pairs have both members classified as AGNs ($\approx 7\%$). Then, the final SDSS-DR4 AGN-pair catalog comprises 606 pairs.

For the purpose of properly assessing the significance of the results obtained from AGN galaxies in pairs, we defined a sample of isolated AGN galaxies from the SDSS by selecting those galaxies without a companion galaxy within $r_p < 100\,\mathrm{kpc\,h^{-1}}$ and $\Delta V < 350\,\mathrm{km\,s^{-1}}$, within the same redshift range of the AGN close pair catalog. The procedure followed to construct the sample of isolated AGN galaxies assures that it has the same selection effects as the AGN galaxy pair sample, and consequently, it can be used to estimate the actual difference between AGN galaxies in pairs and isolated AGNs, unveiling the effect of the interactions. A similar reasoning motivated the definition of a non-AGN galaxy sample with the same luminosity distribution as galaxies in the AGN-pair catalog.

The distributions of absolute magnitude in r-band (M_r) and stellar mass (M^*), of AGNs in pairs, isolated AGNs, and a control sample of non-AGN galaxies with a similar luminosity distribution as the hosts of AGNs are shown in Fig.7.1. It can be seen that the luminosity distribution is similar in the three samples, but the fraction of large stellar mass objects among AGN hosts is larger than that of non-AGN hosts: the percentage of galaxies with $log(M^*) > 11$ is 15.8% for AGNs in pairs, 19.7% for isolated AGNs and 9.8% for non-AGN hosts. In fact, there are very few AGNs in galaxies with $M^* < 10^{10}\ M_\odot$. As it is well know, the majority of low mass galaxies have young stellar populations and a significant fraction are currently experiencing strong star formation activity.

In Fig.7.1*c*, we plotted the $(u-r)$ distributions for the same samples. As it can be appreciated from this figure the colour distribution of the control sample of non-AGN galaxies is clearly bimodal, as expected (e.g. Baldry et al. 2004). However, AGNs, regardless of being in pairs or in isolation, have $(u-r)$ colours consistent with a red host population. Fig.7.1*d* shows the concentration parameter distribution, C, defined as the ratio between the radii enclosing 90% and 50% of the galaxy light in the Petrosian r-band. Recall that Strateva et al. (2001) found that galaxies with $C > 2.5$ are mostly early-type galaxies, whereas spirals and irregulars have $2.0 < C < 2.5$. From the distributions of Fig.7.1*d*, it can be appreciated that AGNs reside preferentially in bulge dominated galaxies in contrast to the control sample of non-AGN galaxies which show the expected C bimodality.

In Fig.7.2 we show the BPT diagnostic diagram, plotting the $[OIII]\lambda5007/H\beta$ ratio versus $[NII]\lambda6583/H\alpha$ ratio for AGN pair galaxies and AGNs without a near companion. As it can be appreciated, there is not an evident difference between isolated AGNs and AGNs in pairs.

Hence, colours, morphology as measured by C, or luminosity, do not provide evidence that interactions could play a role in the triggering or regulation of the AGN activity. AGN

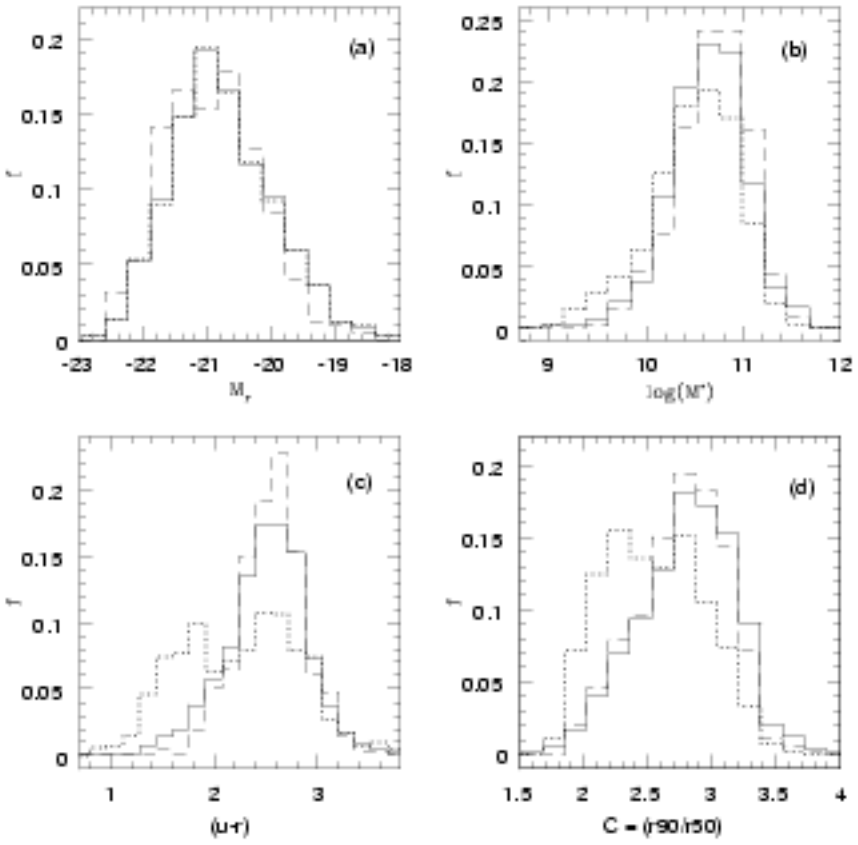

Fig. 7.1: (*a*) r-band absolute magnitude, (*b*) Mass in stars , (*c*) $u-r$ colour and (*d*) Concentration parameter distributions. Solid lines correspond to AGNs in pairs, dashed lines to AGNs without companions, and dotted lines to a control sample of non-AGN galaxies with a similar luminosity distribution than AGNs.

hosts show similar distributions regardless of the presence of a close companion. Howevet, taking into account previous results such as those of Storchi-Bergmann et al.(2001), a clear signal of correlation between AGN activity and interactions could be detected by restricting to active star forming systems. In our previous studies of galaxies in pairs we found that there is an important fraction of galaxies that, although being close in projected space, do not exhibit strong star formation activity. It is very unlikely that at these close projected distances ($r_p < 25$ kpc h^{-1} and $\Delta V < 350$ km s^{-1}) pairs could be strongly affected by interlopers (Chapter 4; Pérez et al. 2006). However, it is possible that, owing to particular characteristics of the projected separation and relative radial velocity or internal structure, these pairs do not experience strong tidal torques that can drive gas inflows. Motivated by

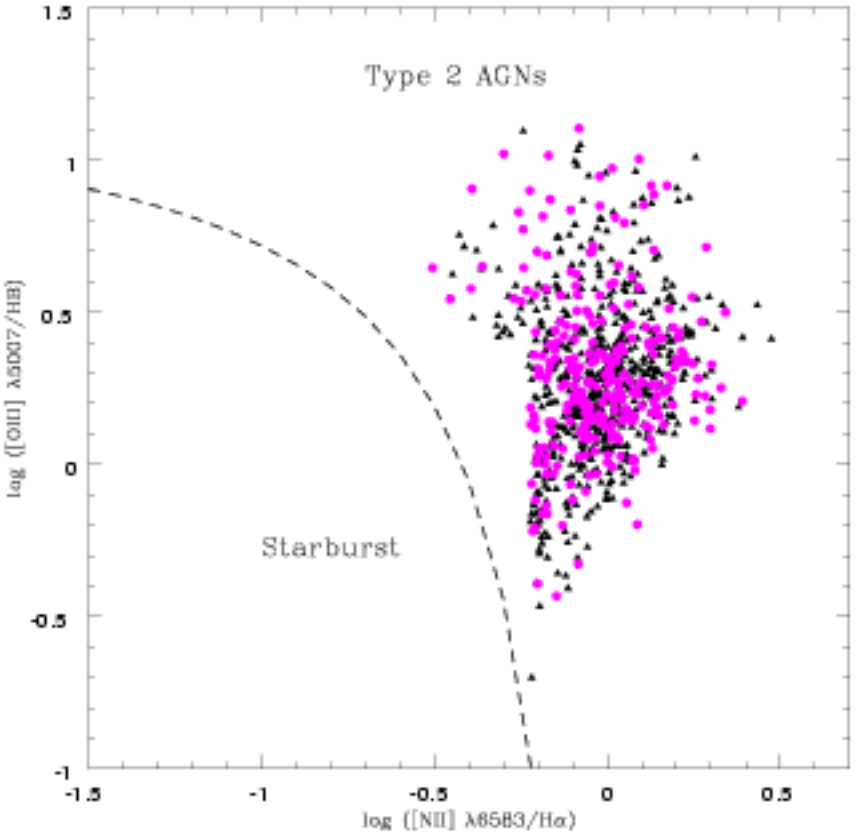

Fig. 7.2: BPT diagnostic diagram. The filled circles correspond to AGN pair galaxies and filled triangles to AGNs without companions. The dashed curve represents the bondary between starburst galaxies and Type 2 AGNs defined by Kauffmann et al. (2003).

these facts, in the next Section we discuss a new classification for close galaxy pairs based on a visual morphological analysis of their members.

7.4.1 Classification of Pair Galaxies

By using the photometric SDSS, we classified all galaxies in the close pair catalog taking into account the eye-ball detection of features characteristic of interactions.

Three categories have been defined:

- Pairs with evidence of an ongoing merging process (*m*: merging pairs)
- Pairs with signs of tidal interactions but not necessarily merging (*t*:tidal pairs)

- Pairs showing no evidence of distorted morphologies (n: non-interacting pairs).

Fig.7.3 shows images of typical examples of close pair galaxies for the three different visual classification: m, t and n. Hereafter we will carry out the analysis by distinguishing them according to these categories. Note that although the m category refers to systems in advanced stages of interactions, both components could be still individualized by the SDSS survey.

Analysis of deblending for merging pair galaxies

In order to analyse the effects of how reliable the SDSS photometric deblending procedure works in merging galaxy pairs (m) for which we expect the largest uncertainties, we have carried out suitable tests to determine independent magnitudes for this sample.

For this purpose we have studied galaxy images extracted from SDSS directly and we have used SExtractor routines to derive galaxy magnitudes. First, we have used a set of isolated galaxies which serve as a control sample for testing the photometry. For this sample, our photometry gives r-band magnitudes with 0.02 rms difference compared to those quoted in SDSS, indicating the consistency of our results with SDSS magnitudes when no deblending procedure is required. The second sample is composed of 50 merging galaxy pairs (m) extracted at random from our total sample of 383 m-pairs (with typical projected separation $r_p < 12$ kpc h^{-1}). We calculated the total magnitude of the pair which according to our previous analysis should be within 0.02 magnitudes compared to SDSS measurements in the case that deblending is accurately working. We find, however, that the deblending procedure in SDSS introduces a larger uncertainty since by adding the quoted luminosities in SDSS, the typical difference raises to 0.12 rms. In Fig.7.4 we show r-band magnitudes derived from SExtractor routines versus r-band magnitudes extracted from SDSS, for a sample of isolated galaxies and for a subsample of 50 merging pairs. This simple and robust test gives useful estimates of the uncertainties introduced by the deblending procedure adopted in SDSS which we argue are about 0.12 mag. We also notice the lack of systematics in SDSS deblending procedures, since the difference between our SExtractor measurements and quoted SDSS magnitudes have an approximately zero mean.

In summary, this analysis indicates that SDSS magnitudes can be suitably used in our analysis in the following sections provided a rms scatter of 0.12 magnitudes is not seriously affecting the results.

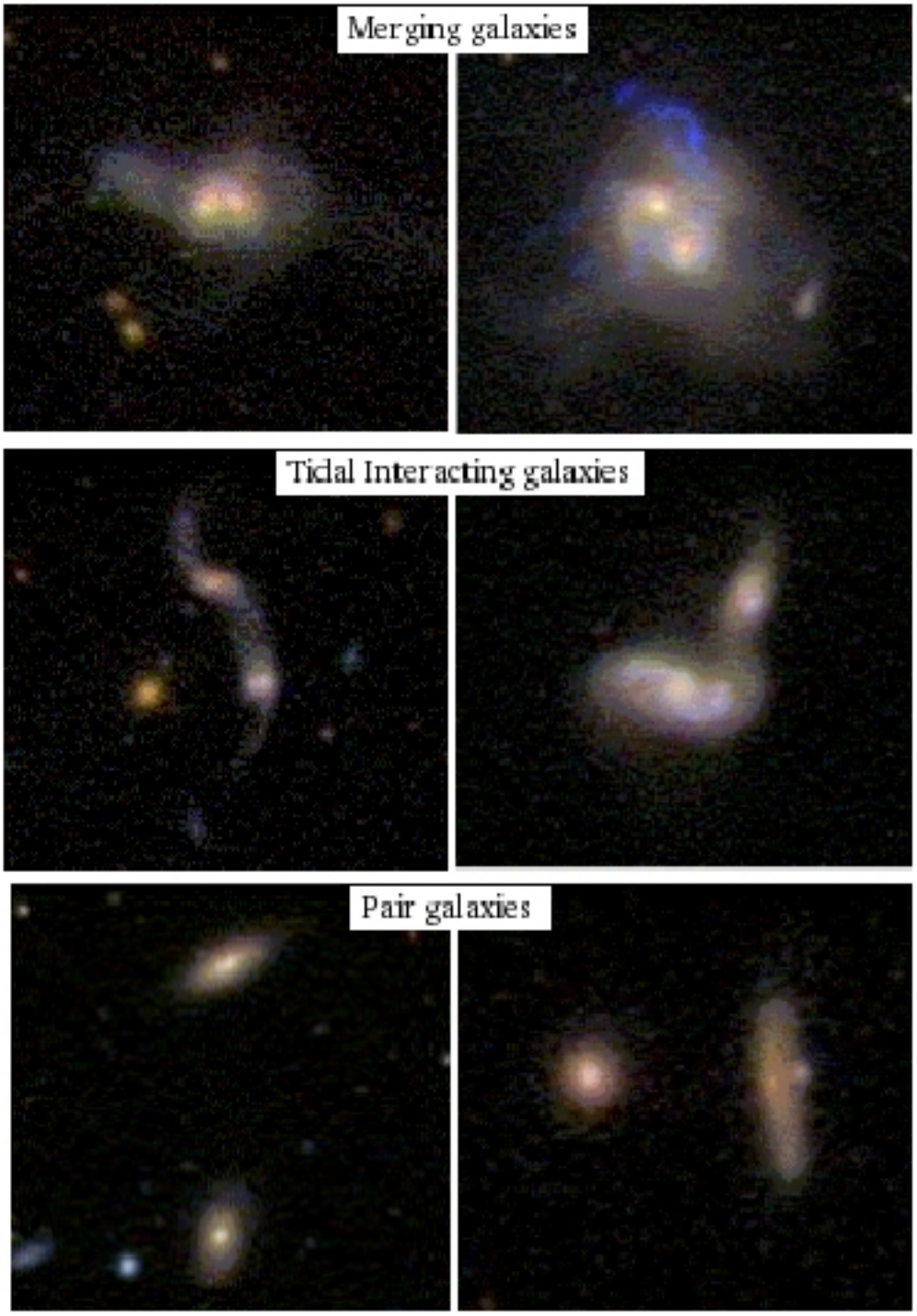

Fig. 7.3: Examples of galaxy images in close pairs with different classification: evidence of an ongoing merging process, *m*, (upper panels), pairs with a sign of tidal interaction but not necessarily merging, *t*, (medium panels) and pair galaxies showing no evidence of distorted morphologies, *n*, (lower panels).

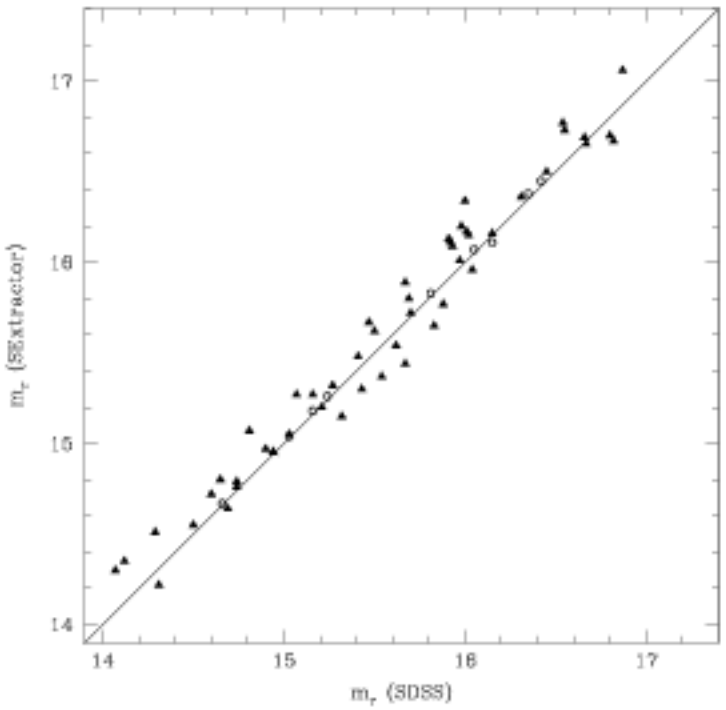

Fig. 7.4: r-band magnitude derived from SExtractor routines versus r-band magnitude extracted from SDSS, for a sample of isolated galaxies (open circles) and for a subsample of close pair galaxies (triangles).

Frequency of AGNs

For the three categories defined above, we calculate the percentage of pairs with AGNs. As we can notice from Table 7.1, we found that $\approx 30\,\%$ of close galaxy pairs host AGNs, regardless of the category they belong to, and that isolated galaxies without companions have a lower AGN frequency ($\sim 23\%$).

Tab. 7.1: Percentages of AGNs

Categories	Total Pairs	m	t	n	Total Control
Number of close pairs	1607	383	688	536	22922
% of AGNs	32%	31%	32%	28%	23%

Note: m: merging pairs t: tidal pairs; n: non-interacting pairs.

Since the AGN phenomenon is a strong function of host luminosity, we analysed the fraction of AGNs in each of the pair categories and in the control sample, for different stellar

mass content and luminosity intervals. In Fig.7.5, we display the fraction of AGNs as a function of r-band luminosity and stellar mass. The results indicate that the fraction of hosts with AGN activity increases with luminosity in a similar fashion for AGNs in pairs or in isolation. However, we notice that, at a given mean luminosity or mean stellar mass, merging pairs tend to have a higher frequency of AGNs than pairs in the two other categories or in the control sample. Nevertheless, this excess is approximately $\approx 10\%$.

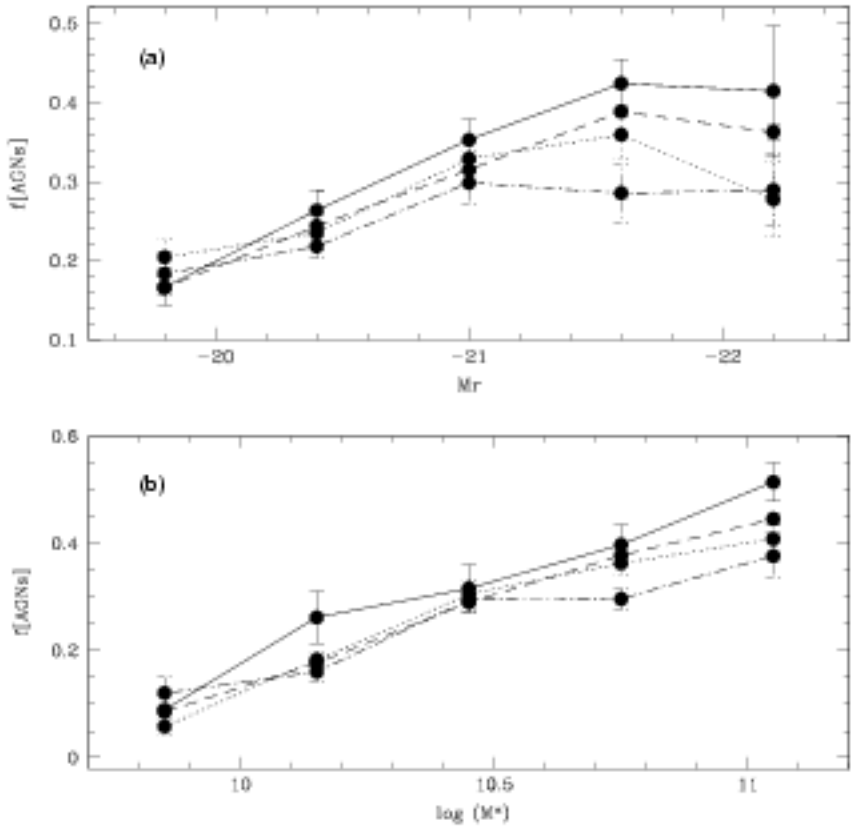

Fig. 7.5: Fraction of AGNs in merging-pair galaxies (solid lines), in tidal pairs (dotted lines), in non-interacting pairs (dot-dashed lines) and in galaxies without companions (dashed lines), as a function of M_r (a) and M^* (b).

Stellar population ages in AGN hosts

The strongest discontinuity occurring at 4000Å in the optical spectrum of a galaxy arises from the accumulation of a large number of spectral lines in a narrow wavelength region where the main contribution to the opacity comes from ionized metals. The break index

$D_n(4000)$ (Kauffmann et al. 2003a) is defined as the ratio of the average flux density by using narrow continuum bands (3850-3950Å and 4000-4100Å). The $D_n(4000)$ indicator is suitably correlated to the mean age of the stellar population in a galaxy and can be used to estimate the star formation rate per unit stellar mass, SFR/M^*, (Brinchmann et al. 2004). The majority of star formation takes place preferentially in galaxies with low $D_n(4000)$ values, for instance, only 12% and 2% of the total SFR density are associated to galaxies with $D_n(4000) > 1.8$ and $D_n(4000) > 2.0$, respectively.

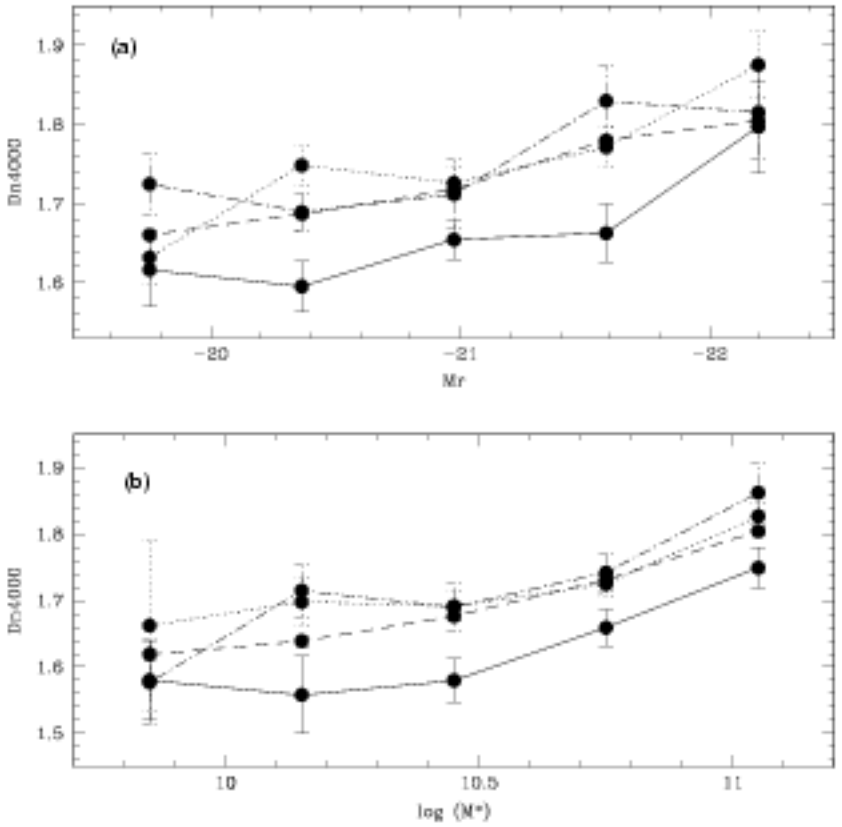

Fig. 7.6: $D_n(4000)$ as a function of (a) M_r and (b) M^*. The different types of lines indicate AGNs in merging-pair galaxies (solid), AGNs in tidal-pairs (dotted), AGNs in non-interacting pairs (dot-dashed) and AGNs in galaxies without companions (dashed).

We have analysed the behaviour of this parameter as a function of stellar mass and luminosity for AGNs in pairs and in isolation. The results are given in Fig.7.6 where it can be seen that AGNs in merging pairs have significantly lower values of $D_n(4000)$. This finding suggests that these galaxies have experienced more recent episodes of star formation as

expected since they are effectively in an ongoing merger event.

The trends shown in Fig.7.5 and Fig.7.6 support the scenario where interactions could drive both star formation and AGN activity via the triggering of gas inflows to the central region. The fact that we are actually detecting the strongest signal for merging pairs could be indicating that fusions could be more efficient than tidal torques produced during the orbital decay to feed both AGN and star formation activity.

7.5 Properties of AGNs in Interacting Galaxies: O[III] Luminosity and Black Hole Mass

As a tracer of the AGN activity, we focus here on the luminosity of the [OIII]λ5007 line, $L[OIII]$, calculated by K03 in SDSS-DR4 AGN galaxies. Although this line can be excited by massive stars as well as by AGNs, it is known to be relatively weak in metal-rich, star-forming galaxies. The [OIII] line also has the advantage of being strong and easily detected in most galaxies. It should be noticed that the narrow-line emission is likely to be affected by dust within the host galaxy (Kauffmann et al. 2003). Thus it is important to correct the $L[OIII]$ luminosities for the effects of extinction. For AGNs in SDSS, Kauffmann et al. (2003) measured the extinction using the Balmer decrement finding that the best approximation for a dust correction to $L[OIII]$ is based on the ratio Hα/Hβ. We will consider the luminosity $L[OIII] = 10^{6.5} L_{\odot}$ as a limit between weak and powerful AGNs. A weak $L[OIII]$ emission indicates that the black hole is not rapidly growing (Heckman et al. 2004).

We estimated black holes masses, $M_{\mathbf{BH}}$, for both AGNs with and without companion, by using the observed correlation between $M_{\mathbf{BH}}$ and the bulge velocity dispersion σ_* (Tremaine et al. 2002):

$$log M_{\mathbf{BH}} = 8.13 + 4.02 log(\sigma_*/200). \tag{7.2}$$

We restrict this analysis to AGN galaxies with $\sigma_* > 70$ km s^{-1}, corresponding to log$M_{\mathbf{BH}}$ > 6.3, because the instrumental resolution of SDSS spectra is $\sigma_* \approx 60$ to 70 km s^{-1}. The aperture corrections to the stellar velocity dispersions are small in early-type galaxies in SDSS (Bernardi et al. 2003), so we do not apply such corrections.

In Fig.7.7a, we show the distribution of $L[OIII]$ for AGNs in galaxies in merging pairs, tidal-pairs, non-interacting pairs and without a close companion. As it can be clearly appreciated, AGNs in pairs with evidence of ongoing merging processes (m) show larger luminosities $L[OIII]$ than AGNs in isolation or in the other two pair categories. In fact, while

62.4% of AGNs in merging pairs have $L[OIII] > 10^{6.5} L_{\odot}$, only 43.3% of isolated AGNs show such a powerful activity. Note that the other two pair categories have AGN luminosity distributions similar to that of isolated AGNs.

In Fig.7.7b, we show the distribution of black holes masses, M_{BH}, for AGNs grouped similarly to Fig.7.7a. In this figure observed that although there is a trend for M_{BH} to be systematically larger for AGNs in merging pairs, the difference is not as significant as the signal detected for $L[OIII]$, being only less than 0.15 dex.

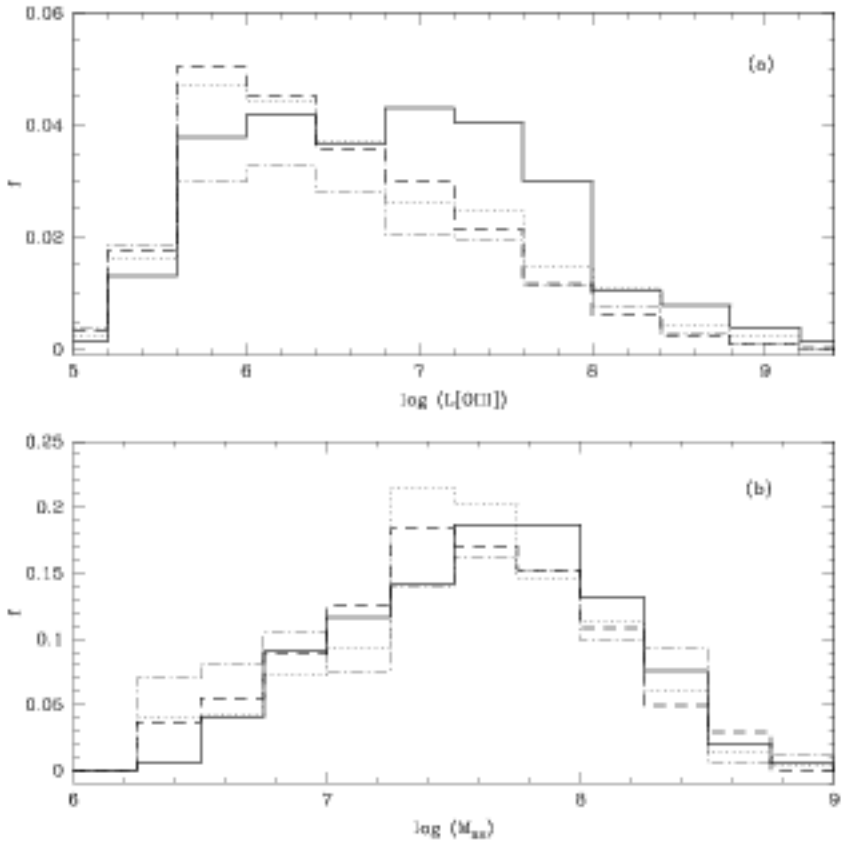

Fig. 7.7: Distributions of $L[OIII]$ (*a*) and Black Hole Mass (*b*) in AGNs merging-pair galaxies (solid lines), AGNs tidal-pairs (dotted lines), AGNs non-interacting pairs (dot-dashed lines) and AGNs galaxies without companions (dashed lines).

It is interesting to further investigate the strength of AGNs as a function of host luminosity and stellar mass. Therefore, we calculated the mean $L[OIII]$ as a function of r-band luminosity and stellar mass content of the corresponding host galaxies. These relations have been estimated for AGNs in the three pair categories (m, t, n) and for isolated AGNs. From

the results shown in Fig.7.8a, it can be clearly appreciated that, in general, the most luminous hosts show the highest $L[OIII]$. We can also see that AGNs in merging pairs show higher $L[OIII]$, regardless of the luminosity and stellar mass of the host galaxy, indicating that the black hole activity is stronger for AGNs in advanced stages of interactions. In fact, for host galaxies with $M^* > 10^{10.5} M_{\odot}$, the mean $L[OIII]$ of merging pairs is larger by half an order of magnitude than the mean $L[OIII]$ of the rest of the samples. A similar estimation for $M_{\mathbf{BH}}$ confirms the trend found in Fig.7.7b. Black hole masses are slightly larger for AGNs in merging pairs than for the rest of the categories.

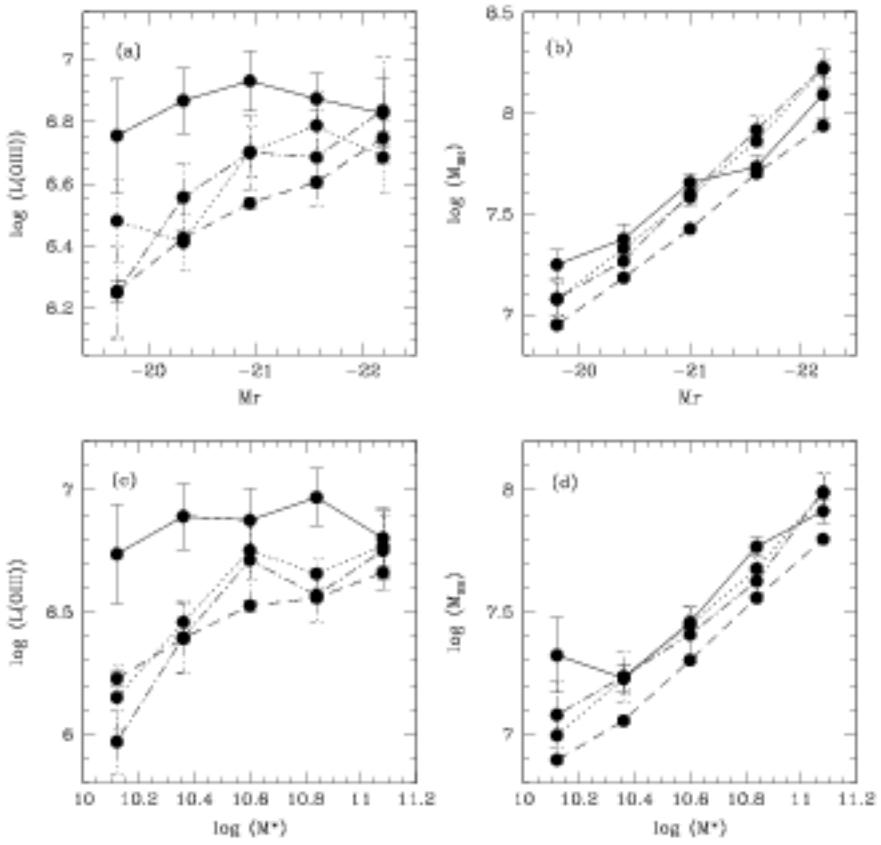

Fig. 7.8: $L[OIII]$ (a,c) and $M_{\mathbf{BH}}$ (b,d) as a function of M_r and M^* for AGNs in merging pairs (solid lines), tidal pairs (dotted lines), non-interacting pairs (dot-dashed lines) and in AGNs galaxies without close companions (dashed lines).

The ratio of $[OIII]$ luminosity to black hole mass ($\mathcal{R} = \log(L[OIII]/M_{\mathbf{BH}})$) provides a useful measure of the accretion rate in a black hole (Heckman et al. 2004). In our calculations we have not converted the $L[OIII]$ to volume-averaged luminosities but by using the

relations displayed in Fig. 2 of Heckman et al. (2004) it is possible to infer an accretion time for AGNs in pairs. In Fig.7.9 we show $\mathcal{R}$ as a function of host luminosity (a), stellar mass (b) and BH mass (c), for AGNs in the three defined pair categories (m, t, n) and in isolated AGN hosts. In agreement with the previous results, we found that black holes in smaller or fainter systems are more active than black holes in larger or brighter systems. Heckman et al. (2004) concludes that the most rapidly growing black holes are those with $M_{\rm BH}$ < few times $10^7 M_{\odot}$ with an implied growth time $\sim$ twice the age of the universe. From Fig.7.9c we can recognize that $M_{\rm BH}$ < few times $10^7 M_{\odot}$ have significantly higher accretion rates than larger ones.

The relations shown in Fig.7.9 indicate that, although in general the smallest black holes are the ones that exhibit the highest rates of accretion, AGNs in merging pairs host the most rapidly growing black holes. In fact, AGNs in merging pairs have the most powerful black holes and the ones that are growing fastest, besides hosting stellar populations which show clear signal of being importantly rejuvenated by recent starbursts.

Finally, we have also investigated the role played by the AGN companion in powering the AGN activity. This was accomplished by calculating, for each AGN in pairs, the OIII luminosity and $L[OIII]/M_{\rm BH}$ as a function of its r-band luminosity and stellar mass content, considering pairs separately with a bright and a faint companion. For that purpose, we adopted $M_r = -20$ as the magnitude threshold. The results shown in Fig.7.10 clearly indicate that AGN activity in hosts with bright companions is significantly enhanced with respect to that of AGNs with faint companions, being both the AGN power and accretion rate significantly larger. This finding provides evidences that nuclear activity is not only affected by the presence of a very close companion but that the relative mass (or luminosity) is also an important issue to take into account.

7.6 Summary

We have performed a statistical analysis of both, host characteristics and nuclear activity, of AGNs in pairs and without close companions. Our study is based on the sample of AGNs derived from the SDSS-DR4 release by Kauffmann et al. (2003) and the pair galaxies obtained from the same data release. We have complemented the SDSS-DR4 data with the addition of a eye-ball classification of images of 1607 close pairs ($r_{\rm p}$ <25 kpc h^{-1}, ΔV < 350 km s^{-1}) according to the evidence of interaction through distorted morphologies and tidal features. Also, we have performed a photometric analysis to assess the reliability of the SDSS magnitude deblending procedure in merging pairs, finding negligible systematic effects.

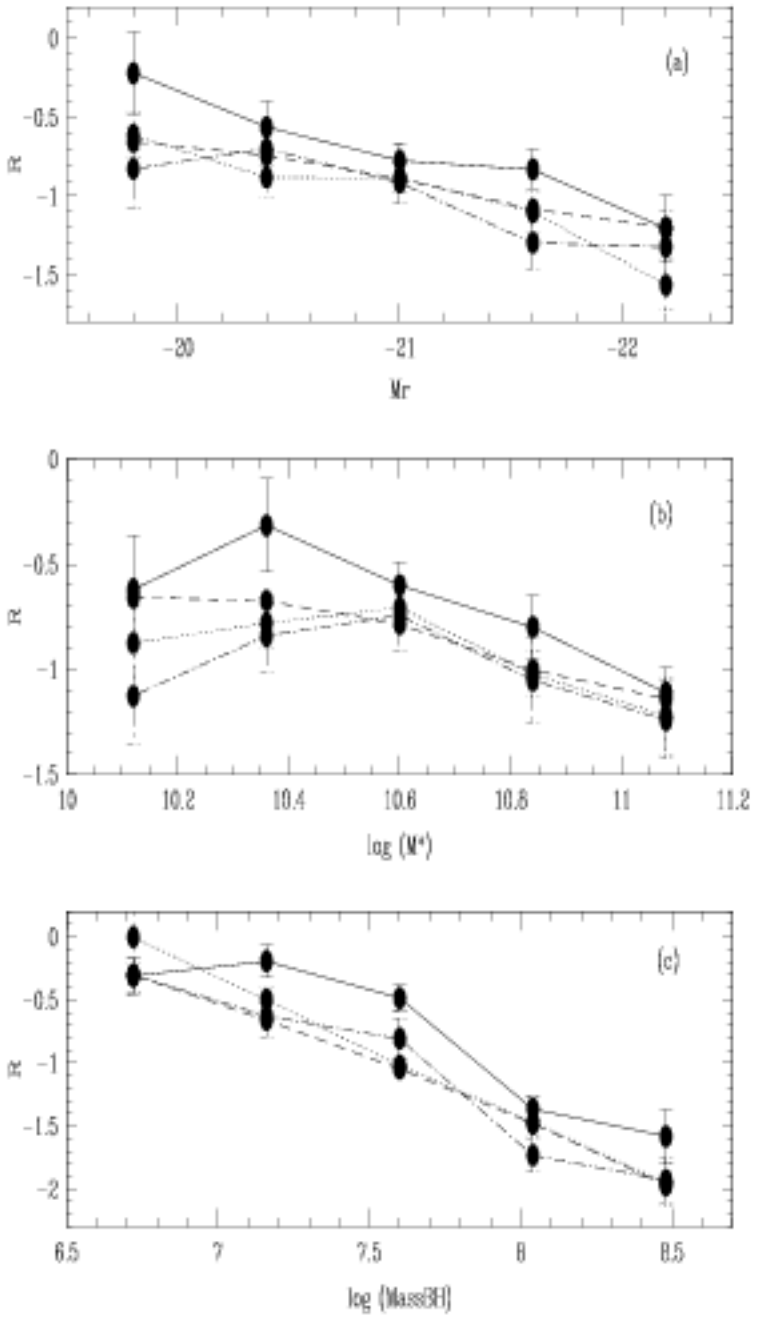

Fig. 7.9: Mean $\mathcal{R} = \log(L[OIII]/M_{\mathbf{BH}})$ as a function of M_r (*a*), M^* (*b*) and $M_{\mathbf{BH}}$ (*c*) for AGNs in merging pairs (solid lines), tidal pairs (dotted lines), non-interacting pairs (dot-dashed lines) and AGNs galaxies without close companions (dashed lines).

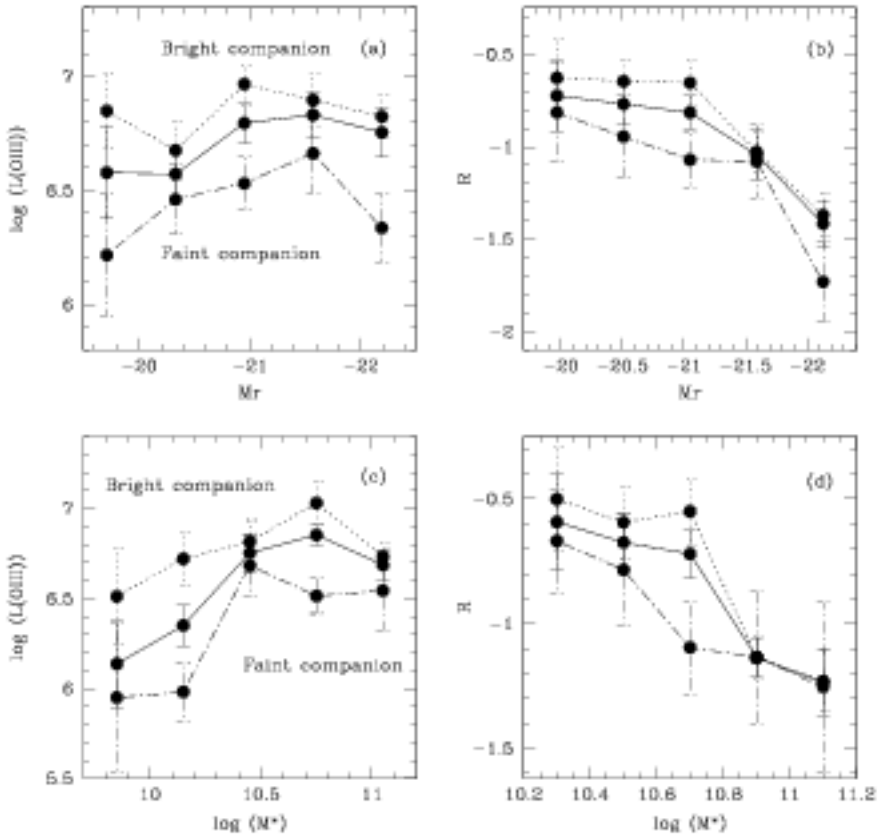

Fig. 7.10: Mean $L[OIII]$ (a, c) and $\mathcal{R} = L[OIII]/M_{BH}$ (b, d) as a function of M_r and M^* for AGNs in pairs (solid lines), AGN galaxy with a bright pair companion ($Mr < -20.0$) (dotted line), and AGN with a faint pair companion ($Mr > -20.0$) (dot-dashed line).

Our main results are:

1- The fraction of AGNs as a function of r-band luminosity or stellar mass is larger for merging pairs. However, this is a relatively small effect accounting for an increase of less $\sim 10\%$ due to tidal interactions.

2- AGN hosts are redder, having a larger concentration morphological index than non-AGN galaxies. This effect is similar for AGN hosts in pairs or in isolation.

3- We find that the locus of AGNs with and without close companions in the BPT diagram are consistent with each other.

4- At a given host r-band luminosity or stellar mass, we find the AGN OIII luminosity to be enhanced by AGNs with strong interaction features (i.e. merging pairs). We found that while 62% of AGNs in merging pairs have $L[OIII] > 10^{6.5}$ this percentage decreases to

43% in the case of isolated AGNs.

5- Estimations of the mean accretion rates onto the black holes of AGNs in pairs in the three defined categories and in isolation indicate that AGNs in merging pairs have more active black holes than other AGNs, at a given r-band luminosity or stellar mass content. We estimated than 27% of AGNs in merging pairs have $L[OIII] > 10^{6.5}$ and $M_{\rm BH} < 3\times10^{7} M_{\odot}$ and can be considered as feeding their black holes with high efficiency (Heckmann et al. 2004). In the case of isolated AGNs (selected to have the same), this percentage decreases to 21%. On the other hand, all AGNs in merging pairs have $Dn4000 < 1.8$ which indicates that they also have active star formation. Interestingly, we also found that 17% of isolated AGNs have powerful emission, $M_{\rm BH} < 3\times10^{7} M_{\odot}$ and have also experienced important star formation activity in the recent past with $Dn4000 < 1.8$. These trends open the possibility that isolated AGNs with active black holes have experienced a recent merger. It is also possible that secular evolution could be responsible for feeding the black hole and the star formation activity if a gaseous disk is present. More detailed data are needed to draw a conclusion on this point.

6- We find that the luminosity (or mass in stars) of the companion galaxy is a key parameter to determine the activity of the black hole. Both the OIII luminosity and the accretion rates $L[OIII]/M_{\rm BH}$ for AGNs with bright close companions are significantly larger than those for AGNs with faint neighbours.

CHAPTER 8

CONCLUSIONS

In this Thesis we have carried out a detailed analysis, from a statistical point of view, on the way that mergers and interactions affect galaxy properties. For this purpose, we have obtained two galaxy pair catalogs from the 2dF Galaxy Redshift Surveys (2dFGRS) and the Sloan Digital Sky Survey (SDSS). These pair catalogs include several thousands objects, and constitute the largest samples of pairs used to analyse statistically into detail the effects of mergers and interactions.

We have analysed samples of interacting galaxy pairs in the field, in groups and clusters, and continuously in different density environments based on a comparative analysis of the properties of galaxies without companions. Moreover, we have studied observations of the Hα emission in a sample of satellite galaxies and we have analysed the current and past star formation rate in interacting satellite galaxies in comparison with satellites without close companions. Finally, we have investigated the role of interactions on active galactic nuclei.

First, we have looked for galaxy pairs in the local universe, $z \leq 0.1$, taken from the 2dF Galaxy Redshift Survey and Sloan Digital Sky Survey (the largest present-day galaxy catalogs). The galaxy pairs where selected by projected separation (r_p) and radial velocity (ΔV) thresholds, criteria determined by analysing the star formation (SF) activity within neighbours of each galaxy. According to this analysis, we have found that $r_p < 100$ kpc h^{-1} and $\Delta V < 350$ km s^{-1} are reliable upper limits to select galaxy pairs. These thresholds are similar for both surveys, which confirm these limits to detect pair galaxies with statistically enhanced star formation activity. Finally, we have obtained two pair catalogs: the 2dF Galaxy Pair Catalog and the SDSS Galaxy Pair Catalog, which comprise 6067 and 11461 pairs respectively.

We have analysed the dependence of star formation activity as a function of r_p and ΔV, for galaxy pairs in different environments with respect to galaxies without a close companion in the same density and luminosity ranges.

For pair galaxies in the field, we have detected a significant correlation between the mean star birthrate parameter $\langle b \rangle = SFR/\langle SFR \rangle$ and both, projected separation and relative velocity. For $r_p < 25$ kpc h^{-1} and $\Delta V < 100$ km s^{-1} we obtain a substantial star formation enhancement with respect to the control sample. The ΔV dependence is less pronounced although we find a systematic increase of star formation activity for decreasing relative velocity.

We have extended this study, analysing the effects of mergets and galaxy-galaxy interactions in high density systems corresponding to groups and clusters of galaxies with vitial masses in the range $10^{13} - 10^{15} M_{\odot}$. Similarly, we found a closer relative projected threshold, $r_p \sim 15$ kpc h^{-1}, for the star formation to be significantly enhanced with respect to that of the control sample of members without close companions. We stress the fact that pairs in groups have a lower SF efficiency than other members.

By characterizing environment through a continuous variable, Σ, (the density derived from the distance to the fifth nearest neighbour) we find an increase of $\langle b \rangle$ in pairs for smaller r_p and ΔV in all environments. However, in the highest density regions, galaxies need to be closer in order to show SF enhancement with respect to galaxies without a close companion. These results indicate that the general lower efficiency of star formation in dense environments is accompanied by a lower enhancement of the star formation induced by interactions, probably associated to early morphology-type galaxies which mostly populate rich systems.

For the purpose to help the understanding of how SF activity is regulated between pair members, we have analysed the dependence of the star formation activity on the luminosity of the galaxy pairs in the field. From this analysis, we have found that there is not an overall dependence of the mean star formation enhancement $\langle \beta \rangle$ (which yields the excess of star formation in galaxies in pairs with respect to an isolated galaxy in the field with the same selection effects and redshift distribution) on luminosity for galaxy pairs. A nearly constant value $\langle \beta \rangle \simeq 1.2$ for the total field galaxy pair catalog and $\langle \beta \rangle \simeq 2$ for the close galaxy pair subsample ($r_p < 25$ kpc h^{-1} and $\Delta V < 100$ km s^{-1}) are determined. However, the fractions of galaxies in pairs that have a higher star formation activity than the corresponding of isolated galaxies, show a clear excess for the brightest members.

We have divided the field close pair sample in minor ($L_2/L_1 < 0.5$) and major ($L_2/L_1 >$

0.5) interactions according to their relative luminosities (L_2/L_1 corresponds to the ratio of luminosities of the faint over the bright member). We found that bright components in minor interactions show a higher probability to have enhanced SF and from larger projected distances than the faint components. This result indicates that a small disturbance produces an effective stimulation of star formation activity over the largest galaxy. On the contrary, the tidal effects of a large companion can make too large disturbances, enough to remove a substantial fraction of the gas reservoir in the minor companion, causing a reduction of the subsequent star formation activity. In the case of major interactions, both components show comparable star formation activity enhancements and with a similar projected distance dependence.

For galaxies in groups and clusters, we have studied whether the pairs have a particular location with respect to other members without close companions. We find that the radial and relative velocity distributions of pairs (normalized to the group virial radius and group mean velocity dispersion) with respect to the group centers are similar to those of group members with no companions.

We have shown that star formation activity strongly increases for larger groupcentric distance for both galaxy pairs and galaxies in the control sample with a similar fashion, approaching the mean SF value for field galaxies in the outskirts. These similar trends in both samples show, that on average, environment has the same effects in all group members.

For the purpose of carrying out a more detailed analysis on star formation activity and environment, we have also calculated the fraction of extremely blue and actively star-forming galaxies in close pairs as a function of local density. The trends found do not behave as the equivalent fraction of the control sample. In low density environment, blue, star-forming galaxies tend to be in pairs. In high density regions, galaxies without a close companion have a higher contribution to blue and actively star-forming systems. The transition densities correspond to group environments. As a complementary analysis, we have studied the extremely red and low star-forming galaxies in pairs which are found to outnumber those without a close companion in all environments. The fraction of red and low star-forming galaxies without a close companion shows an increase in the lowest densities. The corresponding fraction of galaxies in pairs increases in both the low and the high density ends. In low density environments, this effect is more pronounced for pair galaxies owing to the combined effects of the expected lack of gas infall in such regions and the high efficiency of galaxies in pairs using the available gas for new stars at early stages of their evolution.

These results show that galaxy-galaxy interactions are an important mechanism for triggering star formation regardless of environment, although smaller separations are required in high density systems for galaxies to react to the presence of a companion. We also found that in low density environments, extremely blue and star-forming galaxies tend to be in pairs. On the other hand, in high density regions the most intense SF activity is found in galaxies without a close companion and not in very close pairs. The red and low star-forming extreme is dominated by galaxies in pairs in all environments (except for very close pairs). We argue that this trend unveils the ubiquitous effects of interactions also in previous stages of evolution which exhausted the gas reservoir in close systems.

We have also performed observations of the Hα emission in a sample of satellites, orbiting giant isolated spiral galaxies. We have found that all the spiral and irregular satellite galaxies have $H\alpha$ fluxes above 1.15–49.80 x 10^{-14} erg s^{-1} cm^{-2}. We have also obtained the current star formation rates, which span the range between 0.006 and 3.66 $M_{\odot}$ yr^{-1}, and the median of the birth parameter $b = SFR/\langle SFR \rangle$ is 0.68. This result indicates a decrease in the star formation activity with cosmic time.

We have detected a higher star formation activity in satellite galaxies, which show clear signs of interaction with close companions of comparable brightness, at projected distances of 25, 20 and 2 kpc. Nevertheless, the only two galaxies in the sample that do not show star formation activity are members of these interacting systems. It is unclear if this is a consequence of intrinsic properties (both are early Hubble types) or if it is related to a possible disruption of the external parts due to the interaction. On the other hand, we have not detected Hα emission in the filaments associated with these interactions.

Furthermore, we have detected that the object with the largest star formation rate (apart of the interacting systems) corresponds to the satellite galaxy which has the smallest projected distance from its progenitor (19 kpc), and the star formation rate could be due to interaction with the parent galaxy. All of these results indicate that the proximity between galaxies (i.e. satellite-satellite, satellite-progenitor) can produce an efficient enhancement of star formation activity.

From the analysis of active galactic nuclei and galaxy interactions, we have found that the fraction of AGNs as a function of r-band luminosity, or stellar mass, is larger for pairs with evidence of an ongoing merging process. However, this effect is small accounting for an increase of less than $\sim 10\%$ due to pairs with strong signs of tidal interactions.

We have also studied properties of AGN hosts, and we have detected that they are redder

and with a larger concentration morphological index than non-AGN galaxies. This finding is independent of AGN hosts being in pairs or in isolation.

We have also used as tracer of AGN activity the luminosity of the $[OIII]\lambda5007$ emission line, $L[OIII]$ and we have found an enhancement for AGNs with strong interaction features (galaxy pairs with evidence of an ongoing merging process), at a given host r-band luminosity or stellar mass. Moreover, we have detected that while 62% of AGNs in merging pairs have $L[OIII] > 10^{8.5}$ (limit for powerful AGNs) this percentage decreases to 43% in the case of isolated AGNs. Furthermore, we have estimated the mean accretion rates onto the black holes of AGNs in pairs in the three defined categories and in isolation. We have found that at a given r-band luminosity, or stellar mass content, AGNs in merging pairs have more active black holes. On the other hand, all AGNs in merging pairs have $Dn4000 < 1.8$ which indicates that they also have active star formation. These results could be indicating that isolated AGNs have experienced a recent merger. It is also possible that secular evolution could be responsible of feeding the black hole and the star formation activity if a gaseous disk is present, but more detailed data are needed to draw firm conclusions on this point. On the other hand, we have detected that both the OIII luminosity and the accretion rates for AGNs with bright close companions are significantly larger than for those of AGNs with faint neighbours. Then, the luminosity (or mass in stars) of the companion galaxy is a key parameter to determine the activity of the black hole. This finding provides evidence that nuclear activity is not only affected by the presence of a very close companion, but the relative mass (or luminosity) is also an important issue to be taken into account.

To summarize, the analysis of this Thesis has provided the largest catalogs of galaxy pairs available, and detailed studies of interaction-induced star formation and AGN fueling. In short, the main new results are basically the thresholds r_p and ΔV for enhanced star formation activity; the fact that closer interactions are required in groups compared to the field in order to trigger star formation; an excess of red galaxies in pairs in high density environments indicating bursts of star formation in the past; enhanced star formation activity in interacting satellites orbiting late spiral primaries; and the determination that the power of AGNs is substantially larger for galaxies ongoing mergers, in particular with luminous companions.

Although we acknowledge that several issues still remain unclear and deserve further study, we hope to have contributed to a better understanding of the role of interactions on galaxy properties and evolution.

LIST OF FIGURES

LIST OF TABLES

BIBLIOGRAPHY

[1] Abazajian K., Adelman J., Agueros M., et al. 2004, AJ, 128, 502.

[2] Alonso M. S., Tissera P. B., Coldwell G., Lambas D. G. 2004, MNRAS, 352, 1081.

[3] Alonso, M. S., Lambas, D.G., Tissera, P.B. & Coldwell, G., 2006, MNRAS, 367, 1029.

[4] Alonso, M. S., Lambas, D.G., Tissera, P.B. & Coldwell, G., 2007, MNRAS, 375, 1017.

[5] Antonucci, R., 1993, ARA&A, 31, 473.

[6] Arp, H., 1966, ApJS, 14, 1.

[7] Arp, H. & Madore B. S., 1987, *Catalogue of Southern Peculiar Galaxies and Associations*, 2 Vol. New York, Cambridge University Press.

[8] Bahcall J. N., Kirhakos S., Saxe D. H., Schneider D. P., 1997, AJ, 479, 642.

[9] Bagnuolo W. G., 1976, *The stellar content and evolution of irregular and other late-type galaxies.*, PhD thesis. Caltech.

[10] Baldry I. K., et al., 2002, ApJ, 569, 582.

[11] Baldry, I. K.; Glazebrook, K.; Brinkmann, J.; Ivezic, Z.; Lupton, R. H.; Nichol, R. C.; Szalay, A. S., 2004, ApJ, 600, 681.

[12] Baldwin, J. A., Phillips, M. M. & Terlevich, R., 1981, PASP, 93, 5.

[13] Balogh M., Baldry I. K., Nichol R., Miller C., Bower R., Glazebrook K., 2004, ApJ Letters, 615, 101.

[14] Balogh M., et al., 2004, MNRAS 348, 1355.

[15] Barnes J. E., 1988, AJ, 331, 699.

[16] Barnes, J. E. & Hernquist, L., 1992, ARA&A, 30, 705.

[17] Barnes, J., Hernquist, 1996, ApJ, 471, 115.

[18] Barrow, J. D., Bhavsar, S. P., & Sonoda, B. H., 1984, MNRAS, 210, 19p.

[19] Barton E. J., Geller M. J., Kenyon S. J., 2000, ApJ, 530, 660.

[20] Barton E. J., Geller M. J., Kenyon S. J., 2002, ApJ, 582, 668.

[21] Barrow, J. D., Bhavsar, S. P., & Sonoda, B. H., 1984, MNRAS, 210, 19p.

[22] Baugh, C. M., Cole, S. & Frenk, C. S., 1996, MNRAS, 283, 1361.

[23] Begelman, M. C., Blandford, R. D., & Rees, M. J., 1980, Nature, 287, 307.

[24] Bell, E. F., 2003, ApJ, 586, 794.

[25] Bergvall, N., Laurikainen, E., & Aalto, S. 2003, A&A, 405, 31.

[26] Bernardi, M. et al., 2003, AJ, 125, 1817.

[27] Bertin, E. & Arnouts, S, 1996, A&AS, 117, 393.

[28] Bland-Hawthorn, J., 2002 dshg.conf, 373.

[29] Blanton M. R., et al., 2003, AJ, 125, 2348.

[30] Bergvall, N., Laurikainen, E., Aalto, S., 2003, A & A, 405, 31.

[31] Binney, J., Tremaine, S., 1987, Galactic Dynamics, Princeton University Press.

[32] Bond J. R., Cole S., Efsthathiou G., Kaiser N., 1991, ApJ, 379, 440.

[33] Bouwens, R., Broadhurst, T., Silk, J., 1997, ApJ, 489, 21.

[34] Bower, R. J., 1991, MNRAS, 248, 332.

[35] Brinchmann et al 1998, ApJ, 499, 112.

[36] Brinchmann J., Charlot S., White S. D. M., Tremonti C. Kauffmann G., Heetman T., Brinkmann J., 2004, MNRAS, 351, 1151.

[37] Carlberg R. G., 1990, AJ, Lett., 359, 1.

[38] Carlberg R. G., Pritchet C. J. & Infante L., 1994, AJ, 435, 540.

[39] Carlberg R. G., Yee H. K. C., Ellingson E., Abraham R., Gravel P., Morris S., Pritchet C. J., 1996, AJ, 462, 32.

[40] Carter, B. J., Fabricant, D. G., Geller, M. J., Kurtz, M. J., Mclean, B. 2001, ApJ, 559, 606.

[41] Casoli, F., Dickey, J., Kazes, I., Boselli, A., Gavazzi, P., & Baumgardt, K. 1996, A&A, 309, 43.

[42] Chandrasekhar S., 1943, AJ, 97, 255.

[43] Charlton J. C., & Salpeter E. E., 1991, AJ, 375, 517.

[44] Coldwell, G. V. & Lambas, D. G., 2006, MNRAS, 371, 786.

[45] Cole S., Aragon-Salamanca, A., Frenk C. S., Navarro J. F., Zepf S. E., 1994, MNRAS, 271, 781.

[46] Colless, M. M., et al. (the 2dFGRS Team), 2001, MNRAS, 328, 1039.

[47] Colina L., Borne, K., Bushouse, H., Lucas, R. A., Rowan-Robinson, M., Lawrence, A., Clements, D., Baker, A., Oliver, S. 2001, ApJ, 563, 546.

[48] Couchman H. M. P., Thomas P. A., Pearce, F. R., 1995, ApJ, 452, 797.

[49] Dahari, O., 1985, ApJS, 57, 643.

[50] Dijkstra, M., Haiman, Z., Rees, M. J., & Weinberg, D. H. 2004, ApJ, 601, 666.

[51] Domínguez M. J., Zandivarez A. A., Martínez H. J., Merchán M. E., Muriel H., Lambas D. G., 2002, MNRAS, 335, 825.

[52] Donzelli, C. J., Pastoriza, M. G., 1997, ApJS, 111, 181.

[53] Dressler A., 1980, ApJ, 236, 351.

[54] Dressler A., Thompson, I. B., Shectman, S. A., 1985, ApJ, 288, 481.

[55] Ferguson H. C., Sandage A., 1991, AJ, 101, 765.

[56] Friedli, D., Benz, W., 1995, AA, 301, 649.

[57] Fuentes-Williams, T. & Stocke, J.T., 1988, AJ, 96, 1235.

[58] Fukugita M., Ichikawa T., Gunn J. E., Doi M., Shimasaku K., Schneider, D. P., 1996, AJ, 111, 1748.

[59] Gil de Paz, A., Madore, B. F., & Pevunova, O. 2003, ApJSS, 147, 29.

[60] Gómez P., Nichol R., Miller P., et al., 2003, ApJ, 584, 210.

[61] Grogin, N. A. & Geller, M. J., 2000, AJ, 119, 32.

[62] Gunn J. E. et al., 2006, AJ, 131, 2332.

[63] Gutiérrez, C. M., Azzaro, M., & Prada, F. 2002, ApJS, 141, 61.

[64] Gutiérrez, C.M., & Azzaro, M. 2004, ApJSS, 155, 395.

[65] Gutiérrez, C.M., Alonso M. S., Funes J. G., Ribeiro, M. B, 2006, AJ, 132, 596.

[66] Heckman, T. M.; Kauffmann, G.; Brinchmann, J.; Charlot, S.; Tremonti, C.; White, S. D. M., 2004, ApJ, 613, 109.

[67] Hernquist L., Mihos J. C., 1995, 448, 41.

[68] Hickson P., Mendes de Oliveira C., Huchra J. P., Palumbo G. G., 1992, ApJ, 399 353.

[69] Hogg D. W., Finkbeiner D. P., Schlegel D. J., Gunn J, E., 2001, AJ, 122, 2129.

[70] Hogg D. W. et al., 2003, ApJ, 585, 5.

[71] Hopkins, A. M., Schulte-Ladbeck, R. E., Drozdovsky, I. O., 2002, AJ, 124, 862.

[72] Hubble, E, 1926, ApJ, 64, 69.

[73] Huchra J. P., 1977, ApJ, 217, 39.

[74] Kauffmann, G., White, S. D. M. & Guiderdoni, B., 1993, MNRAS, 264, 210.

[75] Kauffmann, G., et al., 2003, MNRAS, 341, 33.

[76] Kauffmann, G., et al., 2003, MNRAS, 346, 1055.

[77] Kauffmann G. et al., 2004, MNRAS, 353, 713.

[78] Keel, W. C. 1996, AJ, 111, 696.

[79] Kelm, B., Focardi, P. & Zitelli, V., 2004, A&A, 418. 25.

[80] Kennicutt, R. C., Keel, W. C., van der Hulst, J. M., Hummel, E. & Roettiger, K. A., 1987, AJ, 93, 1011.

[81] Kennicutt, R. C., 1992, ApJ, 388, 310.

[82] Kennicutt R. Jr., 1998, ApJ, 498, 541.

[83] Klypin, A., Kravtsov, A.V., Valenzuela, O., & Prada, F. 1999, ApJ, 522, 82.

[84] Knebe, A., Gill, S. P. D., & Gibson, B. K. 2004, PASA, 21, 216.

[85] Knebe, A., Power, C., Gill, S. P. D., & Gibson, B. K. 2005, MNRAS, 368, 741.

[86] Kong, X., Cheng, F. Z., Weiss, A., & Charlot, S. 2002, A&A 396, 503.

[87] Kron, R. G., 1980, ApJS, 43, 305.

[88] Lacey C. & Cole S., 1993, MNRAS, 262, 627.

[89] Lambas D. G., Tissera P. B., Alonso M. S., Coldwell G. 2003, MNRAS, 346,1189.

[90] Larson, R. B. & Tinsley, B. M., 1978, ApJ, 219, 46.

[91] Le Fèvre O. et al., 2000, MNRAS, 311, 565.

[92] Lewis, I., et al. (the 2dFGRS Team), 2002, MNRAS, 334, 673.

[93] Lonsdale C. J., Hacking P. B., Conrow T. P., Rowan-Robinson M., 1990, AJ, 358, 60.

[94] Loveday, J., Tresse, L., & Maddox, S., 1999, MNRAS, 310, 281.

[95] Madgwick D. S. et al., 2002a, MNRAS, 333, 133 (M02).

[96] Madgwick D. S., Somerville, R., Lahav, O., Ellis, R., 2003, MNRAS, 343, 871.

[97] Mamon, G. A., 1986, ApJ, 307, 426.

[98] Mamon, G. A., 1987, ApJ, 321, 622.

[99] Martinet, L., 1995, FCPh, 15, 341.

[100] Martínez, H. J., Zandivarez, A., Domínguez, M., Merchán, M. E., Lambas, D. G., 2002, MNRAS, 333, 31.

[101] Mateo, M. L. 1998, ARA&A, 36, 435.

[102] Mayer L., Governato F., Colpi M., Moore B., Quinn T. R., Baugh C. M., 2001, Ap&SS, 276, 375.

[103] Mendez, D. I., Esteban, C.& Balcells, M. 1999, AJ, 117, 1229.

[104] Merchán, M., Zandivarez, A., 2002 MNRAS, 335, 216 (MZ02).

[105] Merchán, M., Zandivarez, A., 2005, ApJ, 630, 759.

[106] Mihos, J. C., Richstone, D. O., Bothun, G. D., 1992, ApJ, 400, 153.

[107] Mihos, J. C., Hernquist, L., 1994, ApJ, 425, 13.

[108] Mihos, J. C., Hernquist, L., 1996, ApJ, 464, 641.

[109] Milosavljevic M., Merritt D., 2001, ApJ, 563, 34.

[110] Moore B., Katz N., Lake G., 1996, ApJ, 457, 455.

[111] Moore, B., Ghigna, S., Governato, F., Lake, G., Quinn, T., Stadel, J., & Tozzi, P. 1999, ApJ, 524, L19.

[112] Nikolic B.; Cullen H.; Alexander P., 2004, MNRAS, 355, 874.

[113] Oke, J. B., 1990, AJ, 99, 1621.

[114] Patton, D. R., Pritchet, C. J., Yee, H. K. C., Ellingson, E. & Carlberg, G., 1996, AJ, 475, 29.

[115] Patton et al. 2002, MNRAS, 565, 208.

[116] Peebles P. J. E., 1974, ApJ, 189, 51.

[117] Pérez M. J., Tissera P., Lambas D. G., Scannapieco C., 2006, A&A, 449, 23.

[118] Petrosian V., 1976, ApJ, 209, 1.

[119] Petrosian A., McLean B., Allen R. J., Leithere C., McKenty J., Panagia N., 2002, ApJ, 123, 2280.

[120] Postman, M. & Geller, M. J., 1984, ApJ, 281, 95.

[121] Press W. H., Schechter P., 1974, ApJ, 187, 425.

[122] Richstone D. O., 1976, ApJ, 204, 642.

[123] Salpeter, E. E., 1955, ApJ, 121, 161.

[124] Sandage A., 1986, A&A, 161, 89.

[125] Sanders, D.B., Soifer, B.T., Elias, J.H., Madore, B.F., Matthews, K., Neugebauer, G.& Scoville, N., 1988, ApJ, 325, 74.

[126] Sanders, D.B., Mirabel I. F., 1996, AR A&A, 34, 92.

[127] Scalo J. M., 1986, FCPh, 11, 1.

[128] Schlegel D. J., Finkbeiner D. P., Davis M., 1998, ApJ, 500, 525.

[129] Schmitt, H. R., 2001, AJ, 122, 2243.

[130] Schwartz, M. P., 1981, ApJ, 247,77.

[131] Searle L., Sargent W. L. W., Bagnuolo W. G., 1973, ApJ, 179, 38.

[132] Sekiguchi, K., & Wolstencroft, R. D. 1992, MNRAS, 255, 581.

[133] Shlosman, I., Begelman, M. C. & Frank, J., 1990, Nature, 345, 679.

[134] Skillman, E. D., Cote, S., & Miller, B. W. 2003, AJ, 125, 593.

[135] Somerville, R., 2002, ApJ, 572, 23.

[136] Stanway, E. R., Bunker, A. J., McMahon, R. G., Ellis, R.S., Treum T., McCarthy, P. J., 2004, ApJ, 607, 704.

[137] Storchi-Bergmann, T.; Gonzlez Delgado, R. M.; Schmitt, H. R.; Cid Fernandes, R.; Heckman, T., 2001, ApJ, 559, 147.

[138] Strateva, I. et al., 2001, AJ, 122, 1861.

[139] Strauss M. et al., 2002, AJ, 124, 1810.

[140] Tegmark, M. & Bromley, B. C., 1999, ApJ, 518, L69.

[141] Tinsley B. M., 1968, ApJ, 151, 65.

[142] Tinsley B. M., 1972, A&A, 20, 96.

[143] Tissera P.B., 2000, ApJ, 534, 636.

[144] Tissera P.B., Domínguez-Tenreiro R., Scannapieco C., Sáiz A., 2002, MNRAS, 333, 327.

[145] Toomre A., 1977, *Evolution of galaxies and stellar populations*, New Haven, Yale Obs. (ed. B.M. Tinsley and R.B. Larson).

[146] Toomre A. & Toomre J. 1972, ApJ, 178, 623.

[147] Tremaine, S. et al., 2002, ApJ, 574, 740.

[148] van Zee, L. 2000, AJ, 119, 2757.

[149] van Zee, L. 2001, AJ, 121, 2003.

[150] van Zee, L., Haynes, M. P., & Salzer, J. J., 1997, AJ, 114, 2479.

[151] Vorontsov-Vel'Yaminov, B. A., Arkhipova V. P., 1968, *Morphological Catalog of Galaxies*, MCG, C04.

[152] White, S. D. M., & Rees, M. J. 1978, MNRAS, 183, 341.

[153] Willman, B., Governato, F., Dalcanton, J. J., Reed, D., & Quinn, T. 2004, MNRAS, 353, 639.

[154] Windhorst R. A. et al., 1995, Nature, 375, 471.

[155] Woods, D., Fahlman, G. G., Richer, H. B., 1995, ApJ, 454, 32.

[156] Yee, H. K. C. & Ellingson, E., 1995, AJ, 445, 37.

[157] York D. O. et al., 2000, ApJ, 120, 1579.

[158] Zaritsky, D., Smith, R., Frenk, C., & White, S. D. M. 1997, ApJ, 478, 39.

[159] Yu Q., 2002, MNRAS, 331, 935.

[160] Zepf, S. E. & Koo, D. C., 1989, AJ, 337, 34.

[161] Zwicky, F. 1971, *Catalogue of selected Compact Galaxies and of Post-eruptive Galaxies*, Guemligen, Switzerland: F. Zwicky.

APPENDIX A

IMAGES OF THE SATELLITE GALAXIES

A.1 Description of the Image Galaxies

This appendix contains a description of the Hα emission maps of each galaxy:

• NGC 488c: This is a low surface brightness irregular galaxy in which we notice four main knots with Hα emission located in the outer parts of the galaxy.

• NGC 772b: What seems to be a bright foreground star is projected on the E side of the galaxy. The Hα emission is concentrated in a few discrete spots, the two brightest being situated NE.

• NGC 772c: There are diffuse and discrete Hα emission features. The two brightest spots are situated roughly symmetrically with respect to the galactic center.

• NGC 1517a: There are about ten Hα regions, which are particularly bright in the external parts of the galaxy. Two of the Hα features through the W are clearly differentiated from the main body of the disk.

• NGC 1620a: The galaxy is irregular with two–three plumes emerging from the W. In one of these plumes there are a few discrete features with Hα emission. The rest of the emission is concentrated in a few features distributed over the full galaxy,

• NGC 1961a: A few clumpy small and faint structures are detected in the image after continuum subtraction.

• NGC 1961b: It is a luminous spiral satellite galaxy which has a bright point-like structure close to the center. The Hα continuum subtracted image shows diffuse Hα emission with a few over-imposed features concentrated along two chains in direction NE–SW enclosing the central part of the galaxy. The brightest spot at 3.8 arcsec from the geometrical center was suspected to be a foreground star but it is the dominant component in the continuum free image, so we think it is a real galactic feature (or an intruder) experiencing a strong starburst.

• NGC 1961c: This galaxy is a face-on spiral, which has a very rich structure in Hα emission with several extended features. The two most intense features are situated in the geometrical center and in a spot NW which is also obvious in the R-band image.

• NGC 2424b: This is a very irregular galaxy which shows a clumpy structure in the broad-band image. The Hα continuum free image shows about six discrete spots, the most intense being the one located to the S W of the galactic center.

• NGC 2718a and NGC 2718b: These galaxies are a clear pair of interacting satellites and have a sharp and very straight bridge ($\approx 92'' = 25$ kpc) connecting both galaxies. Close to NGC 2718a, and perpendicular to the main axis there is what could be a small companion. The continuum-free image shows that the only component with Hα emission is NGC 2718b which has 3–4 intense knots.

• NGC 2775a: The two brightest Hα emission features are projected very close and are only partially resolved. Their position coincides with the geometrical center of the galaxy. Most of the remaining emission is concentrated in a few spots situated to the SE of the galaxy.

• NGC 2775c: This galaxy shows an intense Hα emission with a very irregular spatial distribution concentrated mainly in the northern part. A differentiated feature is to the SE of the galaxy. The broad-band image shows a plume emerging from the main body of the galaxy in that position.

• NGC 2916a: The Hα subtracted image shows an intense and diffuse structure along the major axis. There are two less intense knots situated in the E and W edges of the galaxy.

• NGC 3043a: There is an extended diffuse structure where it is possible to distinguish at least five differentiated regions distributed through the full area (but avoiding the geometrical center) of the galaxy.

• NGC 3154a: The Hα emission is spread over the full projected area of the galaxy in the form of diffuse emission and discrete knots. The most intense spot is located at the geometrical center. This is the galaxy in our sample which has the smallest projected distance from its progenitor and (apart from the interacting galaxies), the one with the largest Hα luminosity. Although this could be related to a possible interaction with its parent, we do not notice any relevant signs of geometrical distortions in the satellite.

• NGC 3735a: The Hα emission is concentrated in the E side of the galaxy. In particular, there is a bright feature at the geometrical center and a few other less intense features in structures resembling arms. In the broad-band image, there is some evidence of a tail connecting this galaxy and another smaller one of unknown redshift situated to the NE. However, this last galaxy does not show any Hα emission.

• NGC 4030b: The majority of the Hα emission is concentrated in four discrete spots. One is located at the center, and another is situated NW coincident with what we have identified as a possible small interacting galaxy. Unfortunately, the redshift of this last object is unknown.

• NGC 4541a: The broad-band image shows a spiral edge-on galaxy with two small structures perpendicular to the major axis on both edges. The Hα continuum-free image shows a diffuse structure that extends over most of the projected area of the galaxy, and some very clumpy structures. This emission seems to be aymetrically distributed through the SW, where one of the features mentioned in the broad-band image shows clear evidence of Hα emission. We think that this could be a small

interacting object that could be enhancing the star formation in the neighbouring regions of the main galaxy.

• NGC 4541b and NGC 4541e: This pair of galaxies is separated by ∼41 arcsec. The galaxies have morphological types E and S0/Sa respectively. In the broad-band image there are two tidal tails emerging from NGC 4541b. One of them is pointing directly to NGC 4541e and it seems clear that its origin is the interaction with this galaxy. The other, pointing nearly in the opposite direction, seems more extended and is possibly the relic of a previous passage of this galaxy near NGC 4541e. The continuum-subtracted Hα image shows an intense structure in NGC 4541e, while NGC 4541b has no Hα emission. The Hα emission in NGC 4541e seems to be composed of at least four major clumps located on the main body of the galaxy. A few faint features seem to follow two arms in approximately opposite directions.

• NGC 4725a: This is the largest satellite in our sample. The morphology corresponds to a late spiral with clear signs of distortions and possibly dust obscuration. In particular, a plume emerges in the NE direction. The Hα emission is concentrated along the major axis with two bright spots, one approximately on the geometric center and the other to the SW.

• NGC 5248a: The Hα features are distributed over the full projected area of the galaxy in about a dozen faint independent features.

• NGC 5248b: The brightest spot is located at the geometrical center with a number of diffuse structures distributed through the disk.

• NGC 5899a: The galaxy shows a rich structure with diffuse Hα features extending over the disk and three major discrete features, one in the center and the other two in direction NW. A line of diffuse Hα emission seems to cross the galaxy in a direction perpendicular to the major axis. We think this is an example of extra-planar diffuse ionized gas.

• NGC 5962d: The Hα emission features are distributed in numerous discrete features in the disk, avoiding the central part of the galaxy.

• NGC 5965a: This really corresponds to two close galaxies, separated by ∼7.4 arcsec as was noted by Zwicky (1971) and Gutiérrez & Azzaro (2004). Following the notation of that paper, we denote them as NGC 5965a_1 and NGC 5965a_2 (other authors have denoted the two members of this pair as SBS 1533+574b and SBS 1533+574a respectively). The continuum-subtracted image shows that both components have Hα emission. In the NW component it is possible to recognize at least two irregular features. The isophotes of the NW component are elongated in the direction of the companion. Additionally, the system is surrounded by a diffuse halo.

• NGC 6181a: This is a late-type spiral with evident signs of distortion in the broad-band image. The Hα continuum free image shows a complex structure dominated by a bright discrete feature which shows at least three bright spots. It seems that this spot corresponds to a structure which is differentiated from the main body of the galaxy and could correspond to a minor merger.

• NGC 7137a: The Hα emission is concentrated in two extended features situated in the E side

of the galaxy. The brightest one runs in direction perpendicular to the main axis.

• NGC 7678a: This nice face-on spiral galaxy has Hα emission in the form of discrete features on the center and in a ring surrounding the galaxy and approximately tracing the spiral structure. A small galaxy is located very close by to the NW. This does not show any Hα emission. The main Hα-emitting regions are located in two extended regions situated in the NE part of the galaxy. Two plumes of diffuse material seem to connect these two structures with the main body of the galaxy. We think that they could be two separate structures in the process of strong interaction with the main galaxy.

AGRADECIMIENTOS

Hay muchas personas a quienes quiero agradecerles por haberme ayudado en esta etapa tan importante de mi vida:

- A Diego G. Lambas, por todo lo que me enseñó y ayudó en cada paso de esta etapa, con gran sabiduría y paciencia. También a su familia, Valeria, Antonia y Emilio, por su amable hospitalidad.

- A Georgina, Rodrigo y Lucas, por su amistad y por haberme brindado su casa durante todos estos años, con la confianza y amabilidad con la que se recibe a un ser muy querido.

- A Patricia Tissera, por haberme enseñado y ayudado durante esta etapa.

- A Hugo Levato, por la ayuda brindada a lo largo de estos años.

- A Carlos Gutiérrez, por lo que me enseñó durante mi estadía en el Instituto Astrofísico de Canarias.

- A Hernán Muriel y Carlos Valoto, por el dictado de sus cursos.

- A Gastón, por acompañarme incondicionalmente en esta etapa y en todas las que decido emprender, ayudándome y dándome fuerzas para seguir siempre adelante. También por su optimismo y alegría que me ayudan en cada momento de mi vida.

- A Gerónimo por brindarme una gran fuerza y seguridad interior y ser la alegría de mi vida.

- A mi mamá Alba, porque siempre está en todos los momentos de mi vida y nunca deja de enseñarme con su ejemplo.

- A mi papá Marcos y a mis hermanos, Anael, Sofi y Kiko, porque siempre están y porque son muy importantes en mi vida.

- A Ana Pacheco, por haber sido mi compañera en la primera etapa de este camino.

- A mis amigos y compañeros de siempre, Natys, Ana, Noelia, Santiago, Carlos, Juan, Lauri.

- A mis compañeros, Silvia, Luisa, Ana, Mónica, Zulema, Stella, Jose Luis y a todo el personal de CASLEO.

- A Anita, Valeria, Laura Checa y en general a todas las personas del grupo IATE.

- A toda mi familia, mis amigos y a muchas personas que de alguna u otra forma me ayudaron!